Titre: Title:	Wavenumber selection in penetrative convection
Auteur: Author:	Xiaoli Zhang
Date:	1989
Type:	Mémoire ou thèse / Dissertation or Thesis
Référence: Citation:	Zhang, X. (1989). Wavenumber selection in penetrative convection [Ph.D. thesis, Polytechnique Montréal]. PolyPublie. https://publications.polymtl.ca/57962/

UNIVERSITE DE MONTREAL

WAVENUMBER SELECTION IN PENETRATIVE CONVECTION

par

ZHANG Xiaoli

DEPARTEMENT DE GENIE CIVIL

ECOLE POLYTECHNIQUE

THESE PRESENTEE EN VUE DE L'OBTENTION

DU GRADE DE PHILOSOPHIAE DOCTOR (Ph.D.)

DECEMBRE, 1989

ISBN 0-315-58214-6

UNIVERSITE DE MONTREAL

ECOLE POLYTECHNIQUE

Cette thèse intitulée:

WAVENUMBER SELECTION IN PENETRATIVE CONVECTION

présentée par: Zhang Xiaoli
en vue de l'obtention du grade de: Philosophia Doctor (Ph.D.)
a été dûment acceptée par le jury d'examen constitué de:

M.	E. Bilgen	Ph.D., président
M.	A. Bejan	Ph.D.
M.	T. Hung Nguyen	Ph.D.
M.	R. Kahawita	Ph.D.
M.	P. Oosthuizen	Ph.D.

SOMMAIRE

Cette thèse est consacrée à l'étude du phénomène de convection naturelle durant le processus de fusion de la glace dans une couche poreuse horizontale. Les trois aspects fondamentaux de ce problème ont été traités successivement, soit la convection pénétrante, la convection avec double diffusion, et la convection en présence du changement de phase. L'accent a été mis sur la détermination des conditions critiques de l'apparition du mouvement convectif, la prédiction de la longeur d'onde, et l'évolution des cellules convectives. L'étude consiste à établir d'abord un modèle mathématique comprenant les équations de Darcy-Boussinesq et l'équation de fermeture de Pomeau-Manneville. Cette dernière représente la condition nécessaire pour obtenir une solution unique qui représente l'écoulement physiquement observable.

Pour traiter le problème de convection pénétrante, on a considéré une couche d'eau froide entre la surface de la glace et une autre couche plus chaude qui est le siège de la convection naturelle. La couche d'eau froide joue alors un rôle déstabilisant. Pour le problème de convection avec double diffusion, on a considéré le cas d'une concentration de sel avec un gradient négatif qui sert d'agent stabilisateur. Dans les deux cas on a observé le phénomène d'instabilité souscritique dont l'existence n'a pas été prévue par la théorie de stabilité linéaire. Dans le processus de la fonte de la glace, l'écoulement et le transfert de chaleur au sein du fluide sont caractérisés par des périodes de transition très courtes. Ces

dernières conduisent à des cellules de convections plus larges et des taux de transfert de chaleur plus élevés.

Les effets de pénétration du fluide chaud dans une couche froide ont été déterminés en fonction des paramètres caractéristiques tels que le nombre de Rayleigh et le paramètre d'inversion. Les effets de la double diffusion, c'est à dire du couplage entre les transferts de chaleur et de masse, ont été déterminés en fonction du nombre de Rayleigh et du nombre de Schmidt.

Pour le problème de convection avec changement de phase, l'effet de la frontière mobile qu'est l'interface liquide-solide a été étudié en déterminant l'évolution du champ d'écoulement, la position et la vitesse du front de fusion, la distribution de température et le taux de transfert de chaleur en fonction du nombre de Rayleigh, du nombre de Stéfan ainsi que des conditions de sous-refroidissement de la glace. Les résultats obtenus sont présentés sous forme d'isothermes et de lignes de courant, ainsi que de courbes donnant les longeurs d'onde et les taux de transfert thermique et massique en fonction des paramètres gouvernant.

Les résultats ont été obtenus par la simulation numérique basée sur la résolution du modèle mathématique par les techniques des différences finies et spectrales.

ABSTRACT

This thesis reports on the results of a numerical investigation into three important aspects of the melting of ice in a horizontal porous layer. In particular, the penetrative convection, the double diffusive convection and convection with a change of phase have been studied and the results reported. Attention has been focused on the critical point defining the onset of convection, the selection of the preferred wavenumber and the evolution of the flow pattern in an axisymmetric system. In an unbounded horizontal porous layer, it was shown that a unique flow pattern, with a preferred wavenumber may be predicted by the closure equation proposed by Pomeau and Manneville. In penetrative convection, the layer of cold water adjacent to the melting front has a destabilizing effect. In double diffusive convection, the negative solute gradient has a stabilizing role. In both cases, subcritical instabilities have been observed with wavenumbers lying outside the neutral linear stability curve. In convection with a phase change, the flow pattern and heat transfer rate have been observed to evolve continuously, with some abrupt transient periods interrupting the melting process. This is followed by larger convection cells and higher heat transfer rates. Effects of penetration into the stable layer, solute concentration and phase change processes on the convective flow and heat transfer, have been investigated in terms of the appropriate governing parameters, namely the thermal and solute Rayleigh numbers, the Schmidt number, the Stefan number, and the inversion parameter.

The results have been obtained by numerical methods based on finite difference and spectral-finite difference techniques.

ACKNOWLEDGEMENT

I would like to express my great gratitude to my advisors, Prof. Nguyen The Hung of the Mechanical Engineering Department, and Prof. René Kahawita of the Civil Engineering Department, for their wise guidance, encouragement and continuous support from the inception to the present form of this project. They have given me invaluable help in many ways.

I would also like to acknowledge the help I received from many friends and members of the personnel of Ecole Polytechnique.

I wish to thank my husband, Dr. Hou Zhang, for his encouragement in this venture and his many useful suggestions during the course of frequent discussions.

Finally, I owe a debt of gratitude to the Ministère de l'Education du Québec for the waiver of the foreign student tuition fees and the Natural Sciences and Engineering Research Council of Canada for the financial support during my studies at Ecole Polytechnique.

CONTENTS

CHAPTER I INTRODUCTION

CHAPTER II CONVECTION IN AN UNBOUNDED HORIZONTAL POROUS LAYER

CHAPTER III CONVECTION WITH PHASE CHANGE IN A BOUNDED POROUS LAYER: THE PROBLEM OF MELTING OF ICE

LIST OF FIGURES

LIST OF TABLES

LIST OF APPENDICES

NOMENCLATURE (for Chapters I and II)

a	: wavenumber
$\mathbf{A}$	: Differential operator in compact form
c	: heat capacity
C	: empirical constant in Forchheimer's term
D	: distance between the two planes
Da	: K/D^2, Darcy number
f_1	: $\|\mathbf{V}\|(1+v^2/\|\mathbf{V}\|^2)$
f_2	: $\|\mathbf{V}\|(1+u^2/\|\mathbf{V}\|^2)$
f_3	: $-uv/\|\mathbf{V}\|$
F, G, H	: solutions of the adjoint equations
g	: gravity
K	: permeability
N_f	: number of Fourier expansion terms
N_g	: number grid points in the vertical direction
Nu^s	: Solute Nusselt number
Nu^T	: Thermal Nusselt number
P	: pressure
$\mathbf{P}$	: $(\varphi,\ T)$ or $(\varphi,\ T,\ S)$, solution vector
Pr	: ν/α_T, Prandtl number
r	: radial coordinate
R	: characteristic radial scale
Ra^e	: $Ra(1-\beta)^3$, effective Rayleigh number
Ra_s	: $\lambda_s g \Delta S D^3/\nu\alpha_T$, solute Rayleigh number

Ra : $\lambda_T g \Delta T K D / \nu \alpha_T$, thermal Rayleigh number

Ra_m : $RaDa$, modified Rayleigh number

S : solute concentration

S_b : constant solute concentration on the lower plane

S_u : constant solute concentration on the upper plane

S_c : α_s / α_T, Schmidt number

$f(a)$: function that defines the solvability condition $f(a) = 0$

T : temperature

T_b : temperature at the lower plane (constant)

T_c : 3.98°, maximum density point

T_u : temperature at the upper plane (constant)

u, v : radial and vertical velocity components, respectively

V : velocity vector

z : vertical coordinate

α_s : mass diffusivity

α_T : thermal diffusivity

β : $(T_u - T_c)/(T_u - T_b)$

λ_s : concentration expansion coefficient

λ_T : thermal expansion coefficient

μ : viscosity

φ : stream function

ϕ : porosity of porous medium

σ : ratio of porous medium to fluid heat capacity

ρ : density

ν : kinematic viscosity

δ_s : solute boundary layer thickness

δ_T : thermal boundary layer thickness

ΔS : $S_b - S_u > 0$

ΔT : $T_b - T_u > 0$

τ : $C/(PrDa^{1/2})$

τ_m : $\tau Da = CDa^{1/2}/Pr$.

Superscripts:

0 : quantities of the zeroth order

1 : quantities of the first order

$*$: dimensional quantities

c : quantity values at the onset of convection

Subscripts:

r : derivative with respect to r

z : derivative with respect to z.

NOMENCLATURE (for Chapter III)

a	: wavenumber
c_p	: heat capacity
$\mathbf{e}^{\mathbf{i}}$	: contravariant vector in the curvilinear coordinate
$\mathbf{e}_{\mathbf{i}}$	: covariant vector in the curvilinear coordinate
$\tilde{\mathbf{e}}^{\mathbf{i}}$	: contravariant vector in the curvilinear coordinate
$\tilde{\mathbf{e}}_{\mathbf{i}}$	: covariant vector in the curvilinear coordinate
$\mathbf{E}_{\mathbf{i}}$	: covariant vector in Cartisian coordinate
g	: gravitational acceleration
g_{ij}	: covariant metric tensor
g^{ij}	: contravariant metric tensor
$\tilde{g}_{ij}$	: covariant metric tensor
$\tilde{g}^{ij}$	: contravariant metric tensor
H	: height of the cavity
J	: Jacobi determinant of the coordinate transformation
k	: conductivity
K	: permeability
L	: length of the cavity
$\mathbf{n}$	: normal direction of the interface
Nu^b	: average Nusselt number at the bottom surface
Nu^u	: average Nusselt number at the upper surface
q	: 1.894816, constant in the water density expression
R	: α^s/α^l, diffusivity ratio
Ra	: $\lambda g(\Delta T^l)^q KH/\nu\alpha^l$, Rayleigh number

Ra^e : $Ra * S * (1-\beta)^{1+q}$, Effective Rayleigh number based on the potentially unstable layer thickness

S : S^*/H, dimensionless interface position

Ste^l : $C_p^l \Delta T^l / \phi \Delta h_f$, Stefan number of the liquid phase

Ste^s : $C_p^l \Delta T^s / \phi \Delta h_f \left(k^s/k^l\right)$, Stefan number of the solid phase

t : $t^*/\alpha^l H^2$, dimensionless time

T^l : $(T^{l*} - T_f)/\Delta T^l$, dimensionless temperature in the water layer

T^s : $(T_f - T^{s*})/\Delta T^s$, dimensionless temperature in the ice layer

T_b : temperature at the bottom surface

T_u : temperature at the upper surface

T_f : fusion temperature

T_m : 4.029325^oC, maximum density temperature

u^i : contravariant velocity component

$\mathbf{V}$: Velocity vector

V_n : Moving velocity of the interface in its normal direction

$x^1,\ x^2$: $x^{1*}/H,\ x^{2*}/H$, dimensionless cartesian coordinate

XL : L/H, the geometry ratio

α : diffusivity

β : $(T_m - T_f)/(T_b - T_f)$

λ : $9.297173 * 10^{-6}\ {}^o\mathrm{C}^{-q}$, constant in the water density expression

ξ^1, ξ^2 : transformed coordinates in the water region

η^1, η^2 : curvilinear coordinates in the ice region

τ : t, dimensionless time

Δh_f : latent heat of fusion

ΔT^l : $T_b - T_f$, temperature difference across the melt layer

ΔT^s : $T_f - T_u$, temperature difference across the ice layer

φ : φ^*/α^l, dimensionless stream function

ϕ : porosity

Φ : quanlities representing φ or T

ν : kinematic viscosity

ρ : density

ρ_m : $999.972 kg/m^3$, maximum density

Superscript:

s : quantity in the ice region

l : quantity in the water region

$*$: dimensional variables

o : quanlities of the previous time or iteration step

Subscript:

c : critical value at the onset of convection

m : refers to maximum density point

p : point being currently discussed

nb : the points nearby

CHAPTER I INTRODUCTION

1.1 Review of Literature

Natural convection heat transfer can significantly affect the energy transport processes in nature as well as in engineering systems. For example, convection dominates in stars wherever radiation is not sufficiently strong. It warms the earth atmosphere by upward transfer of heat absorbed at ground. Convective motions are responsible for much of the mixing of water masses in the oceans, and it is believed that thermal convection is the cause of most tectonic processes in the earth's crust, including the phenomenon of continental drift. In industrial applications, natural convection enters in various forms and creates a continuing demand for a better understanding of its properties in nuclear reactors, in crystallization processes, in solar heating devices, etc..

While a great amount of fundamental knowledge, data and correlations has been accumulated during the last few decades, convective flow and heat transfer cannot still be predicted with enough accuracy for many systems of interest. This is due to a number of difficulties, including unbounded domains, complex interactions involving multi-component heat and mass transfer, moving boundaries, etc.. Of course, beyond all these difficulties lies many a hazardous route leading to the ultimately fascinating domain of turbulence. One of these routes

has been proposed by Landau (1944) some forty years ago, who conjectured that the transition to turbulence consists of the development of successive instabilities with an increasing number of characteristic frequencies (like the bifurcation of branches and leaves in a tree) until the flow becomes chaotic which is of course the fundamental characteristic of turbulence.

A phenomenon which encompasses all the above mentioned problems is the natural convection in a horizontal layer of fluid heated from below. This so-called Bénard problem (named after the French physician who first studied it experimentally) is without any doubt one of the most attractive test grounds for studies in convective flow and heat transfer.

The history of natural convection in a horizontal layer may be traced back to the beginning of this century when Bénard (1900) heated a thin layer of spermaceti oil from below, and observed the famous hexagonal flow pattern. Thereafter, it was demonstrated that if the buoyancy force is stronger than a certain value, convection in the form of a cellular pattern will set in or else the fluid remains motionless. The critical values when convection sets in, the size of the cell and the transport properties of the convective flow have been the subjects of numerous studies. In 1940, Pellew and Southwell (1940) published a paper entitled "On maintained convective motion in a fluid heated from below", which solved the critical stability problem. They found that the critical Rayleigh number (i.e. the ratio of buoyancy forces to the viscous forces) was

about 1708 while the value of the corresponding wavenumber was 3.117 (nearly square cell) for the case of two rigid horizontal boundaries. A classical review of the critical stability problem is presented in the book by Chandrasekhar (1961). Since then, all efforts have been devoted to both theoretical and experimental studies of the convection form after the onset of motion, with as yet, no unified results. The difficulties lie in the fact that the evolution of the convection form is completely dependent on the initial state of the system. However, while linear stability theory predicts that a finite band of wavenumbers is possible for a given Rayleigh number above the critical value (as shown in Fig. 1.1), Koschmeider and Pallas (1969), Pocheau and Croquette (1984), Willis et al. (1972) and Chen and Whitehead (1968), demonstrated that a unique wavenumber would exist under certain conditions. McDonough and Catton (1982) numerically showed that the heat transfer rates calculated using the observed wavenumbers are in good agreement with the measured values. Schluter, Lortz and Busse (1965) proved theoretically that only two-dimensional convection rolls are realizable in the range of lower Rayleigh number. It is based on the notion that the real physical world is full of noises and an observable phenomenon should be the one that can stand these noises, otherwise it will be replaced quickly. This stability criterion greatly reduces the range of possible steady solutions which, however, still form an infinite set contained within the so-called stability balloon (Busse, 1967) as shown in Fig. 1.2. The question of wavenumber selection is therefore still open.

In the classic Bénard problem discussed above, only one unstable layer of fluid is involved. In nature, there often exists multi-layer systems where convection that arises from an unstable layer can penetrate into an adjacent stable layer and drive it into motion. Examples can be found in the areas of geophysical fluid dynamics, meteorology, oceanography and astronomy (Veronis, 1963):

In the atmosphere bounded below by the ground (or the ocean), the air layer is heated by solar radiation and becomes gravitationally unstable. When convection occurs, the warm air is carried aloft into regions that are stably stratified.

In the ocean, evaporation is the primary physical process which gives rise to instabilities near its surface. As the cool surface water convects downwards, it also penetrates into regions that are stably stratified.

In stars, the surface layer is stable. At some distance from their surface, the increase in temperature due to adiabatic compression causes negative hydrogen to form. The latter is opaque to photons. The temperature gradient therefore rises to a value greater than the adiabatic gradient, making the region unstable. Depending on the type of star, this superadiabatic gradient can extend far into the interior to a point where the very high temperature causes the gas to become completely ionized and the gradient is no longer superadiabatic. An unstable layer is formed, with stable fluid both above and below.

The onset and evolution of the flow pattern and heat transfer in such systems can be quite different from the case of a single fluid layer and should be regarded with special attention. Most studies on this subject focused on the onset of convection, and on the development of flow pattern in enclosures, i.e. with fixed wavenumber. The question of wavenumber selection still remains untouched.

In the past three decades, considerable attention has been directed to the problem of double diffusive convection. A saltwater layer confined between two infinite planes is a typical example. In this kind of flow, more than one solute component is involved and can make opposite contributions to the vertical density gradient. The competition between their contributions to the density gradient, and the large difference between their diffusivities (for example, about 1/80 in the thermohaline system) lead to some new phenomena which are not observed in pure Bénard convection. For instance, it is found that convection can appear in the form of narrow "fingers" even when the net density decreases upwards, as in the case of a saltwater layer heated from above, if a positive salinity gradient is present. For the case of heating from below with a negative salinity gradient, oscillations can arise since heat diffuses much faster than salt. The oscillation could be explained by simply noting that if a parcel of saltwater is displaced upward, it will loose more heat than salt since its thermal diffusivity is about eighty times higher than the diffusivity of salt, and it will be heavier than its surroundings because of the negative salinity gradient. The buoyancy force will therefore drive

it back towards its initial position with a speed faster than it leaves, because of the lag in temperature between the parcel and its surroundings, thus producing an oscillation.

Much of the theoretical work in this field has developed directly from the linear stability analysis for a fluid layer heated from below. In order to explain experimental observations, many works have been made of stability and flow regimes in the nonlinear region by Veronis (1965, 1968), Hupper and Moore (1976), Toomre et al. (1982), etc. In all these studies, the wavenumbers were not selected according to any closure equation, but were supposed known a priori.

So far, the foregoing review considers only convective flows between fixed boundaries. There exists another class of problems where the flow is driven within a moving boundary. The simplest physical description of the phenomenon is a solid mass that, under the influence of external heat sources, undergoes a phase change and forms a layer of liquid melt that coexists with the remaining solid phase. The subsequent evolution of the two phases will essentially depend on the behavior of the net heat transfer to the system. Earlier studies on this problem considered conduction as the only heat transfer mechanism during the phase change process. More recently, an increasing number of studies have been devoted to the studies of convective flow and heat transfer in the liquid phase as it has been found that conduction is dominant only at the very early stage of the melting process. The major difficulties in solving this type of problems

are due to the fact that one has to deal with an essentially transient flow in a continuously changing domain. The interplay between the convective flow and the liquid-solid interface movement is one of the most complicated and fascinating subjects in heat transfer. This domain is still wide open, and much work needs to be done to arrive at a comprehensive and unified description of the flow patterns and heat transfer rates during the whole phase change process. Recent literature reviews on this subject may be found in the articles of Viskanta (Viskanta, 1983, 1985).

In the context of this thesis, all the topics discussed above, namely the wavenumber selection, the penetrative convection, the double diffusive convection and convection with a phase change, have been studied for the case of a porous layer heated from below and will be presented in the following chapters.

1.2 Description of the Research Project

Let us consider a horizontal porous layer saturated with an incompressible fluid. The fluid can be multi-component, such that two (or more) stratifying agents can affect its density. A specific example is that of a layer of soil saturated with saltwater.

Suppose that the fluid within the porous layer has been completely frozen to a temperature below its freezing point T_f. At time $t = 0$, let the lower boundary of the layer be heated to a temperature $T_b > T_f$ while the upper boundary is kept at a constant temperature $T_u < T_f$. As a consequence of this heating, a liquid layer is formed whose thickness increases as the melting progresses in time, until a steady state is attained in which the heat input through the lower boundary is equal to the heat loss through the upper boundary (which is maintained at a temperature below the fusion temperature). As the thickness of the melt layer increases, convection can set in and greatly influence the melting process, as heat transfer is then controlled not only by conduction but more and more by convection. If some solute is present in the fluid, the convective flow and heat transfer may also be significantly affected.

For the specific case of melting of ice within a porous medium, another phenomenon which can influence the convective heat transfer is the inversion of density of cold water in the melt region, giving rise to penetrative convection.

To solve the problem of the melting of a layer of frozen soil, we have studied the following four aspects:

(1) The Preferred Convection Pattern: This question arises when the layer is unbounded in the horizontal direction (the aspect ratio length /height >> 1). In fact, it is well-known that convection rolls will arise in such layer, but their horizontal size is not known a priori, and must be found according to some closure equation.

(2) The Penetrative Convection: This type of convective flow arises due to the fact that cold water in the 0^oC to 10^oC temperature range presents a peculiar behavior: its density increases between 0^oC to 4^oC and then steadily decreases. The maximum density at 4^oC has the consequence of creating a stable layer of cold water (between 0^oC to 4^oC) overlying the unstable hotter layer (above 4^oC) in which the convective motion is induced, which then penetrates into the upper stable layer. This problem is not only typical of cold water, but also occurs in other systems as discussed earlier.

(3) The Double Diffusive Convection: In the presence of a solute gradient such as salt, the problem of mass transfer is coupled to the heat transfer through the density-induced flow. Influence of such coupling on the preferred flow pattern and heat transfer is still an unsolved aspect of the problem which needs to be investigated.

(4) Convection with a Moving Boundary: During the melting process,

the convection regime is limited to the liquid phase, i.e. cold water. The main difficulty that characterizes this problem lies in the fact that the flow domain is bounded by a moving surface, namely the solid-liquid interface, whose form and melting speed are not specified, but have to be solved as one of the unknowns of the problem. Attention has to be focused on the onset of convection and the evolution of the flow pattern and heat transfer rates as the melting proceeds.

These four aspects of natural convection within a porous layer heated from below are not only closely related to the physical situation of a layer of frozen soil, but each one clearly represents in its own right an important research topic in the domain of convective heat transfer. Each topic has therefore been studied separately, and presented independently in the following sections so that the results obtained may be applied to other systems where only one effect, or some combination of them is relevant.

1.3 General Mathematical Formulation

1.3.1 The Forchheimer-Darcy Boussinesq Equations

Most studies of convective flow and heat transfer in porous media are based on the framework of Darcy's law which substitutes for the momentum equation in fluid dynamics and was formulated after numerous experimental observations (Darcy, 1856).

Darcy's law, however, does not correctly describe the flow field when the local Reynolds number based on the mean pore diameter is of order 1 or greater, as inertial forces then become comparable to the viscous forces, and can significantly reduce both the velocity and thermal boundary layer thicknesses, broaden the temperature distribution and decrease the heat transfer rate. Modelling the inertial forces in a porous medium is a delicate task with an uncertain result. The simplest and perhaps most popular model is due to Forchheimer with a quadratic term of the form $|\mathbf{V}|\mathbf{V}$ which makes the momentum equation a nonlinear one. This Forchheimer-Darcy equation will be presented here, and will be applied in a later section to solve the classical Bénard problem in order to evaluate the effects of inertial forces and thereby to assess the validity of the Darcy model that will be used (within its validity domain) in the subsequent studies presented in Chapter II and Chapter III.

Within the Forchheimer-Darcy and Boussinesq approximation, the following assumptions will be adopted:

- The saturated fluid and the porous matrix are incompressible.

- The porous medium is homogeneous, isotropic and in thermal equilibrium with the saturated fluid.

- All physical properties of the medium, except the fluid density that gives rise to the buoyancy force, are taken to be constant and independent of the temperature.

– The diffusion of vorticity from a boundary is negligible.

– All boundaries are impermeable.

– Viscous dissipation is negligible.

The system of equations (usually referred to as the Forchheimer-Darcy- Boussinesq Equations) governing the fluid flow and the heat and mass transfer then consists of

1– The continuity equation

$$\nabla \cdot \mathbf{V} = 0 \tag{1.1}$$

2– The momentum equation

$$-\nabla P - \rho \mathbf{g} - \frac{\mu}{K}\left(1 + \frac{CK^{1/2}\rho}{\mu}|\mathbf{V}|\right)\mathbf{V} = 0 \tag{1.2}$$

3– The energy equation

$$\sigma \frac{\partial T}{\partial t} + \nabla \cdot (\mathbf{V}T - \alpha_T \nabla T) = 0 \tag{1.3}$$

4– The mass diffusion equation

$$\phi \frac{\partial S}{\partial t} + \nabla \cdot (\mathbf{V}S - \alpha_s \nabla S) = 0 \tag{1.4}$$

5– The state equation

$$\rho = \rho_0 \left(1 - \sum_n \lambda_n (T - T_0)^n\right) \tag{1.5}$$

where $\mathbf{V}$, P, ρ, T and S represent the velocity, pressure, density, temperature and solute concentration, respectively. Other parameters $\mathbf{g}$, μ, λ_n are the gravitational acceleration, viscosity and thermal expansion coefficients of the fluid, K is the permeability of the porous medium, σ and α_T are the heat capacity ratio and thermal diffusivity of the fluid-saturated medium. C the empirical parameter in the inertial term has a value of approximately 0.55 according to Chen (1979), ϕ and α_s are the porosity and molecular diffusivity of the solute.

It should be noted from Eq.(1.2) that the term $\mu/K\mathbf{V}$ is the Darcy force, $\rho\mathbf{g}$ is the buoyancy force while $CK^{-1/2}\rho|\mathbf{V}|\mathbf{V}$ is the Forchheimer one that accounts for inertial effects. At first sight, the Forchheimer force (which is absent in the original Darcy's equation), seems negligible compared to the Darcy force when the Reynolds number based on $K^{1/2}$ does not exceed $O(1)$. In fact, a more sophisticated criterion will be developed in the next section. It should also be noted that the foregoing equations are written for the primitive variables $\mathbf{V}$, P, T and S. In subsequent studies concerning specifically two-dimensional flows, a vorticity-stream function formulation will be used which has the advantage of eliminating both the pressure term and the continuity equation.

1.3.2 The Closure Equation

In an unbounded horizontal fluid layer heated from below, spatially

periodic convection rolls can be observed when the Rayleigh number exceeds a certain critical value. Linear stability theory, however, predicts that a whole band (i.e. an infinite set) of wavenumbers at a given supercritical Rayleigh number is possible (as in Fig. 1.1). In other words, for an infinite layer, (or for a large aspect ratio (length/height) cavity), the foregoing system of equations admits an infinite number of possible solutions. However, experimental observation indicates that only a single wavenumber out of this spectrum is selectively amplified and dominates the convection. How and why this preferred wavenumber is selected still remains an open question.

In order to obtain a unique solution, one needs to find a closure equation based on some physical ground. To this end, Malkus (1954) proposed a maximum heat transfer principle, which stated that the realizable convection form should be the one giving the maximum heat transfer rate. This quite plausible principle, unfortunately, does not agree well with experimental data.

Glansdorff and Prigogine (1971) proposed a global non-equilibrium thermodynamic stability condition from a generalization of the minimum entropy principle, the application of which required some experimental data. Georgiadis and Catton (1986) applied this principle to the Bénard convection in a porous layer and obtained not a unique, but two convection patterns for a given Rayleigh number.

Another approach was proposed by Pomeau and Manneville (1981)

who succeeded in determining a unique wavenumber for Bénard convection in both a fluid and a porous layer. Their approach may be considered as a geometric one: By considering an axisymmetric horizontal layer, they argued that the preferred convection rolls must be able to survive the constraint of small curvature imposed by an axisymmetric system which is considered as a geometric perturbation of the straight convection rolls. Mathematically, this idea leads to a condition of solvability which serves as a closure equation for the prediction of the preferred flow pattern. The formulation of this constraint can be explained as follows:

Let us suppose that the flow is axisymmetric with an axisymmetric constraint imposed on the system as shown in Fig.1.3. The curvature effect ($\epsilon = 1/r$) is assumed to be very small at a position far from the point of symmetry. The number of solutions $\mathbf{P}(0) = (\varphi^0,\ T^0)$ without the curvature constraint are infinite as stated before. The idea of Pomeau and Manneville (1981) is that the solutions $\mathbf{P}(\epsilon) = (\varphi,\ T)$ with the constraint should be slightly different from those of the infinite set $(\varphi^0,\ T^0)$ as the constraint, i.e. ϵ, is small. Mathematically, $\mathbf{P}(\epsilon)$ is at least a continuous function at $\epsilon = 0$, and

$$\lim_{\epsilon \to 0} \mathbf{P}(\epsilon) = \mathbf{P}(0) \tag{1.6}$$

In order to simplify the description that follows, the homogeneous equations of the governing system Eq.(1.1) to Eq.(1.4) are rewritten in compact form using the polar coordinates as

$$\mathbf{A}(\epsilon)\mathbf{P} = 0 \tag{1.7}$$

where $\mathbf{A}(\epsilon)$ is the differential operator, $\mathbf{P}$ the vector with components φ and T, and $\epsilon = 1/r$ the small curvature.

The unknown variable $\mathbf{P}$ and the differential operator $\mathbf{A}$ are subsequently expanded in a series of ϵ as follows:

$$\mathbf{P} = \mathbf{P}_0 + \epsilon\mathbf{P}_1 + O(\epsilon^2) \tag{1.8}$$

$$\mathbf{A}(\epsilon)\mathbf{P} = \mathbf{A}_0\mathbf{P}_0 + \epsilon(\mathbf{A}_1\mathbf{P}_1 + \mathbf{N}\mathbf{P}_0) + O(\epsilon^2) \tag{1.9}$$

where the operator $\mathbf{A}_1$ includes all linear terms related to $\mathbf{P}_1$, while nonlinear terms are included in $\mathbf{N}\mathbf{P}_0$. Eq. 1.7 can thus be ordered as :

$$\mathbf{A}_0\mathbf{P}_0 = 0 \tag{1.10}$$

$$\mathbf{A}_1\mathbf{P}_1 = -N\mathbf{P}_0 \tag{1.11}$$

....

The zero-th order equation (1.10) describes the convection in an infinite horizontal porous layer and possesses a multitude of solutions at supercritical Rayleigh numbers. The first order equation (1.11), however, will admit a solution only if its solvability condition is satisfied, since it is a linear non-homogeneous equation with a nonzero kernel. It can be stated that Eq.(1.11) is solvable if the non-homogeneous part $\mathbf{N}\mathbf{P}_0$ is perpendicular to any solutions of the adjoint equation of Eq. (1.11), i.e.

$$f(a) =< \mathbf{P}_1^*, N\mathbf{P}_0 >= 0 \tag{1.12}$$

where $< *, * >$ denotes the inner product in L_2 space, $\mathbf{A}_1^*$ the adjoint operator of $\mathbf{A}_1$, and $\mathbf{P}_1^*$ the solutions of the adjoint equation

$$\mathbf{A}_1^* \mathbf{P}_1^* = 0 \tag{1.13}$$

Any given wavenumber a that satisfies the solvability condition $f(a) = 0$ is called the preferred wavenumber, and the solution associated with this wavenumber is called the selected solution, which is realizable under the curvature constraint. Thus Eq.(1.12) serves as a closure to Eq.(1.10).

1.4 Methods of Solutions

From the above discussion, it follows that the zero-th order equation (1.10) should be solved first with a given wavenumber. To judge if the obtained solution is the "real" one, equation (1.12) should be evaluated, after having solved the adjoint equation (1.13). In the following, two methods, the spectral-finite difference method and the finite-difference method will be used to solve the zero-th order and the adjoint equations and an iterative procedure will be given to coordinate the whole system.

1.4.1 Linear Stability Analysis

Within the context of linear stability theory, $\mathbf{P}$ is expanded in the following Fourier series

$$\varphi = \sum_{k=1}^{N_f} \varphi_k \sin(k\pi z) \sin(a\pi r) \tag{1.14}$$

$$T = \sum_{k=1}^{N_f} T_k \sin(k\pi z)\cos(a\pi r) \tag{1.15}$$

These expressions are substituted into the linear part of Eq.(1.10) that finally results in the algebraic system of the form

$$L_{i,j}T_j = 0 \tag{1.16}$$

where L is a matrix, belongs to $R^{N_f \times N_f}$ and is a function of Rayleigh number Ra as well as the wavenumber a. The neutral stability curves may, therefore, be determined by

$$f_L(Ra, a) = \text{Determinant of } (L_{i,j}) = 0 \tag{1.17}$$

1.4.2 Spectral-Finite Difference Method

Since we are looking for a periodic solution in the radial direction with wavenumber a, the spectral approximation by Fourier expansion is used in this direction. By observing the parity of the momentum equation and the energy equation in Eq.(1.10), solutions of the zero-th order equations can be chosen, for the homogenized boundary conditions, as:

$$\varphi = \sum_{k=1}^{N_f} \varphi_k(z)\sin(a\pi(k-1)r) \tag{1.18}$$

$$T = \sum_{k=1}^{N_f} T_k(z)\cos(a\pi(k-1)r) \tag{1.19}$$

Substituting these expressions into Eq.(1.10) and applying the general Galerkin procedure to these equations results in a two-point boundary value ordinary differential system. A central difference operator coupled with a relaxation technique is then used to solve these equations in the vertical direction. For a given wavenumber, the φ's are solved from the momentum equation, the T's are subsequently obtained from the energy equation by using the new φ, then φ is recalculated with the new T's ... . This procedure is repeated until the maximum absolute difference between the solutions obtained in two consecutive steps was less than some tolerance (10^{-4} in this study). The numbers of Fourier terms N_f and grid points N_g required to satisfy the accuracy criterion were obtained by numerical tests. It was found that $N_f = 13$ and $N_g = 51$ were sufficient to provide accurate results in the range of parameters considered in this study.

The solutions to the adjoint equations are obtained in a similar fashion by expanding $\mathbf{P}_1^* = (F, G)$ as

$$F = \sum_{k=1}^{N_f} F_k(z) \cos(a\pi(k-1)r) \tag{1.20}$$

$$G = \sum_{k=1}^{N_f} G_k(z) \sin(a\pi(k-1)r) \tag{1.21}$$

1.4.3 Finite-Difference Method

The spectral-finite difference method transforms the partial differential equations into a group of ordinary differential equations. This task

can be tedious when nonlinear terms are involved: the Forschheimer term in the momentum equation is such an example that will be discussed later. The finite-difference method has its advantages for such situations.

In the finite difference method, the governing equations are written in conservative form, and the power law scheme (Patankar, 1980) is applied to obtain the discretized equations. The discretized equations are solved using a line under-relaxation iteration technique. At each iteration step, φ is first improved by solving the momentum equation and the current T is corrected from the energy equation using the improved φ values. The iteration is continued until the maximum absolute difference between the solutions obtained in two consecutive iteration steps is smaller than a given tolerance. It was found that a grid of $51 * 51$ points was sufficient to provide accurate results, say, for a given tolerance of order 10^{-4}. The solutions $\mathbf{P}_1^*$ to the adjoint equation (1.13) were obtained in a similar manner.

1.4.4 Iteration Procedure for the Wavenumber Selection

For a group of given physical parameters in the system, the zero-th order equation (1.10) and the adjoint equation (1.13) are solved using either of the above methods with an initial guess for the wavenumber a, $f(a)$ is evaluated from the solvability condition (1.12). The secant method is used for providing an updated estimate of the wavenumber

as follows: let the superscript n denote the iteration counter and $f^n = f(a^n)$, then

$$a^{n+1} = \frac{\left(a^{n-1}f^n - a^n f^{n-1}\right)}{\left(f^n - f^{n-1}\right)} \tag{1.22}$$

This iteration is repeated until the residue between two consecutive iteration steps is smaller than a given tolerance which is of order 10^{-4}. Convergence is usually achieved, within 4 to 6 iteration steps.

1.5 The Bénard Problem Revisited

Let us consider the problem of natural convection in a fluid saturated layer heated from below. Most of the literatures on this subject has been devoted to convective heat transfer in enclosed spaces subjected to various types of boundary conditions. For example, Poulikakos and Bejan (1985) and Prasad and Tuntomo (1987) have studied the case of a rectangular cavity with adiabatic horizontal walls and differentially heated isothermal side walls. Poulikakos (1985) considered the same problem with side walls subjected to a uniform heat flux. A more recent reference, on the subject of Prandtl number influence on natural convection in a porous layer heated from side, can be found in the article of Wang and Bejan (1987). All these studies lead to the conclusion that inertia forces can significantly influence the heat transfer as well as flow velocity if the Prandtl number is "small" and the Darcy number is "large".

For a layer of infinite extent, the scale of the convection pattern (wavenumber) is still unknown. In this section, we will investigate the dependence of the preferred wavenumber on parameters such as the Darcy and Prandtl numbers that are related to the inertia effects. To the author's knowledge, this question has been considered only by Georgiadis and Catton (1986) who have investigated the Prandtl number effect on Bénard convection in a porous layer by including both the Brinkman and Forchheimer terms in the Darcy-Boussinesq formulation. To determine the preferred wavenumber, they proposed a closure based on the theory of non-equilibrium thermodynamics of Glansdorff and Prigogine (1971). Their results showed that inertia effects can become important when the Prandtl number is small and the Darcy number is large, in agreement with the results obtained by previous authors in the case of side heating. However, it was found that

1) The Glansdorff-Prigogine principle, when applied to the Brinkman-Forchheimer-Darcy-Boussinesq formulation, leads to two possible wave-numbers instead of a unique one as found by Somerton et al. (1983) using the same principle for the case of a porous layer governed by the Brinkman-Darcy-Boussinesq formulation (i.e., in the absence of inertia forces).

2) The predicted wavenumber increases with increasing Prandtl number contrary to the tendency observed in a pure fluid layer by Buell and Catton (1986) where the geometric principle of Pomeau and Manneville (1981) was used.

3) The predicted wavenumber was only qualitatively rather than quantitatively in agreement with the data of Jonsson (1984).

From these results, it seems that the inclusion of inertial effects does lead to some "confusion". A more definitive study is necessary to determine if indeed the inclusion of the Forchheimer term is the cause of the ambiguity or if it is the result of the closure principle employed. The present section was focused therefore on the formation of Bénard cells under the effects of inertia forces by using the Forchheimer-Darcy-Boussinesq formulation with the principle of Pomeau and Manneville (1981) to determine the preferred wavenumber. A comparison with the theoretical results of Georgiadis and Catton (1986), and with the available experimental data of Jonsson (1984) was made to assess the validity of the various formulations.

Consider the Bénard convection and heat transfer in a porous medium including the inertia effect, as shown in Fig.1.4. The conventional state equation (1.5) for this problem takes a linear form

$$\rho = \rho_0 \Big[1 - \lambda_T (T - T_0) \Big] \tag{1.23}$$

The two-dimensional axisymmetric dimensionless equation may be expressed as

$$\frac{\partial}{\partial r} \left[(\varphi_r + \varphi/r)\,(1 + \tau_m |\mathbf{V}|) + Ra_m T \right] + \frac{\partial}{\partial z} \left[\varphi_z \,(1 + \tau_m |\mathbf{V}|) \right] = 0 \tag{1.24}$$

$$T_{rr} + T_{zz} + T_r/r - \varphi_z T_r + (\varphi_r + \varphi/r) T_z = 0 \tag{1.25}$$

using the stream function φ and the following scales

$$\begin{aligned} \mathbf{V} &= \mathbf{V}^*/(\alpha_T/D) \\ T &= (T^* - T_u)/\Delta T \\ r &= r^*/D \\ z &= z^*/D \end{aligned} \tag{1.26}$$

one obtains two dimensionless parameters in the dimensionless governing system, Ra_m and τ_m which are defined as

$$Ra_m = Ra^* Da \tag{1.27}$$

and

$$\tau_m = \frac{CDa^{1/2}}{Pr} \tag{1.28}$$

where the Rayleigh number Ra, the Prandtl number Pr and the Darcy number Da are defined as

$$Ra^* = \frac{\lambda_T g \Delta T D^3}{\nu \alpha_T} \tag{1.29}$$

$$Pr = \frac{\alpha_T}{\nu} \tag{1.30}$$

$$Da = \frac{K}{D^2} \tag{1.31}$$

τ_m is a parameter characterizing the inertial force.

The details of the ordered equations and the solvability condition are given in Appendix 1.1. A finite difference method was used to solve the zero-th order and adjoint equations, since the nonlinearity of the

added Forschheimer term made the manipulation long and tedious if the spectral-finite difference method was used.

The empirical parameter C was taken to be 0.55 as suggested by Cheng (1979). Five typical values of τ_m, namely, 0., 0.00111, 0.0035, 0.0065 and 0.028, were chosen in this study. It is worth noting that the solutions with $\tau_m = 0$ are identical to those without the inertia effect.

The preferred wavenumbers are presented in Fig.1.5. One can see that they decrease monotonically as Rayleigh numbers Ra_m increase. The wavenumbers selected with the inertia effect involved are greater than those without it and, finally, approach them as τ_m is small. The difference between them is negligible when τ_m becomes smaller than about 0.0011 in the range of Rayleigh number less than 160. The case of $\tau_m = 0.0065$ is equivalent to that investigated by Georgiadis and Catton(1986) and Jonsson(1984) in steel-water. For comparison, the present results and those obtained by previous authors are shown in Fig.1.6. The Nusselt numbers versus Rayleigh numbers Ra_m are drawn in Fig.1.7 which indicates that the heat transfer monotonically increases as τ_m decreases and, when τ_m is very small, say about 0.00111, approaches the limiting case of no inertia effect. The streamlines and isotherms with and without inertia terms are also presented in Fig.1.8. As can be expected, the flow and heat transfer rates are reduced by inertia effects, i.e. when τ_m is increased.

From the results presented above, the following conclusions may be

drawn:

1) By using the concept of slightly curved rolls in an axisymmetric configuration, it was possible to uniquely determine the preferred wavenumbers as a function of Rayleigh number. It was found that the preferred wavenumber decreases (i.e. the convective cells become larger) as the Rayleigh number is increased, in agreement with the tendency observed in the experiments of Jonsson(1984). It should be remembered at this point that Georgiadis and Catton(1986) have investigated the same problem (including the Brinkman term) using the Glansdorff-Prigogine theory of non-equilibrium thermodynamics to determine the preferred wavenumber, but have found two possible wavenumbers for a given Rayleigh number instead of a unique one as expected. By choosing only the values that are closer to those observed in Jonsson's experiments, they also predicted the tendency of decreasing wavenumber with increasing Rayleigh number. Quantitatively, the values obtained from the present computations lie midway between the results of Jonsson(1984) and those of Georgiadis and Catton(1986) (Fig.1.6).

2) The effects of inertia forces have been investigated by using the Forchheimer-Darcy-Boussinesq formulation so that the problem depends, besides the Rayleigh number, on one additional parameter, namely $\tau_m = CDa^{1/2}/Pr$. It was found that inertia effects may be neglected when $\tau_m < 0.001$, i.e., $Pr > 550Da^{1/2}$. As τ_m is increased, inertia effects can become important. For example, for $Ra_m = 200$ the preferred

wavenumber increased from 2.3 to 2.6 when τ_m was increased from 0 to 0.028 (Fig.1.5). The corresponding Nusselt number, on the contrary, decreased from 3.5 to 2.9 (Fig.1.7). These results may be interpreted in terms of the Prandtl numbers: For a given Rayleigh number, the preferred wavenumber increased as the Prandtl number decreased. This tendency is contrary to that predicted by Georgiadis and Catton(1986) using a closure based on the Glansdorff-Prigogine theory, but in agreement with their results obtained for a pure fluid layer (Buell and Catton, 1986) using the principle of Pomeau and Manneville (1981).

3) As far as inertia effects on the preferred wavenumbers are concerned, the present study shows that the results predicted by the geometric principle of Pomeau and Manneville are both qualitatively and quantitatively different from those obtained using the Glansdorff-Prigogine theory.

1.6 Summary

In this chapter, the mathematical background has been laid for the study of natural convection in a horizontal porous layer. The system of governing equations and the proposed methods of solution have been assessed by solving the classical Bénard problem for a Non-Darcy fluid. It has been found that the small curvature constraint can be chosen as a criterion to uniquely determine the convection pattern, and inertial forces influences on the flow pattern and heat transfer are negligible if

$\tau_m < 10^{-3}$, i.e. if the Prandtl number is sufficiently large to satisfy the condition $Pr > 550 Da^{1/2}$.

CHAPTER II CONVECTION IN AN UNBOUNDED HORIZONTAL POROUS LAYER

2.1 Penetrative Convection

2.1.1 General Description

In natural convection phenomena, the process of thermal convection often involves penetration into a stably stratified fluid. Examples can be found in the areas of geophysical fluid dynamics, meteorology, oceanography and astronomy (Veronis, 1963).

In order to study the phenomenon of penetrative convection which is free of other difficulties and complexities encountered in the natural phenomena mentioned above, Furumoto and Rooth (Veronis, 1963) carried out an experiment in a layer of water with an upper boundary at a temperature below 4^oC and a lower boundary at a temperature above 4^oC. In the static state the temperature gradient is constant, and the layer of maximum density is at the 4^oC level. The fluid below 4^oC is potentially unstable while the fluid above the 4^oC level is stable. They observed that when convection occurs in the lower region, it is in a cellular form and penetrates into the stable fluid. The onset of convection, the wavenumber and the transport properties of the convective flow are, therefore, quantities being determined. The following study is devoted

to these subjects for the case of axisymmetric convection of cold water in an unbounded horizontal porous layer.

2.1.2 Governing Equations

It is well known that water has a maximum density at about 4^oC. According to Goren (1966), and Moore and Weiss (1973), the density of water may be approximated by the state equation

$$\rho = \rho_m[1 - \lambda(T - T_m)^2] \tag{2.1}$$

which is valid in the range $0 - 8^oC$, where λ is a constant with a value of $7.94 \times 10^{-6}[^oC]^{-2}$, and the subscript m refers to quantities at 3.98^oC.

For a layer of water-saturated porous medium confined between two horizontal infinite planes at a distance apart of D, and kept at constant temperatures T_u and T_b, respectively, as shown in Fig. 2.1, let us define the following dimensionless quantities

$$\begin{aligned} r &= r^*/D \\ z &= z^*/D \\ T &= (T_b + \Delta T - z^*\Delta T/D - T^*)/\Delta T - 1 \\ \varphi &= \varphi^*/\alpha \\ \Delta T &= T_b - T_u \end{aligned} \tag{2.2}$$

where all quantities are defined in the Nomenclature (with reference to this chapter). Note in particular that φ is the stream function.

The axisymmetric conservations of momentum and energy equations may be expressed as

$$\varphi_{rr} + \varphi_{zz} + \varphi_r/r - \varphi/r^2 + Ra(T + 1 - z - \beta)T_r = 0 \qquad (2.3)$$

$$T_{rr} + T_{zz} + T_r/r - \varphi_z T_r + (\varphi_r + \varphi/r)(T_z - 1) = 0 \qquad (2.4)$$

with boundary conditions

$$\varphi = T = 0, \qquad \text{at} \qquad z = 0,\ 1 \qquad (2.5)$$

There are two dimensionless parameters in the system, Ra and β, defined as:

$$Ra = \frac{2\lambda g \Delta T^2 K D}{\alpha_T \nu} \qquad (2.6)$$

and

$$\beta = \frac{T_u - T_m}{T_u - T_b} \qquad (2.7)$$

respectively.

Here β represents the thickness of the stable layer to the whole layer, for example, $\beta = 0.5$ means that the thickness of the stable layer is half of the water layer. Ra is the Rayleigh number based on the thickness of the whole layer and the temperature difference across the layer. The effective Rayleigh number,

$$Ra^e = Ra(1 - \beta)^3 \qquad (2.8)$$

which is based on the thickness and the temperature difference across the potentially unstable layer will be used later.

The spectral-finite difference method is used. The details of the ordered equations, the adjoint equation, the solvability condition and the related ordinary differential equations are listed in Appendix 2.1.

2.1.3 Linear Stability Analysis

Figure 2.2 exhibits the results from a linear stability analysis and Fig.2.3 is an alternative presentation, with the wavenumber being normalized vs the effective Rayleigh number Ra^e. Note that $8\pi^2$ is the critical Rayleigh number for $\beta = 0$.. It can be seen that although the critical Rayleigh number Ra is increased (Fig.2.2), the effective Rayleigh number Ra^e (which is based on the thickness and the temperature difference of the unstable layer) decreases (Fig. 2.3) and the rate of change of Ra^e versus β is decreased as β is increased from 0 to 0.5. It appears that β has no influence on the onset of convection as β further increases (Fig.2.3). For example, Ra_c^e is $8\pi^2$ for $\beta = 0$, and Ra_c^e are about $6.18\pi^2$, $4.77\pi^2$, $3.92\pi^2$, $3.76\pi^2$ and $3.76\pi^2$ for β values of 0.1, 0.2, 0.3, 0.4 and 0.5 respectively. This results from the density inversion effect, which divides the water into two layers, a stable and potentially unstable layer near the upper and lower boundaries, respectively. Convection can only develop in the lower unstable layer from its time of inception, and the "soft" boundary reduces the rigid upper

boundary constraint. Increasing the thickness of the stable layer continuously reduces the critical Rayleigh number, which however does not go to zero as the thickness of the stable layer tends to infinity, but rather tends to an asymptotic value. It could be concluded, therefore, that the stable layer on the top of the layer has a destabilizing effect (compared to the rigid boundary).

2.1.4 The Preferred Convection Forms

The selected wavenumbers versus Rayleigh number Ra are presented in Fig.2.4 to Fig.2.9, for β values of 0., 0.1, 0.2, 0.3, 0.4 and 0.5 respectively, where the dashed lines are the neutral stability curves, the dotted lines correspond to the points where a maximum heat transfer rate is achieved, and the solid lines represent the preferred wavenumbers. They indicate that there exists a unique convection form which can stand the small curvature constraint and which becomes larger (a smaller) as the convection becomes stronger for fixed β values. This tendency is the same as that observed by Buell and Catton (1986) for a fluid layer of infinite Prandtl number. It should be noted that the preferred convection form is different from the one proposed by Malkus (1954) on the basis of a maximum heat transfer rate, except in the vicinity of the critical point where convection begins. They diverge further as convection becomes stronger.

A rather interesting phenomenon can be seen by comparing Figs.2.4

to 2.9 that the curves of the preferred wavenumber versus Rayleigh numbers move closer and closer to the left boundary of the neutral stability curve as β increases from $\beta = 0$, and finally leave the linear unstable region when $\beta = 0.5$. Also note that the curve passes through the critical point only for cases when β is small. This may be explained from the finite amplitude analysis by expanding the solutions and Rayleigh number in a small amplitude ϵ, for example:

$$Ra = Ra_c + \epsilon R_1 + \epsilon^2 R_2 + O(\epsilon^2) \tag{2.9}$$

where Ra_c is the critical Rayleigh number obtained from the linear stability analysis. One can observe supercritical or subcritical instability, if $R_1 = 0$ with $R_2 > 0$ or $R_2 < 0$, respectively. The subcritical case means that convection can set in even at some subcritical point $Ra = Ra_c + \epsilon^2 R_2 \leq Ra_c$ where an initial disturbance with infinitesimal amplitude would die out according to the linear stability analysis. The present penetrative convection system is subcritical. It was pointed out (Veronis, 1963) that R_2 becomes larger as β is increased. It may be reasonable therefore, to expect that the point of the preferred wavenumber can lie outside the unstable region predicted from the linear stability analysis.

It may be speculated that there exists a nonlinear unstable region which includes the linear unstable region and the subcritical unstable region. It may be possible that the curve of preferred wavenumber would

pass by the nonlinear minimum critical point, but not the linear one, as for cases with small β (Fig.2.4 and Fig.2.5 for $\beta = 0.,\ 0.1, ...$).

Figure 2.10 illustrates the average velocity profiles (average in the horizontal direction) for different β with the selected convection form. Here the Rayleigh number is chosen to be close to the critical Rayleigh number for each case ($Ra \approx Ra_c$). It can be seen that the center of the convection is in a lower position and the velocity increases as β increases while a counter circulation is produced in the upper stable layer when $\beta = 0.5$.

Fig.2.11 and Fig.2.12 show the Nusselt number versus wavenumber for $\beta = 0.3$ and 0, respectively with some different values of Rayleigh number, where the marks square and diamond correspond to the selected wavenumber and the wavenumber with a maximum heat transfer.

Some typical streamline and isotherm patterns are shown in Fig.2.13 and Fig.2.14. In Fig.2.14, there are two circulations in the vertical direction with the upper one much weaker than the lower one. The penetrative phenomenon can be seen by comparing the vertical sizes of the two cells, for $\beta = 0.5$ there. In Fig.2.13, there is only one circulation in the vertical direction since $\beta = 0$ (no stable layer on the top being involved). From these figures, it can also be seen that the convection cells are not symmetric about their center even in the absence of a stable layer on the top, in contrast to the results of the linear density approximation. It is simply due to the nonlinear relationship between density

and temperature of cold water.

2.1.5 Concluding Remarks

From the above discussion it may be concluded that a stable layer on the top of an unstable layer has a destabilizing influence and can lead to subcritical instability. The criterion of small curvature constraint has been successful in uniquely determining the convection form. The preferred wavenumber, which is not the one that yields a maximum heat transfer rate, decreases as Ra is increased, i.e., axisymmetric convection cells become wider (in horizontal size) as buoyancy force is increased.

2.2 Double Diffusive Convection

2.2.1 General Description

In the previous section, only one fluid component was involved, and the instability had its origin only in the temperature gradient. In nature, convective flows often involve more than one fluid component. The thermohaline system is such an example. In this section, attention will be paid to this kind of phenomenon without involving the penetration (linear density approximation for the buoyancy term).

Examples and applications can be found in the areas of geophysical fluid dynamics, oceanography, chemistry, astronomy etc. (Turner, 1974, Chen and Johnson, 1983 and Turner, 1985). For example, layers of 5 meters thick of colder fresher water over lying warm salty water were found underneath a drifting ice island in the Arctic ocean (Neal, Neslyba and Denner 1969, 1971). In oceans, when heated by the sun, water evaporates, causing a layer of salty water forms on the sea surface.

Stern (1960) was the first to consider the case of linear opposing gradients (of two properties) between horizontal boundaries at fixed concentrations, and since then many others, including Gershuni and Zhukhovitskii (1963), Veronis (1965,1968), and Nield (1967) have developed the ideas. Experiments such as the heating from below of a layer of water with a salinity gradient make it clear that a series of diffusive layers

and interface can only be properly explained theoretically using nonlinear theories, as the oscillatory instabilities predicted by linear theory are rapidly swamped by monotonic motion and convective mixing within the layers. Veronis (1965, 1968) has extended the stability calculations into the nonlinear region. Huppert and Moore (1976) tackled the "diffusive" system numerically and found two different solution branches, one oscillatory and one steady. Toomre et al. (1982) have extended Hupper and Moore's (1976) calculation to high Rayleigh numbers and lower diffusivity ratios. All these nonlinear analyses were based on wavenumbers that were not chosen according to any closure equation.

The present section will concentrate on the wavenumber selection for double diffusive convection in a porous layer with an unstable thermal and stable solute stratification for an axisymmetric system.

2.2.2 Governing Equations

Consider a fluid-saturated porous medium contained between two infinite horizontal planes separated by a distance D. The lower plane is kept at constant temperature and constant concentration $T_u + \Delta T$, $S_u + \Delta S$, (ΔT and ΔS are both positive), and the upper plane is kept at T_u, S_u, respectively. According to the Darcy-Boussinesq model, the steady state temperature, solute concentration and velocity fields may be described by

The continuity equation

$$\nabla \cdot V = 0 \tag{2.10}$$

The momentum equation

$$-\nabla P + \rho_0 \left[1 - \lambda_T (T - T_u) + \lambda_s (S - S_u)\right] \mathbf{g} - \frac{\mu}{K}\mathbf{V} = 0 \tag{2.11}$$

The energy equation

$$\nabla \cdot (\mathbf{V}T - \alpha_T \nabla T) = 0 \tag{2.12}$$

The solute concentration equation

$$\nabla \cdot (\mathbf{V}S - \alpha_s \nabla S) = 0 \tag{2.13}$$

For two-dimensional axisymmetric flow, Eq.2.10 to Eq.2.13 may be rewritten in the dimensionless form

$$\frac{\partial}{\partial r}(\varphi_r + \varphi/r) + \frac{\partial^2}{\partial z^2}\varphi + RaT_r - R_s S_r = 0 \tag{2.14}$$

$$T_{rr} + T_{zz} + T_r/r - \varphi_z T_r + [\varphi_r + \varphi/r]T_z = 0 \tag{2.15}$$

$$S_c[S_{rr} + S_{zz} + S_r/r] - \varphi_z S_r + [\varphi_r + \varphi/r]S_z = 0 \tag{2.16}$$

where stream function φ and the following dimensionless scales were used

$$\begin{aligned} \mathbf{V} &= \mathbf{V}^*/(\alpha_T/D) \\ T &= (T^* - T_u)/\Delta T \\ S &= (S^* - S_u)/\Delta S \\ r &= r^*/D \\ z &= z^*/D \end{aligned} \tag{2.17}$$

There are three dimensionless .parameters governing the system, namely the thermal Rayleigh number Ra, the solute Rayleigh number R_s and the Schmidt number S_c, defined as

$$Ra = \frac{\lambda_T g \Delta T K D}{\nu \alpha_T} \tag{2.18}$$

$$R_s = \frac{\lambda_s g \Delta S K D}{\nu \alpha_T} \tag{2.19}$$

and

$$S_c = \frac{\alpha_s}{\alpha_T} \tag{2.20}$$

respectively.

Ra and R_s provide the destabilizing and stabilizing contribution to the system since the temperature gradient and the solute gradient are negative and positive upward, respectively, S_c is a parameter representing the ratio of the solute and thermal diffusivities.

In order to study the effect of the stabilizing influence of the solute concentration and the effect of the diffusivity ratio on the formation of the convection cells, results have been obtained for various values of R_s, and S_c: $R_s = 0.,\ 10,\ 40,\ 80$ and $S_c = 0,\ 10^{-1/2},\ 2^{-1/2},\ 1$. The special case of $R_s = 0$ and $S_c = 1$, is identical to Bénard convection.

The details of the ordered equations and solvability condition and

the related ordinary differential equations are listed in Appendix 2.2. The spectral-finite difference method is used.

2.2.3 Results and Discussion

The selected wavenumbers versus the thermal Rayleigh number Ra are presented in Fig.2.15 and Fig.2.16. The solute Rayleigh number influence is demonstrated in Fig.2.15 with a fixed Schmidt number of $10^{-1/2}$. Comparing the curves (a), (b) and (c) in Fig. 2.15, with $R_s =$ 80, 40 and 10 respectively, it can be seen that the stabilizing parameter R_s makes the preferred convection cell much narrower (as R_s increases), especially in regions where the thermal Rayleigh number Ra is not much higher than the solute Rayleigh number R_s.

The Schmidt number influence on the preferred wavenumber is illustrated in Fig.2.16 with a solute Rayleigh number of 40. It can be seen that as the Schmidt number is increased, i.e. for higher solute diffusivity, the curve of preferred wavenumbers is shifted to the left, resulting in a more elongated flow pattern. This shifting is considerable at thermal Rayleigh numbers Ra a few times larger than the solute Rayleigh number R_s, but becomes negligible when $Ra/Rs > 5$.

These two figures also show that the preferred wavenumber decreases as the thermal Rayleigh number increases, as has been observed in Bénard convection (Buell and Catton, 1986). The tendency of these curves indicates that the influence of the solute Rayleigh number and

the Schmidt number is important only at low thermal Rayleigh numbers as should be expected. Note that in these figures, the curve of preferred wavenumbers for Bénard convection (i.e., in absence of solute concentration) is also drawn for reference.

Fig.2.17 and Fig.2.18 are the thermal Nusselt number Nu^T and "solute Nusselt number" Nu^s versus the thermal Rayleigh number Ra for the preferred convection rolls. They indicate the influences of R_S and S_c on the heat and mass transfer, where the two Nusselt numbers are defined as

$$Nu^T = \frac{1}{a}\int_0^{1/a} \left.\frac{\partial T}{\partial z}\right|_{z=0,or\ z=1} dr \tag{2.21}$$

and

$$Nu^s = \frac{1}{a}\int_0^{1/a} \left.\frac{\partial S}{\partial z}\right|_{z=0,or\ z=1} dr \tag{2.22}$$

respectively. The Nusselt number values at $z = 0$ and $z = 1$ should be equal at the steady state. This is therefore chosen as a criterion to judge the convergence of the solutions.

These figures clearly show that both the heat and mass transfer rates are reduced when the solute Rayleigh number or the Schmidt number increases.

From a linear stability analysis (Nield, 1968), it has been shown that the critical thermal Rayleigh number and corresponding wavenum-

ber are $Ra_c = 4\pi^2 + R_s/S_c$ and π respectively. Subcritical instabilities are possible since steady convection has been obtained at $Ra = 112$, which is much smaller than $Ra_c = 166$ for $R_s = 40$ and $S_c = 10^{-1/2}$. In Bénard convection subcritical instability does not exist and the curve of Rayleigh number versus the preferred wavenumber starts from the critical point of Rayleigh number and wavenumber (Pomeau and Manneville, 1981; Buell and Catton, 1986). In the present study, the curve does not traverse the critical point predicted by the linear stability analysis but seems to originate from a wavenumber significantly greater than the linear critical value π (Fig.2.15 and Fig.2.16); this is most probably due to the subcritical instabilities.

Some typical streamlines, isotherms and iso-concentration lines are presented in Fig.2.19 for $Ra = 120$, $R_s = 40$, and $S_c = 2^{-1/2}$, $10^{-1/2}$, respectively. It can be observed that the boundary layers of the solute concentration become thinner, and the thermal boundary layer is thicker than that of the solute concentration as the Schmidt number becomes smaller. This can be seen from a scale analysis which indicates that the thermal boundary layer thickness δ_T and the solute boundary layer thickness δ_s are related by

$$\frac{\delta_s}{\delta_T} \approx S_c \tag{2.23}$$

It is worth noting that the curves of Nusselt number Nu^T in Fig.2.17 all start at values of Nu^T greater that 1.5. Lower values at lower

Rayleigh numbers could not have been obtained as we had difficulty in getting converged solutions.

2.3 Summary

In this chapter, the phenomena of penetrative and double diffusive convection in an infinite horizontal layer of saturated porous medium have been investigated. It was found that the small curvature constraint can be chosen as an effective criterion to uniquely determine the convection pattern. The stability effect (solute concentration with negative vertical gradient) makes the convection cell narrower, while the destabilizing effect (overlying stable layer) makes the convection cell larger. Both the destabilizing force produced by an overlying stable layer and the stabilizing force resulting from the negative solute gradient are responsible for the subcritical and oscillatory phenomena. These latter subjects definitely deserve further investigation.

CHAPTER III NATURAL CONVECTION WITH PHASE CHANGE IN A BOUNDED POROUS LAYER: THE MELTING OF ICE

3.1 Introduction

Heat transfer with a solid-liquid phase change is a topic of current interest in both fundamental and applied researches as well as in practical applications. Some naturally occurring examples are in the freezing and subsequent breakup of ice in lakes and rivers as well as in the melting of the upper permafrost in the Artic due to a buried pipeline. To this may be added several other problems relevant to the areas of soil and groundwater physics. Numerous technical applications, for example, in thermal energy storage, the design of buried heat exchangers for heat pump applications as well as in the food processing industry also exist.

In this chapter, a study is made of a two phase ice water problem in a bounded layer saturated with a porous medium. In early work, convection in the melt was neglected, and some analytical solutions were obtained such as the classic Stefan solution. However, it has been found that the conduction in the liquid is the dominant mode of heat transfer only at the early stage of melting. Subsequently, the liquid motion becomes stronger and stronger and can significantly influence the heat transfer and the position of the interface (Boger and Westwater, 1967;

Gau, and Viskanta, 1985). The presence of the convective activity complicates analytical studies due to the fact that the moving interface is an unknown transient factor. Most of the available literature concentrates mainly on cylinders and cavities with side heating (Beckman, and Viskanta, 1988; Ho and Chen, 1986; Ho and Viskanta, 1984; Webb and Viskanta, 1986; Bejan, 1989: Jany and Bejan, 1988). Recent literature reviews may be found in the articles of Viskanta (Viskanta, 1983, 1985).

3.2 Governing Equations

The physical system considered here is the melting of ice in a rectangular cavity containing a porous medium as shown in Fig.3.1, the two vertical boundaries being insulated and the other two being kept at constant temperatures T_u and T_f respectively at times less than zero. As $t \geq 0$, their temperatures are changed to T_u and T_b, with T_u and T_b respectively smaller and larger than the fusion temperature T_f.

Using the two dimensional Darcy-Boussinesq approximation, neglecting the volume change during the phase change process, the governing equations can be written as

the continuity equation

$$\nabla \cdot \mathbf{V} = 0 \tag{3.1}$$

the momentum equation

$$\mathbf{V} = \frac{K}{\mu}(-\nabla P + \rho \mathbf{g}) \tag{3.2}$$

the energy equation in the water region

$$\sigma \frac{\partial T^l}{\partial t} + \nabla \cdot \left(\mathbf{V} T^l - \alpha^l \nabla T^l \right) = 0 \tag{3.3}$$

the energy equation in the ice region

$$\sigma \frac{\partial T^s}{\partial t} - \alpha^s \nabla^2 T^s = 0 \tag{3.4}$$

and the energy balance equation at the interface

$$\rho \phi \Delta h_f V_n = -k^l \nabla T^l \cdot \mathbf{n} + k^s \nabla T^s \cdot \mathbf{n} \qquad \text{at} \qquad x^2 = S \tag{3.5}$$

where V_n is the melting velocity of interface in the direction $\mathbf{n}$ normal to the interface.

The nonlinear variation of density in the water layer is given as (Gebhart and Mollendorf, 1977)

$$\rho = \rho_m \left(1 - \lambda |T - T_m|^q \right) \tag{3.6}$$

The dimensionless governing equations can be written as

$$\nabla^2 \varphi + Ra \frac{\partial}{\partial x^1} |T - \beta|^q = 0 \tag{3.7}$$

$$\frac{\partial T^l}{\partial t} + \nabla \cdot \left(\mathbf{V} T^l - \nabla T^l \right) = 0 \qquad 0 \le x^2 \le S \tag{3.8}$$

$$\frac{\partial T^s}{\partial t} - R \nabla^2 T^s = 0 \qquad S \le x^2 \le 1 \tag{3.9}$$

and

$$\frac{\partial S}{\partial t} \mathbf{E_2} \cdot \mathbf{n} = \left(-Ste^l \nabla T^l + Ste^s \nabla T^s \right) \cdot \mathbf{n} \qquad x^2 = S \tag{3.10}$$

where the stream function-vorticity formulation

$$\mathbf{V} = \nabla \times (\varphi \mathbf{E}_3) \tag{3.11}$$

and the dimensional scales

$$\begin{aligned} x^i &= x^{i*}/H \\ S &= S^*/H \\ T^l &= (T^{l*} - T_f)/\Delta T^l \\ T^s &= (T_f - T^{s*})/\Delta T^s \\ \varphi &= \varphi^*/\alpha^l \\ t &= t^*/(\alpha^l \sigma)H^2 \\ \Delta T^l &= T_b - T_f \\ \Delta T^s &= T_f - T_u \end{aligned} \tag{3.12}$$

are used.

The dimensionless parameters are the Rayleigh number (Ra), density inversion parameter β, the diffusivity ratio R, the Stefan numbers in the water (Ste^l) and ice (Ste^s) region, defined as

$$Ra = \frac{\lambda g (\Delta T^l)^q K H}{\nu \alpha^l} \tag{3.13}$$

$$Ste^l = \frac{C_p^l \Delta T^l}{\phi \Delta h_f}, \quad \beta = \frac{T_m - T_f}{\Delta T^l} \tag{3.14}$$

$$Ste^s = \frac{C_p^l \Delta T^s}{\phi \Delta h_f} \left(k^s/k^l\right) \tag{3.15}$$

$$R = \frac{\alpha^s}{\alpha^l} \tag{3.16}$$

As melting proceeds, a moving interface denoted here by $S(x^1, t)$ is formed. Due to the existence of this moving interface, the solid and liquid domains are irregular and time dependent. To avoid this difficulty, a curvilinear system of coordinates is used to transform the physical domain into a rectangular region for the computations. The transformations

$$x^1 = \xi^1, \qquad x^2 = S\xi^2, \qquad t = \tau \tag{3.17}$$

and

$$x^1 = \eta^1, \qquad x^2 = (1 - S)\eta^2 + S, \qquad t = \tau \tag{3.18}$$

transform the two irregular regions into two rectangles,

$$0 \leq \xi^1 \leq XL, \qquad 0 \leq \xi^2 \leq 1 \tag{3.19}$$

and

$$0 \leq \eta^1 \leq XL, \qquad 0 \leq \eta^2 \leq 1 \tag{3.20}$$

respectively. The dimensionless momentum, energy and interface energy balance equations may be written in the curvilinear coordinate system as follows:

In the water region:

$$\frac{\partial}{\partial \tau}\left(J^l T^l\right) + \frac{\partial}{\partial \xi^i}\left[G^{ij}\left(\hat{u}_j T^l - \frac{\partial T^l}{\partial \xi^j}\right)\right] = 0 \tag{3.21}$$

$$\frac{\partial}{\partial \xi^i}\left(G^{ij}\frac{\partial \varphi}{\partial \xi^j}\right) + Ra\frac{\partial}{\partial \xi^i}\left(J^l \xi^i_{x^1} |T^l - \beta|^q\right) = 0 \qquad (3.22)$$

where

$$J^l = \frac{\partial(x^1, x^2)}{\partial(\xi^1, \xi^2)}$$

$$G^{ij} = J^l g^{ij}$$

$$g^{ij} = \frac{1}{J^l} g_{ij}(-1)^{i+j}$$

$$g_{ij} = \frac{\partial x^k}{\partial \xi^i}\frac{\partial x^k}{\partial \xi^j} \qquad (3.23)$$

$$\hat{u}_j = u^k g_{kj} + g_{jk}\xi^k_t$$

$$u^1 = \varphi_{\xi^2}\frac{1}{J^l}$$

$$u^2 = -\varphi_{\xi^1}\frac{1}{J^l}$$

In the ice region:

$$\frac{\partial}{\partial \tau}\left(J^s T^s\right) + \frac{\partial}{\partial \eta^i}\left[\tilde{G}^{ij}\left(\hat{v}_j T^s - R\frac{\partial T^s}{\partial \eta^j}\right)\right] = 0 \qquad (3.24)$$

where

$$J^s = \frac{\partial(x^1, x^2)}{\partial(\eta^1, \eta^2)}$$

$$\tilde{G}^{ij} = J^s \tilde{g}^{ij}$$

$$\tilde{g}^{ij} = \frac{1}{J^s}\tilde{g}_{ij}(-1)^{i+j} \qquad (3.25)$$

$$\tilde{g}_{ij} = \frac{\partial x^k}{\partial \eta^i}\frac{\partial x^k}{\partial \eta^j}$$

$$\hat{v}_j = \tilde{g}_{jk}\eta_t^k$$

A consideration of the energy balance at the interface provides the following equation:

$$\frac{\partial S}{\partial \tau} = -Ste^l \frac{(x^1_{\xi^1})^2 + (x^2_{\xi^1})^2}{x^1_{\xi^1} J^l} \frac{\partial T^l}{\partial \xi^2}\Big|_{\xi^2=1} + Ste^s \frac{(x^1_{\eta^1})^2 + (x^2_{\eta^1})^2}{x^1_{\eta^1} J^s} \frac{\partial T^s}{\partial \eta^2}\Big|_{\eta^2=0} \tag{3.26}$$

The details of the derivation of these equations are given in Appendix 3.1.

The boundary conditions for the dimensionless stream function φ and dimensionless temperatures T^l and T^s are:

$$\begin{aligned} T^l = 1, \quad \varphi = 0, \qquad & at \quad \xi^2 = 0 \\ T^l = \varphi = 0, \qquad & at \quad \xi^2 = 1 \\ T^l_{\xi^1} = \varphi = 0, \qquad & at \quad \xi^1 = 0,\ XL \end{aligned} \tag{3.27}$$

and

$$\begin{aligned} T^s = 0, \qquad & \text{at} \quad \eta^2 = 0 \\ T^s = -1, \qquad & \text{at} \quad \eta^2 = 1 \\ T^s_{\eta^1} = 0, \qquad & \text{at} \quad \eta^1 = 0,\ XL \end{aligned} \tag{3.28}$$

Other parameters are defined in the nomenclature. For a fixed choice of fluid properties, the parameters β and Ste^l are interrelated. In

fact, they both remain functions of the temperature at the lower surface T_b. β although expressed as the ratio of two temperature differences, is in fact the thickness of the upper stable layer divided by the total thickness of the melt, this being the consequence of the linear conduction profile established prior to the onset of convection. Thus a value of $\beta = 0.5$ will fix the value of Ste^l at 0.1674 and implies that the thickness of the upper stable layer occupies 50% of the melt region. Ste^s represents the influence of the steadily maintained temperature at the upper surface. For example, an imposed temperature of -4^oC at the upper surface will give a $Ste^l = 0.3068$ while a temperature of -8^oC will yield a value twice as large or $Ste^s = 0.6136$. The definition of the Rayleigh number Ra is based on the height of the cavity and the temperature difference across the melt. A modified Rayleigh number Ra^e based on the thickness of the lower unstable layer and the temperature difference $T_b - T_m$ across it will be defined and used later.

3.3 Solution Method

As the numerical simulation of the phase change phenomenon is relatively complicated, a detailed description of the method of solution is given in this section, in addition to those given in Chapter I.

In order to initiate the numerical simulation, a very thin layer of melt with a constant thickness S_0 was assumed to be present for simulating the ice melting from below. This initial condition is obtained from

the Stefan solution in the melt and a linear temperature distribution in the ice region. Tests revealed that the influence of S_0 could be neglected as S_0 was sufficiently small (typically, $S_0 = 0.05$ was used in this study).

3.3.1 Discretization

A finite-difference method based on a control volume formulation was used to obtain the numerical solutions. The discretized equations were derived by using a power law interpolation scheme for the spatial discretization and a standard forward difference approximation for the time step. The use of a non-orthogonal coordinate transformation results in the appearance of cross derivative terms which were treated in a special manner so as to deal with instabilities. Denoting the relevant contravariant component of the flux as

$$J^{ij}(\Phi) = G^{ij}\left(\hat{u}_j\Phi - r\frac{\partial\Phi}{\partial\xi^j}\right) \qquad \text{(no summation here)} \qquad (3.29)$$

where Φ can be either T or φ, r equals 1 as Φ represents T^l and φ, and r equals R as Φ represents T^s. The diffusion-convection equation may then be written as

$$\frac{\partial}{\partial t}(J\Phi) + \frac{\partial}{\partial\xi^i}\left(J^{i1}(\Phi) + J^{i2}(\Phi)\right) = 0 \qquad (3.30)$$

Integrating on the control volume as shown in Fig.3.2 yields

$$\frac{J\Phi - J^0\Phi^0}{\Delta t}\Delta x\Delta y\Big|_p + \left[J^{11}(\Phi) + J^{12}(\Phi)\right]\Delta y\Big|_w^e + \left[J^{21}(\Phi) + J^{22}(\Phi)\right]\Delta x\Big|_s^n = 0 \qquad (3.31)$$

where P represents the current point under discussion, E, W, N, S the neighbors of P at the east, west, north and the south, respectively, and e , w, n, s are the mid points of the control volume interface.

The value of J^{ii} are approximated using the power law scheme. For example, the value of the non-cross term J^{11} at point e is approximated using the power law scheme directly as

$$J^{11}(\Phi)\Big|_e = G^{11}\left[(\hat{u}_1 + b_1)\Phi_P - b_1\Phi_E\right]\Big|_e \qquad (3.32)$$

where

$$b_1 = \max\{0,\ -\hat{u}_1\} + \max\left\{0,\ \left(1 - 0.1\left|\frac{\hat{u}_1}{r}\right|\right)^5\right\}\Big|_e \qquad (3.33)$$

Similarly, the term $J^{12}(\Phi)$ at point e may also be represented as

$$J^{12}(\Phi)\Big|_e = G^{12}\left[(\hat{u}_2 + b_2)\Phi_{i+1/2,j-1/2} - b_2\Phi_{i+1/2,j+1/2}\right]\Big|_e \qquad (3.34)$$

where

$$b_2 = \max\{0,\ -\hat{u}_2\} + \max\left\{0,\ \left(1 - 0.1\left|\frac{\hat{u}_2}{r}\right|\right)^5\right\} \qquad (3.35)$$

$\Phi_{i+1/2,\ j-1/2}$ and $\Phi_{i+1/2,\ j+1/2}$ are interpolated as

$$\Phi_{i+1/2,\ j-1/2} = \begin{cases} \frac{1}{2}(\Phi_{i,j} + \Phi_{i+1,j-1}) & \text{if } G^{12} < 0 \\ \frac{1}{2}(\Phi_{i+1,j} + \Phi_{i,j-1}) & \text{if } G^{12} > 0 \end{cases} \tag{3.36}$$

and

$$\Phi_{i+1/2,\ j+1/2} = \begin{cases} \frac{1}{2}(\Phi_{i,j+1} + \Phi_{i+1,j}) & \text{if } G^{12} < 0 \\ \frac{1}{2}(\Phi_{i,j} + \Phi_{i+1,j+1}) & \text{if } G^{12} > 0 \end{cases} \tag{3.37}$$

These interpolations were obtained from geometric arguments. Since

$$G^{12} = -\frac{1}{J} g_{12} = -\frac{1}{J} \mathbf{e}_1 \cdot \mathbf{e}_2 \tag{3.38}$$

$G^{12} < 0$ means that the angle between the directions $\mathbf{e}_1$ and $\mathbf{e}_2$ is smaller than $\pi/2$ and therefore, the position at "$(i + 1/2,\ j - 1/2)$" is closer to the points P and $(i + 1,\ j - 1)$ than to the points S and E. The inverse conclusion may also be made for the positive value of G^{12}. One may show that, the interpolations in Eqs.(3.36) and (3.37) further ensures that the coefficients of the discretized equations

$$a_p \Phi_p = \sum a_{nb} \Phi_{nb} \tag{3.39}$$

usually satisfy the discretizing rules (Patankar, 1980), in order to avoid the instability caused by the cross terms under the non-orthogonal curvilinear coordinate.

3.3.2 Energy Balance Equation at the Interface

The energy balance equation at the interface can be written in a simple form as other variable being treated as known

$$\frac{\partial S}{\partial \tau} = \left[\frac{A}{S} + \frac{B}{1-S}\right]\left[1 + \left(\frac{\partial S}{\partial \xi^1}\right)^2\right] \tag{3.40}$$

under the present curvilinear coordinate, where

$$A = -Ste^l \left.\frac{\partial T^l}{\partial \xi^2}\right|_{\xi^2=1} \tag{3.41}$$

$$B = Ste^s \left.\frac{\partial T^l}{\partial \eta^2}\right|_{\eta^2=0} \tag{3.42}$$

The forward and central difference methods are used to discretize S for the time and space derivatives, respectively. As the temperature is assumed known, the Newton-Raphson iteration is used to solve the discretized equations to obtain the interface position.

3.3.3 Iteration Algorithm

At each time step or iteration, the interface position S was determined from the energy balance equation (Eq.3.40) at the interface. The stream function φ, temperature T^l and T^s were solved using an ADI technique. The position of the interface S was then recalculated using the new φ and T's..., this procedure being repeated until convergent solutions were obtained. Usually, 3 to 10 iterations were needed at

each time step except at some critical points where the convection pattern changed rapidly and more iterations were necessary. In the present study, a 51 by 31 computational grid for each domain was used with a dimensionless time step of about 10^{-2}. The incorporation of the conductive heat transfer in the ice region results in the establishment of a final steady state solution, in contract to the classic Stefan problem where the phase change process continues until the solid is completely melted. The criterion for acceptance of steady solutions being attained is when the difference between the two Nusselt numbers, defined at the top of the ice layer and the bottom of the cavity, differ by less than some predetermined tolerance, typically 1%. However, as will be discussed later, this criterion should be applied with care.

3.4 Results and Discussion

In studies of the phenomenon of melting from below, it has been observed experimentally (Gau and Viskanta, 1985) and predicted analytically (Sparrow and Shamsundar, 1976) that the melt remains motionless at the early stage of melting until an effective Rayleigh Number exceeds some critical value. The initial appearance of convective activity has been generally observed to be of cellular form. The primary characteristics of this problem are the onset of convection, the convective pattern in the melt, the position of the interface and the heat transfer rates at the upper and lower boundaries. This study therefore concentrates on these subjects. The influence of the Rayleigh number Ra, the

temperature ratio β, the Stefan number of the liquid phase Ste^l (which is dependent on the temperature of the lower boundary T_b), the Stefan number Ste^s (dependent on the upper boundary temperature T_u) and the geometry ratio XL on the system will be discussed and illustrated. In the following, it is implied that when the influence of a parameter is being examined, the other parameters are being kept constant.

The numerical experiments performed within the scope of this section are summarized in Table 3.1.

3.4.1 Onset of Convection

The primary parameter influencing the natural convection in a fluid layer heated from below is the Rayleigh number which is usually based on the thickness and the temperature difference within the potentially unstable layer. Ra^e is such a parameter in this section, while the symbol Ra has been reserved (as mentioned earlier) to denote the overall Rayleigh number.

Table 3.2 summarizes, for each experiment, the critical values of the relevant parameters at the onset of convection.

It is instructive to compare the results tabulated in Table 3.2 for experiments 1, 2, 3 and 4. Referring to Table 3.1, the overall Rayleigh number Ra for this series of experiments were respectively 478, 300, 200, and 120 with a constant value for β of 0.2. As expected, increasing the

Rayleigh number results in convection being initiated at an earlier time (lower t_c) with a thinner (dimensionless) melt layer (S_c) at the critical point. It must be noted however, that in this discussion, an increase in the Rayleigh number (due to the manner in which it is defined) implies a larger cavity size, other parameters remaining fixed. A simple calculation indicates that the actual dimensional critical thickness of the melt layer does increase with increasing Rayleigh number, the rate of increase being marked at the lower Rayleigh numbers and tapering off at the higher Ra. One would expect therefore that, at very high Rayleigh numbers, the thickness of the melt at the onset of convection would be virtually independent of the Rayleigh number. This same behavior is exhibited in the series of experiments 7, 8 and 11 which have a β value of 0.5 (Note that in experiment 11, the combination of β and Ra was such that only the pure conduction mode was realized). It is also reasonable to speculate that, as the cavity size increases, the influence of the side walls on the critical point is being reduced due to their physical distance from the bulk of the fluid. If now, the critical Rayleigh number Ra_c^e is computed for the unstable portion of the melt, it appears that this value increases as Ra is increased. This interesting behavior is probably due to the fact that keeping β, Ste^l and Ste^s fixed while increasing Ra amounts to increasing the height H of the cavity as mentioned earlier. Consequently, the loss through the ice layer would be impeded with a resultant increase in the melting rate. Any small disturbance (although supposedly initially amplified exponentially according to linear stability theory) would take a

finite time to manifest itself as an observable phenomenon during which time the interface has continued to move due to melting. The critical Rayleigh number Ra_c^e would thus appear to have increased due to this transient effect.

We now direct our attention to the influence of β on the onset of convection. To this end, it is useful to examine the results of experiments 1, 6, and 11 tabulated in Table 3.2, which have β values of 0.2, 0.4 and 0.5 respectively. These results indicate that as β increases, t_c and S_c also increase, all other quantities being constant. (It should be noted here that changing β while keeping other parameters fixed corresponds to changing both T_b and H). For $\beta = 0.5$, convection is suppressed so that the final steady state is in the pure conduction regime. The bottom temperature is then 8^oC with an overall Rayleigh number of 478 and an effective Rayleigh number Ra^e for the unstable layer of 22.8. This value is not sufficiently large to initiate convection and therefore the only mode of heat transfer is by conduction. Experiments 1 and 6 although performed at the same overall Rayleigh number Ra have descending values of the critical effective Rayleigh number Ra_c^e based on the unstable layer. The upper stable layer or "inversion" has a "softening" effect compared to the "rigid" upper boundary condition as demonstrated by Oguro and Kondo (1970) on the basis of a linear stability analysis.

The results of experiments 1 and 5 indicate that a higher Ste^s (lower T_u) reduces the melting rate as well as the value of the effective critical

Rayleigh number Ra_c^e. Comparing the two values of S_c, it appears that the influence of Ste^s on the onset of convection is not very strong. One explanation may be the fact that in these experiments the melt is relatively very thin compared to the ice region. It may be expected that the influence of the parameter Ste^s on the onset of convection would be more pronounced for the cases where convection sets in with a larger value of S_c.

The influence of the lateral boundary on the onset of convection may be seen in the results of experiments 8, 9 and 10 where $XL = 1,\ 1.1$ and 0.8 respectively. From the results shown in Table 3.2 and Fig.3.8 to Fig.3.10, it appears that convection is developing into a symmetric, nearly square form, but narrower cells arise at higher critical effective Rayleigh number, in agreement with the fact that the lateral boundary has a stabilizing effect, as mentioned by Beck (1972).

In obtaining the results presented here, it was verified that any small disturbance imposed on the system would be attenuated and die away without the inception of convection, provided that the effective Rayleigh number was subcritical. However, if the initial thickness of the melt S_0 was not small enough, convection would be initiated with a cell pattern that was strictly dependent on the form of the initial disturbance.

3.4.2 Evolution of the Flow and Isotherm Pattern

The streamlines and isotherms from some simulations are illustrated

in Fig.3.3 to Fig.3.10. It can be seen that in some of them, the same cell or wave number is preserved from the inception of convection to the final steady state, while in some other cases, evolution of wavenumber with time is evident. For convenience, this effect will be referred to as "convection form transition".

The time evolution of the streamlines and isotherms for experiments 1, 2 and 3, where $Ra = 478$, 300 and 200, respectively are presented in Fig.3.3 to Fig.3.5 which indicate the Ra influence on the convection form. For $Ra = 478$ (Fig.3.3), convection is initiated with six cells, the cells becoming narrower as the melting proceeds. Subsequently, some of them shrink while others grow. Finally, the six cells break down into an irregular pattern of four cells, which do not persist for very long, but are quickly bypassed to arrive at a two cell configuration. The two-cell form then persists for the rest of the melting process with a steady state being attained at $S = 0.8907$. For $Ra = 300$ (Fig.3.4), convection is initiated with a pattern of four cells which persist for a long time and appear to approach a sort of "quasi" steady state. However, convection form transition occurs albeit slowly with a slight freezing in the areas of descending water flow during which a two-cell pattern gradually replaces the four cell form. The two cell form remains for the rest of the melting process with a steady state being obtained with $S = 0.8739$. Finally, at the lowest Rayleigh number $Ra = 200$ (Fig.3.5), convection is initiated with two cells, and there is no convection form transition during the whole melting process, its steady state being approached with an $S =$

0.8284.

In Fig.3.7, where $\beta = 0.4$, a four cell form was initiated and persisted for a long time in a quasi-steady state, subsequently followed by the same freezing phenomenon in areas of descending liquid. A two cell convection form was finally established. Comparison with Fig.3.3 indicates that a higher β slows down the melting rate and retards the convection transition effect. Another interesting feature which may be noted in these two figures is that the convection penetrates into the upper statically stable water layer even at inception, when the thickness of the static stable layer is 1/5 and 2/5 of the total melt thickness in Fig.3.3 and Fig.3.7 respectively.

The influence of Ste^s on the cell pattern can be seen in Fig.3.3 and in Fig.3.6. Fig.3.6 presents the convective history of experiment 5 in which all relevant parameters are the same as in experiment 1 except for Ste^s. The two convection forms are very similar, the only difference being a slight time lag at the early stage of convection. At this time, the melt is much thinner than the ice region so that the influence of the upper temperature on the water region would be small. The convection patterns evolve in different ways as further melting proceeds with a demonstrated dependence on the Ste^s parameter. For $Ste^s = 0.3068$, the convection form transition occurs earlier, quickly passing through an irregular four cell pattern and terminating with a two cell pattern. For $Ste^s = 0.61036$, the initial form persists during a long quasi-steady

period. The convection form transition happens much later with the attendant refreezing phenomenon mentioned earlier. The six cell form is transformed into a four cell pattern and no further transition observed afterwards. Clearly, the Ste^s parameter has an increasing effect on the convection pattern as further melting develops.

It is reasonable to expect that more than one convection form transition may exist if the convective activity in the water layer was enhanced, for example, by increasing Ra, or decreasing β or Ste^s, which would result in more convection cells being initiated at the onset with smaller values for S_c.

The cause and the "preferred" new convection pattern after the convection form transition, are interesting questions. It was predicted by Clever and Busse (1974) and also by Strauss (1974) that a secondary stability problem exists after the onset of convection in the Bénard problem. They pointed out that the two dimensional convection solutions are unstable when the (Ra^e, a) point remains outside their stability envelope. The convection form transition observed in this study may be the result of unstable convection forms being encountered during the melting process. As melting proceeds, the convection cells become narrower and some disturbances sensible to this convection form are encountered. It was checked that the point (Ra^e, a) where convection form transition began to appear is out of Strauss's stability balloon.

As mentioned earlier, the initial convection form appeared to be

strictly dependent on the initial melt thickness S_0 and the initial disturbance if S_0 is not very small. In order to verify if the final steady solutions were still dependent on these initial conditions, some further tests were performed for experiment 8. One such test was to start the simulation with an initial melt of $S_0 = 0.35$ and a disturbance which could initiate a three cell convection pattern. It was observed that convection was initiated with a three cell pattern which was later replaced by a two cell form, and the steady solution was obtained as before. Another test was the simulation of freezing from above. A thin layer of ice and pure conduction in the water layer were used as the initial conditions. A two cell pattern was initiated, which was subsequently replaced by a four cell pattern as the frozen continued, the steady solution obtained being identical to the previous case. It was concluded therefore, that the final steady solutions (the interface position, the convection form and the heat transfer rate) were indeed independent of the initial conditions.

3.4.3 Heat Transfer Rate and Interface Position

The bottom and upper Nusselt numbers are defined as:

$$Nu^b = \frac{1}{XL}\int_0^{XL} T^l_{\xi^2}/S|_{\xi^2=0}\, d\xi^1 \tag{3.43}$$

and

$$Nu^u = Ste^s/Ste^l \frac{1}{XL}\int_0^{XL} T^s_{\eta^2}/(1-S)|_{\eta^2=1}\, d\eta^1 \tag{3.44}$$

respectively.

Fig.3.11 to Fig.3.18 indicate the variation of the average interface position and Nusselt numbers versus time for several experiments. Some sharp jumps may be observed during the melting process, the earliest one corresponding to the point of initiation of convection, while others (if they exist) to the convection form transition. It can be seen that during the time when heat is by conduction only, the interface movement and heat transfer rates proceed smoothly and slowly compared with the transition period, which correspond to the onset of convection and to a convection form transition. These periods are accompanied by a sharp increase in both the interface movement and in the heat transfer rates. It appears that the convection form transition to a new cell pattern occurs in order to augment the heat transfer rate, i.e. to transfer heat more efficiently.

The influence of β, Ste^s, XL on the heat transfer rate and interface position can be seen in Fig.3.13 to Fig.3.18, respectively. Higher β, Ste^s, and lower XL have stabilizing effects, they reduce the heat transfer rates, slow down the interface movement, and postpone or even eliminate the convection form transition.

Figure 3.11 and Fig.3.13 indicate two types of convection form transition. One occurs at a time when the two Nusselt numbers are very different, the other one at a time long after an apparent steady state is approached. It was observed that slight refreezing in certain regions

of the water layer exists before and during a convection form transition of the second type but is absent during the evolution of the first type. (Fig.3.4, Fig.3.6, Fig.3.7, Fig.3.12, especially Fig.3.7 and Fig.3.12).

The convergence of the two Nusselt numbers can not, therefore, be used as a unique criterion to determine the approach to the final steady solution. Other aspects such as whether the cells have the same size and shape or the position of the (Ra^e, a) point with respect to Strauss's stability envelope will have to be considered simultaneously with the convergence of the two Nusselt numbers in order to ascertain if a true steady state has been reached.

Finally, results at the steady state using only the pure conduction mode, and with convection are presented in Table 3.3 to show the overall effects of convection on the interface position and the heat transfer rates.

3.5 Concluding Remarks

The melting of ice in a rectangular cavity filled with a porous medium and heated from below has been investigated numerically. By increasing the bottom temperature,or reducing the upper temperature, convection is initiated earlier. The initial convection pattern may pass through many intermediate stages in its transition to a final steady state. A special "quasi" steady state in which refreezing occurs in parts of the water layer were noted, this quasi steady state being eventually destroyed

to be replaced by a new convection pattern. The convection form transition results in an abrupt increase of interface movement and heat transfer rates. This transition effect may arise from an instability in the narrow convection cells and results in a new convection pattern which exhibits a local maximum in the heat transfer rate at the lower (heated) boundary.

Table 3.1 Definition of Investigated Problems

experiment	β	Ste^l	Ste^s	XL	Ra
1	0.2	0.4184	0.306825	1.	478.
2	0.2	0.4184	0.306825	1.	300.
3	0.2	0.4184	0.306825	1.	200.
4	0.2	0.4184	0.306825	1.	120.
5	0.2	0.4184	0.61370	1.	478.
6	0.4	0.2092	0.306825	1.	478.
7	0.5	0.1674	0.306825	1.	900.
8	0.5	0.1674	0.306825	1.	700.
9	0.5	0.1674	0.306825	1.1	700.
10	0.5	0.1674	0.306825	0.8	700.
11	0.5	0.1674	0.306825	1.	478.

Table 3.2 Critical Values at the Onset of Convection

experiment	S_c	t_c	Ra_c^e	cell number	a
1	0.2000	0.0628	50.10	6	0.8334
2	0.3000	0.1563	47.17	4	0.8333
3	0.4426	0.4188	46.40	2	1.1297
4	0.5648	2.8000	35.56	2	0.8853
5	0.1930	0.0700	48.36	6	0.8635
6	0.3659	0.7500	39.84	4	0.6832
7	0.3127	0.7800	42.32	6	0.5330
8	0.3502	2.1250	32.96	4	0.7139
9	0.3486	1.8125	32.81	4	0.7172
10	0.3534	2.8125	33.26	4	0.7074
11		$+\inf$		0	

Table 3.3 Steady State Solution Obtained with and without Convection

experiment	$S_{cond.}$	$S_{conv.}$	$Nu_{cond.}$	$Nu_{conv.}$	S_{min}	S_{max}
1	0.5769	0.8449	1.7333	5.5100	0.6886	0.8907
2	0.5769	0.8184	1.7333	4.4370	0.7273	0.8739
3	0.5769	0.7673	1.7333	3.4830	0.6887	0.8284
5	0.4054	0.7220	2.4667	5.3740	0.6794	0.7465
6	0.4054	0.5897	2.4667	3.680	0.5225	0.6471
8	0.3530	0.4650	2.8329	3.4170	0.4603	0.4678
9	0.3530	0.4739	2.8329	3.486	0.4647	0.4778
10	0.3530	0.4177	2.8329	3.184	0.4164	0.4191
11	0.3530	0.3530	2.8329	2.8329	0.3530	0.3530

CHAPTER IV CONCLUSION

This thesis is comprised of three interrelated studies, each of which have been described in the previous chapters that include the principal results obtained together with a summary of the work accomplished.

The present chapter is devoted to a general overview of the research proposed, and to the description of some topics warranting further investigation.

The basic thrust of this research was to investigate the possibility of obtaining solutions to a certain class of thermoconvective problems using a set of auxiliary constraint equations to form a closed system. Specifically, the Darcy-Boussinesq equations together with the Pomeau-Manneville closure equation were chosen to investigate three important aspects of natural convection in porous media, namely, convection in a double layer, double component convection and mixed phase convection, respectively.

Whether all these three problems will arise simultaneously will depend on the situation under consideration. As an example, during the freezing/melting process of a layer of soil saturated with saltwater, one has to deal with all of them while in the cooling of a plate of (pure) steamed rice, none of these phenomena are present. From the study of penetrative convection and double diffusive convection, it was found

that the preferred convection pattern can be the one that would be excluded (i.e. considered as impossible) by a linear stability analysis as its wavenumber actually lies outside the neutral stability curve. This somewhat unexpected result is due to the fact that penetrative and double diffusive convection can be both subcritically unstable.

In a double layer, the critical Rayleigh number predicted by linear stability theory is based on the static thickness of the potentially unstable layer. As a finite amplitude perturbation is imposed on the system, the effective thickness of the unstable layer becomes actually greater as a result of penetration of hot fluid into the stable layer, resulting in an effective Rayleigh number that is higher than the nominal (originally defined) one, thus leading to the subcritical instability phenomenon. A similar interpretation can be given to double diffusive systems where a finite amplitude perturbation can reduce the solute inhomogeneity by the effect of convective mixing.

Besides subcritical instabilities, a double layer is more unstable than a single layer (having the same unstable thickness), and the curve of Rayleigh number versus preferred wavenumber is shifted towards the left as the thickness of the stable layer is increased. In other words, the preferred convection cell is more elongated in a double layer than in a single one. Of course, there is a limit corresponding to the case of a semi-infinite stable layer overlying an unstable layer.

In the case of double component systems, two additional parameters

enter into play: the solute Rayleigh number and the Schmidt number. The present study has considered the case of a negative solute gradient that has a stabilizing effect on the thermal buoyancy-driven flow. By increasing the concentration gradient, the preferred wavenumber is increased and the convection cells become narrower. The inverse effect was obtained by increasing the solute diffusivity.

In the melting process, convection starts to play an important role as the melt thickness attained a certain value corresponding to the critical Rayleigh number for the onset of convection. The newly formed convection cells appear to have a nearly square form. As melting continues, these cells become more slender, and suddenly break up sequentially. The transition period (i.e. duration of the breaking process) is quite short, but is followed by a very long (i.e. quasi-steady) period. The final steady state (which in fact exists when the upper boundary is maintained at a temperature below the melting point) is sometimes difficult to attain as it can be preceded by very long quasi-steady states. This phenomenon is reflected in the evolution of the heat transfer rate: The curve of Nusselt number versus time exhibits a jump each time a convection cell disappears. It is therefore reasonable to conclude that the new convection pattern is formed to augment the heat transfer, in agreement with the principle of maximum heat transfer proposed by Malkus. This change in the convection pattern may be interpreted with reference to the stability theory of Busse: As melting continues, the convection cells become narrower and narrower until a point is reached where they be-

come unstable with respect to a certain kind of perturbation and cannot survive. This is in fact the point at which increasing wavenumber crosses threshold to fall outside Busse's stability balloon. Moreover, during the transition from one flow pattern to another, the inverse phenomenon of refreezing was sometimes observed together with a decrease in the heat transfer rate.

A final remark should be made concerning the specific melting of ice: Here the melt is comprised of a stable layer of cold water (below 4^oC) lying between the ice surface and an unstable layer of warmer water (above 4^oC). As a consequence, if the lower surface is maintained at a temperature below 4^oC, no convection would occur. The presence of a stable layer adjacent to the ice surface also greatly reduces the heat transfer, and thereby the melting rate, when the heated surface is maintained at temperatures below 10^oC. Furthermore, the cold stable water at the ice surface also attenuates the effect of the impinging flow rising from the unstable layer. Thus the water-ice interface, when heated from below, is less wavy than when heated from above.

It appears appropriate now to consider the perspective of some future studies.

Firstly, it appears from Chapter I that the concept of small curvature can lead to a closure equation capable of predicting a unique convection pattern. The interesting question is then to relate the preferred wavenumber-Rayleigh number curve to Busse's stability balloon.

Secondly, as subcritical instabilities have been observed in both penetrative and double diffusive convection, there remains the question of how to determine the lower bounds for subcritical Rayleigh numbers, and to obtain a kind of nonlinear neutral stability curve. This task may best be done by numerical analyses using spectral methods on a fast computer.

Besides steady state solutions, oscillatory regimes also arise in both penetrative and double diffusive convection, for small as well as large values of some governing parameter. This type of flow should be investigated with a high accuracy numerical method.

In Chapter III, the melting process has been considered in a bounded layer to focus attention on the moving solid-liquid interface. There remains the case of melting in an unbounded layer. The prediction of the flow pattern is a challenging task requiring a great effort in both mathematical and numerical modelling.

The melting in the presence of double diffusion is also an interesting but as yet untouched problem.

Finally, even in the simplest case without penetration or double diffusion, the practical task of constructing a unified correlation for the heat transfer rate still requires a considerable amount of work. Analytical, numerical and dimensional analyses should be coordinated in solving this type of problem.

In retrospect, it might be concluded that this research project has opened more questions than it has solved. But, after all, is not that the best motivation for a venture of this kind?

REFERENCES

Baines, P.G. and Gill, A.E., (1969), "On Thermohaline Convection with Linear Gradients", J. Fluid Mech., 37, 289-306.

Beck, J.E., (1972), "Convection in a Box of Porous Material Saturated with Fluid", The Physics of Fluids, 15(8), 1377-1383.

Beckman, C., and Viskanta., (1988), "Natural Convection Solid/Liquid Phase Change in Porous Media", Int. J. Heat Mass Transfer, 31(1), 35-46.

Bejan, A., (1985), "Convection Heat Transfer", A Wiley-Interscience Publication, John Wiley & Sons.

Bejan, A., (1987), "The Basic Scales of Natural Convection Heat and Mass Transfer in Fluid and Fluid-Saturated Porous Media," Int. Comm. Heat Mass Transfer, Vol.14, pp. 107-123.

Bejan, A., (1989), "Theory of Melting with Natural Convection in an Enclosed Porous Medium", J. Heat Transfer, Vol.111, 407-415.

Boger, D.V. and Westwater, J.W., (1967), "Effect of Buoyancy on the Melting and Freezing Process", J. Heat Transfer, Vol. 89, 81-89.

Bénard, H., 1900, Rev. Gen. Sci. Pur. Appl., 12, 1261-1309.

Buell, J.C. and Catton, I., (1986), "Wavenumber Selection in Large-Amplitude Axisymmetric Convection," Phys. Fluids, 29(1), 23-33.

Busse, F.H., (1967), "On the Stability of Two-Dimensional Convection in a Layer Heated from Below", J. Math. & Phys., 46, 140-149.

Busse, F.H., (1969), "On Howard's Upper Bound for Heat Transport by Turbulent Convection", J. Fluid Mech., 37, 457-477.

Busse, F.H., (1978), "Nonlinear Properties of Thermal Convection," Rep. Progr. Phys., 41, 1929-1967.

Catton, I. and Buell, J.C., (1986), "The Wavenumber at Supercritical Rayleigh Numbers," In "Stability in Convective Flows", HTD. 54, 17-29, Ed. W.S.Saric and A.A.Szewczyk.

Chandrasekhar, S., (1961), "Hydrodynamic and Hydromagnetic Stability," Oxford: Clarendon.

Chen, C.F. and Johnson, D.H., 1984, "Double-Diffusive Convection: A Report on an Engineering Foundation Conference," J. Fluid Mech., 138, 405-416.

Chen, M.M. and Whitehead, J.A., 1968, "Evolution of Two-Dimen sional Periodic Rayleigh Convection Cells of Arbitrary Wave-Number", J.Fluid Mech., 31, 1-15.

Cheng, P., (1979). "Heat Transfer in Geothermal System," Adv. Heat Transfer, Vol.14, 1-105.

Clever, R.M, and Busse, F.H., (1974), "Transition to Time-Dependent Convection", J. Fluid Mech., Vol. 65(4), 625-645.

Darcy, H., (1856), "Les Fontaines Publiques de la Ville de Dijon", Damont, Paris.

Gau, C. and Viskanta, R., (1985), "Effect of Natural Convection on Solidification from Above and Melting from Below of a Pure Metal", Int. J. Heat Mass Transfer, Vol. 28, 573-587.

Gebhart, B. and Mollendorf, J., (1977), "A New Density Relation for Pure and Saline Water", Deep-Sea Research, Vol. 124, 831-848.

Georgiadis, J.G. and Catton, I., (1986), "Prandtl Number Effect on Bénard Convection in Porous Media," J. Heat Transfer, Vol.108, pp. 284-290.

Gershuni, G.Z. and Zhukhovitskii, E.M., (1963), J. Appl. Math. Mech., 27, 441-452.

Glansdorff, P., and Prigogine, I., (1971), "Thermodynamic Theory of Structure, Stability and Fluctuations," Wiley-Interscience, New York.

Goren, S., 1966, "On Free Convection in Water at 4^oC", Chem. Engeg. Sci., 21, 515-518.

Howard, L.N., (1963), "Heat Transport by Turbulent Convection", J. Fluid Mech., 17, 405-412.

Ho, C.J., and Chen, S., (1986), "Numerical Simulation of Melting of Ice around a Horizontal Cylinder", Int. J. Heat Mass Transfer, 29(9), 1359-1369.

Ho, C.J., and Viskanta, R., (1984), "Heat Transfer during Melting from an Isothermal Vertical Wall", J. Heat Transfer, 106, 12-19.

Huppert, H.E. and Moore, D.R., (1976), "Non-Linear Double-Diffusive Convection", J. Fluid Mech., 78, 821-854.

Jany, P. and Bejan, A., (1988), "The Scales of Melting in the Presence of Natural Convection in a Rectangular Cavity Filled with Porous Medium", J. Heat Transfer, Vol. 110, 526-529.

Jonsson, T., (1984), "Natural Convection in Porous Media: Prandtl Number Effects," M.S. thesis, Dept. of Engrg., UCLA, Los Angeles.

Koschmieder, E.L. and Pallas, S.G., 1974, "Heat Transfer through a Shallow Horizontal Convecting Fluid Layer", Int.J.Heat Mass Transfer, 17, 991-1002.

Landau, L.D., (1944), "On the Problem of Turbulence", Doklady, 44, 339. (papers of the Academy of Science of the USSR).

Malkus, W.V.R., (1954), "The Heat Transport and Spectrum of Thermal Turbulence", Proceedings of the Royal Society, 225, l85, Series A.

Malkus, W.V.R., and Veronis, G., (1958), "Finite Amplitude Cellular Convection," J. Fluid Mech., Vol.4, pp. 225-260.

McDonough, J.M. and Catton, I., 1982, "Accuracy of the Mean Field Approximation and Physical Effect of Prandtl Number in Bénard Convection", Phys. Fluid, 25(9), 1502-1505.

Moore, D.R. and Weiss, N.D., 1973, "Nonlinear Penetrative Convection", J. Fluid Mech., 61, 553-581.

Neal, V.T., Neshbya, S. and Denner, W., (1969), Science 166, 373-374.

Neshyba, S., Neal, V.T. and Denner, W., (1971), J. Geophys. Res. 76, 8117-81120.

Nield, D.A., (1967), J. Fluid Mech., 29, 545-558.

Nield, D.A., (1968), "Onset of Thermohaline Convection in a Porous Medium," Water Resources Research, 4(3), 553-560.

Nield, D.A., and Joseph, D.D., (1985), "Effects of Quadratic Drag on Convection in a Saturated Porous Medium," Phys. Fluids, Vol.28(3), pp. 995-997.

Ogura, Y., and Kondo, H., (1970), "A Linear Stability of Convective Motion in a Thermally Unstable Layer below a Stable Region", J. Meteorological Society of Japan, Vol. 48(3), 204-215.

Patankar, S.V., (1980), "Numerical Heat Transfer and Fluid Flow," Hemisphere, New York.

Pellew, A. and Southwell, R.V., 1940, "On Maintained Convection Motion in a Fluid Heated from Below", Proc.R.Soc.A., 176, 312-343.

Pomeau, Y. and Croquette, V., 1984, "Dislocation Motion: A Wavenumber Selection Mechanism in Rayleigh-Bénard Convection", J. Physique, 45, 35-48.

Pomeau, Y. and Manneville, P., (1981), "Wavelength Selection in Axisymmetric Cellular Structure," J. Phys., 42, 1067-1074.

Poulikakos, D., (1985), "A Departure from the Darcy Model in Boundary Layer Natural Convection in a Vertical Porous Layer with Uniform Heat Flux from the Side ," J. Heat Transfer, Vol.107, pp. 716-720.

Poulikakos, D., and Bejan, A., (1985), "The Departure from the Darcy Flow in Natural Convection in a Vertical Porous Layer," Phys. Fluids, Vol.28(12), pp. 3477-3483.

Prasad, V., and Tuntomo, A., (1987), "Inertia Effects on Natural Convection in a Vertical Porous Cavity," Num. Heat Transfer, Vol.11, pp. 295-320.

Rudraiah, P.K., Srimani, P.K. and Friedrich, R., (1982), "Finite Amplitude Convection in a Two-Component Fluid Saturated Porous Layer," Int. J. Heat Mass Transfer, 25(5), 715-722.

Schluter, A., Lortz, D. and Busse, F., 1965, "On the Stability of Steady Finite Amplitude Convection", J. Fluid Mech., 23, 129-144.

Segel, L.A., (1966), "Non-linear Hydrodynamic Stability Theory and Its Applications to Thermal Convection and Curved Flows," In Non-Equilibrium Thermodynamics, Variational Techniques and Stability. Ed. by R.J.Donnelly, R.Herman and I.Prigogine, University of Chicago Press.

Somerton, C.W., McDonough, J.M., and Catton, I., (1983), "Natural Convection in Porous Media: A Mixed Finite Difference-Galerkin Solution with Wavenumber Prediction," Proc. VII Int. Heat Transfer Conference, Hemisphere, New York, 1983, Vol.2, pp. 347-350.

Sparrow, E.M., and Shamsundar, N., (1976), "Convective Stability in a Melting Layer Heated from Below", J. Heat Transfer, Vol. 98, 88-94.

Stern, M.E., (1960), "The 'Salt Fountain' and Thermohaline Convection", Tellus, 12, 172-175.

Strauss, J.M., (1974), "Large Amplitude Convection in a Porous Media", J.Fluid Mech., 64, 51-63.

Tien, C.L. and Hong, J.T., (1985), "Natural Convection in Porous Media under Non-Darcian and Non-Uniform Permeability Conditions", In "Natural Convection", Fundamentals and Applications, Ed. by Kakaç, S., Aung, W. and Viskanta, R., Hemisphere Publishing Corporation.

Toore, J., Gough, D.O. and Spiegel, E.A., (1982), "Time-Dependent Solutions of Multimode Convection Equations", J. Fluid Mech., 125, 99-122.

Trevisan, O.V. and Bejan, A., (1985), "Natural Convection with Combined Heat and Mass Transfer Buoyancy Effects in a Porous Medium," Int. J. Heat Mass Transfer, 28, 1597-1611.

Trevisan, O.V. and Bejan, A., (1986), "Mass and Heat Transfer by Natural Convection in a Vertical Slot Filled with Porous Medium," Int. J. Heat Mass Transfer, 29(3), 403-415.

Trevisan, O.V. and Bejan, A., (1987), "Mass and Heat Transfer by High Rayleigh Number Convection in a Porous Medium Heated from Below," Int. J. Heat Mass Transfer, 30, 2341-2356.

Turner, J.S., (1974), "Double-Diffusive Phenomena," Ann. Rev. Fluid Mech., 6:37-56.

Turner, J.S., (1985), "Multicomponent Convection," Ann. Rev. Fluid Mech., 17, 11-44.

Vafai, K., and Tien, C.L., (1981), "Boundary and Inertia Effects on Flow and Heat Transfer in Porous Media," Int. J. Heat Mass Transfer, Vol.24, pp. 195-203.

Veronis, G., (1963), "Penetrative Convection", Astrophy. J., 137, 641-663.

Veronis, G., (1965), "On Finite Amplitude Instability in Thermohaline Convection", J. Mar. Res. 23, 1-17.

Veronis, G., (1968), "Effect of a Stabilizing Gradient of Solute on Thermal Convection", J. Fluid Mech., 34, 315-336.

Viskanta, R., (1983), "Phase Change Heat Transfer", in " Solar Heat Storage: Latent Material", Vol. 1, Edited by Lane, G. A..

Viskanta, R., (1985), "Natural Convection in Melting and Solidification", in "Natural Convection: Fundamentals and Applications", Edited by Kakaç, S., Aung, W., and Viskanta, R..

Wang, M. and Bejan, A., (1987), "Heat Transfer Correlation for Bénard Convection in a Fluid Saturated Porous Layer", Int. Comm. Heat Mass Transfer. Vol. 14, 617-626.

Webb, B.W., and Viskanta, R., (1986), "Analysis of Heat Transfer during Melting of a Pure Metal from an Isothermal Vertical Wall", Num. Heat Transfer, 9, 539-558.

Willis, G.E., Deardorff, J.W. and Somerville, R.C.J., 1972, "Roll-Diameter Dependence in Rayleigh Convection and Its Effect upon the Heat Flux", J.Fluid Mech., 54, 351-367.

Zhang, X., Nguyen,T.H., Kahawita,R., and Pu,W.,(1987), "Spectral and Spectral-Finite Difference Methods in Wavenumber Prediction of Penetrative Convection." Proceedings of 5th Intern. Conf. on Numerical Methods in Thermal Problems, Montréal, Québec, Part I, 773.

Zhang, X., Nguyen,T.H., and Kahawita,R., (1987), "Wavenumber Selection in Axisymmetric Penetrative Convection." Proceedings of CANCAM, Vol.2, C-50, Edmonton, Alberta.

Zhang, X., Nguyen,T.H., and Kahawita,R., (1987), "Formation des Cellules de Convection dans une Couche d'Eau à Basse Température." Recueil des Résumés de Communications, Les Annuales de L'Association Canadienne-Française pour L'Avancement des Sciences, Ottawa, Ontario, Vol.55, 162.

Zhang, X., Nguyen,T.H., and Kahawita,R., (1987), "Selection of Cell Size in Axisymmetric Penetrative Convection," Premiére Conférence Internationale sur les Mathématiques Appliquées et Industrielles, Paris.

Zhang X., Nguyen,T.H., and Kahawita,R., (1988), "Non-Darcy Effect on Bénard Convection in Porous Medium." Intern. Symp. on Convection in Porous Medium: Nondarcy Effects, 25th National Heat Transfer Conf., Houston, Texas.

Zhang, X., Nguyen,T.H., and Kahawita,R., (1988), "Wavenumber Selection of Double-Diffusive Convective Flow in a Porous Medium," Proceedings of the ASME International Computer in Engineering, Conference Exhibition, Aug.1-Aug.3, 1988, San Francisco, California.

Zhang, X, Nguyen. T.H., and Kahawita, R., (1989) "Numerical Simulation of Ice Melting from Below in a Cavity Saturated with a Porous Medium," Proceedings of CANCAM, 1989, Vol. 1, 112, Ottawa.

Zhang, X., Nguyen, T.H., and Kahawita,R., (1989), "Melting of Ice Heated from Below in a Porous Medium", submitted to Int. J. Heat and Mass Transfer.

Zhang, X., Nguyen, T.H., and Kahawita,R., (1989), "Melting of Ice in an Inclined Porous Layer", to be submitted to Int. J. Heat and Mass Transfer.

Appendix 1.1 Detailed Equations for Nondarcy Fluid

The zeroth order equations:

$$\frac{\partial}{\partial r}\left(\varphi_r^0(1+\tau_m|\mathbf{V^0}|)+Ra_m T^0\right)+\frac{\partial}{\partial z}\left(\varphi_z^0(1+\tau_m|\mathbf{V^0}|)\right)=0$$

$$\frac{\partial}{\partial r}\left(\varphi_z^0 T^0-T_r^0\right)+\frac{\partial}{\partial z}\left(-\varphi_r^0 T^0-T_z^0\right)=0$$

The first order equations

$$[(1+\tau_m f_1)\varphi_r^1+\tau_m f_3\varphi_z^1]_r+[(1+\tau_m f_2)\varphi_z^1+\tau_m f_3\varphi_r^1]_z+Ra_m T_r^1$$
$$=-\tau_m[(f_1\varphi^0)_r+(f_3\varphi^0)_z]-\varphi_r^0$$
$$[\varphi_z^0 T^1-T_r^1]_r+[-\varphi_r^0 T^1-T_z^1]_z+\varphi_z^1 T_r^0-\varphi_r^1 T_z^0=\varphi^0 T_z^0+T_r^0$$

The adjoint equation

$$\frac{\partial}{\partial r}\left((1+\tau_m f_1)F_r+\tau_m f_3 F_z-GT_z^0+G\right)+$$
$$\frac{\partial}{\partial z}\left((1+\tau_m f_2)F_z+\tau_m f_3 F_r+GT_r^0\right)=0$$
$$\frac{\partial}{\partial r}\left(-\varphi_z^0 G-G_r+Ra_m F\right)+\frac{\partial}{\partial z}\left(\varphi_r^0 G-G_z\right)=0$$

Solvability condition

$$f(a)=\int_0^{1/a}\int_0^1 -F[\varphi_r^0+\tau_m(f_3\varphi^0)_z+\tau_m(f_2\varphi^0)_r]$$
$$+G[T_r^0+\varphi^0 T_z^0]\,dz\,dr$$

where f_1, f_2 and f_3 are defined as follows:

$$f_1 = |\mathbf{V}^0|(1 + v^2/|\mathbf{V}^0|^2)$$

$$f_2 = |\mathbf{V}^0|(1 + u^2/|\mathbf{V}^0|^2)$$

$$f_3 = -uv/|\mathbf{V}^0|$$

Appendix 2.1 Detailed Equations for Penetrative Convection

Zero-th Order Equation

$$\varphi^0_{rr} + \varphi^0_{zz} + Ra(T^0 + 1 - z - \beta)T^0_r = 0$$

$$T_{rr} + T_{zz} - \varphi^0_z T^0_r + \varphi^0_r (T^0_z - 1) = 0$$

First Order Equations:

$$\varphi^1_{rr} + \varphi^1_{zz} + Ra(T^0 + 1 - z - \beta)T^1_r + RaT^1 T^0_r + \varphi^0_r = 0$$

$$\begin{aligned} T^1_{rr} + T^1_{zz} - \varphi^0_z T^1_r + \varphi^0_r T^1_z + \varphi^0 (T^0_z - 1) \\ - \varphi^1_z T^0_r + \varphi^1_r (T^0_z - 1) + T^0_r = 0 \end{aligned}$$

Adjoint Equations

$$F_{rr} + F_{zz} + T^0_r G_z - (T^0_z - 1)G_r = 0$$

$$G_{rr} + G_{zz} + \varphi^0_z G_r - \varphi^0_r G_z - Ra(T^0 + 1 - z - \beta)F_r = 0$$

Solvability Condition

$$f(a) = \int_{-1/a}^{1/a} \int_0^1 [F\varphi^0_r + G(T^0_r + \varphi^0 T^0_z - \varphi^0)\, dzdr$$

The Related Ordinary Differential Equations

The Zero-th Order

$$\varphi_k^{(2)} - a_{k-1}^2 \varphi_k - Ra(1-z-\beta)a_{k-1}T_k -$$
$$\frac{1}{2}\left[F1(N_f, Ng, a, k, i, T, T) - F3(N_f, Ng, a, k, i, T, T)\right] = 0$$

$$T_k^{(2)} - a_{k-1}^2 T_k + a_{k-1}\varphi_k +$$

$$\frac{1}{2}\begin{bmatrix} -F1(N_f, Ng, a, k, i, D\varphi, T) + F2(N_f, Ng, a, k, i, D\varphi, T) \\ +F1(N_f, Ng, a, k, i, DT, \varphi) + F2(N_f, Ng, a, k, i, DT, \varphi) \end{bmatrix} = 0$$

The Adjoint Equations

$$F_k^{(2)} - a_{k-1}^2 F_k + a_{k-1}G_k -$$

$$\frac{1}{2}\begin{bmatrix} -F1(N_f, Ng, a, k, i, DG, T) + F2(N_f, Ng, a, k, i, DG, T) \\ +F1(N_f, Ng, a, k, i, DT, G) + F2(N_f, Ng, a, k, i, DT, G) \end{bmatrix} = 0$$

$$G_k^{(2)} - a_{k-1}^2 G_k + a_{k-1}Ra(1-z-\beta)F_k -$$

$$\frac{1}{2}\begin{bmatrix} -RaF1(N_f, Ng, a, k, i, T, F) + RaF3(N_f, Ng, a, k, i, T, F) \\ -F1(N_f, Ng, a, k, i, D\varphi, G) - F3(N_f, Ng, a, k, i, D\varphi, G) \\ +F1(N_f, Ng, a, k, i, DG, \varphi) + F3(N_f, Ng, a, k, i, DG, \varphi) \end{bmatrix} = 0$$

Solvability Condition

$$f(a) = \int_0^1 u(z)\, dz = 0$$

where

$$u(z) = \sum_{k=1}^{N_f} (a_{k-1}\varphi_k F_k - \varphi_k G_k - a_{k-1} T_k G_k) +$$
$$\frac{1}{2} \sum_{k=1}^{N_f} G_k \left\{ \sum_{m=1}^{k} \varphi_{k-m+1} T_m^{(1)} + \sum_{m=1}^{N_f-k-1} \left(\varphi_{k+m-1} T_m^{(1)} - \varphi_m T_{k+m-1}^{(1)} \right) \right\}$$

Functions F1, F2 and F3

$$F1(N1, N2, a, k, i, P, G) = \sum_{m=1}^{k} a_{m-1} P_{k-m+1,i} G_{m,i}$$

$$F2(N1, N2, a, k, i, P, G)$$

$$= \sum_{m=1}^{N1-k+1} a_{m-1} P_{k+m-1,i} G_{m,i} + a_{k+m-2} P_{m,i} G_{k+m-1,i}$$

$$F3(N1, N2, a, k, i, P, G)$$

$$= \sum_{m=1}^{N1-k+1} a_{m-1} P_{k+m-1,i} G_{m,i} - a_{k+m-2} P_{m,i} G_{k+m-1,i}$$

where $N1$, $N2$, k, i are integers, $k \leq N1$, $i \leq N2$ and P and G are matrices of order $N1 * N2$, and

$$D\varphi = \frac{d\varphi}{dz}$$

$$T_m^{(i)} = \frac{d^i T_m}{dz^i} \quad i = 1,\ 2$$

Appendix 2.2 The Detailed Equations for Double Diffusion Convection

The zero-th order equations:

$$\varphi^0_{rr} + \varphi^0_{zz} + RaT^0_r - R_s S^0_r = 0$$

$$T^0_{rr} + T^0_{zz} - \varphi^0_z T^0_r + \varphi^0_r (T^0_z - 1) = 0$$

$$S_c(S^0_{rr} + S^0_{zz}) - \varphi^0_z S^0_r + \varphi^0_r (S^0_z - 1) = 0$$

The first order equations

$$\varphi^1_{rr} + \varphi^1_{zz} + RaT^1_r - R_s S^1_r = -\varphi^0_r$$

$$(\varphi^0_z T^1 - T^1_r)_r + (-\varphi^0_r T^1 - T^1_z)_z + \varphi^1_z T^0_r - \varphi^1_r (T^0_z - 1) = \varphi^0 (T^0_z - 1) + T^0_r$$

$$(\varphi^0_z S^1 - S_c S^1_r)_r + (-\varphi^0_r S^1 - S_c S^1_z)_z + \varphi^1_z S^0_r - \varphi^1_r (S^0_z - 1) = \varphi^0 (S^0_z - 1) + S_c S^0_r$$

Adjoint equation

$$F_{rr} + F_{zz} - \left[G(T^0_z - 1)\right]_r + \left[GT^0_r\right]_z - \left[H(S^0_z - 1)\right]_r + \left[HS^0_r\right]_z = 0$$

$$(-\varphi^0_z G - G_r)_r + (\varphi^0_r G - G_z)_z - RaF_r = 0$$

$$(-\varphi^0_z H - S_c H_r)_r + (\varphi^0_r H - S_c H_z)_z + R_s F_r = 0$$

Solvability condition

$$f(a) = \int_0^{1/a} \int_0^1 [F\varphi^0_r + G(T^0_r + \varphi^0 T^0_z - \varphi^0)$$

$$+ H(S_c S^0_r + \varphi^0 S^0_z - \varphi^0)] dz dr$$

The Related Ordinary Differential Equations

The Zero-th Order

$$\varphi_k^{(2)} - a_{k-1}^2 \varphi_k - a_{k-1}(RaT_k - R_s S_k) = 0$$

$$T_k^{(2)} - a_{k-1}^2 T_k + a_{k-1}\varphi_k +$$

$$\frac{1}{2}\begin{bmatrix} -F1(N_f, Ng, a, k, i, D\varphi, T) + F2(N_f, Ng, a, k, i, D\varphi, T) \\ +F1(N_f, Ng, a, k, i, DT, \varphi) + F2(N_f, Ng, a, k, i, DT, \varphi) \end{bmatrix} = 0$$

$$S_c\left(S_k^{(2)} - a_{k-1}^2 S_k\right) + a_{k-1}\varphi_k +$$

$$\frac{1}{2}\begin{bmatrix} -F1(N_f, Ng, a, k, i, D\varphi, S) + F2(N_f, Ng, a, k, i, D\varphi, S) \\ +F1(N_f, Ng, a, k, i, DS, \varphi) + F2(N_f, Ng, a, k, i, DS, \varphi) \end{bmatrix} = 0$$

The Adjoint Equations

$$F_k^{(2)} - a_{k-1}^2 F_k + a_{k-1} G_k -$$

$$\frac{1}{2}\begin{bmatrix} -F1(N_f, Ng, a, k, i, DG, T) + F2(N_f, Ng, a, k, i, DG, T) \\ +F1(N_f, Ng, a, k, i, DT, G) + F2(N_f, Ng, a, k, i, DT, G) \\ -F1(N_f, Ng, a, k, i, DH, S) + F2(N_f, Ng, a, k, i, DH, S) \\ +F1(N_f, Ng, a, k, i, DS, H) + F2(N_f, Ng, a, k, i, DS, H) \end{bmatrix} = 0$$

$$G_k^{(2)} - a_{k-1}^2 G_k + a_{k-1} Ra F_k -$$

$$\frac{1}{2}\begin{bmatrix} -F1(N_f, Ng, a, k, i, D\varphi, G) - F3(N_f, Ng, a, k, i, D\varphi, G) \\ +F1(N_f, Ng, a, k, i, DG, \varphi) + F3(N_f, Ng, a, k, i, DG, \varphi) \end{bmatrix} = 0$$

$$S_c\left(H_k^{(2)} - a_{k-1}^2 H_k\right) - a_{k-1} R_s H_k +$$

$$\frac{1}{2}\begin{bmatrix} -F1(N_f, Ng, a, k, i, D\varphi, H) - F3(N_f, Ng, a, k, i, D\varphi, H) \\ +F1(N_f, Ng, a, k, i, DH, \varphi) + F3(N_f, Ng, a, k, i, DH, \varphi) \end{bmatrix} = 0$$

Sovlability Condition

$$f(a) = \int_0^1 u(z)\, dz = 0$$

where

$$u(z) = \sum_{k=1}^{N_f} (a_{k-1}\varphi_k F_k - \varphi_k G_k - a_{k-1} T_k G_k - \varphi_k H_k - S_c a_{k-1} S_k H_k) +$$
$$\frac{1}{2}\sum_{k=1}^{N_f} G_k \left\{ \sum_{m=1}^{k} \varphi_{k-m+1} T_m^{(1)} + \sum_{m=1}^{N_f y-k-1} \left(\varphi_{k+m-1} T_m^{(1)} - \varphi_m T_{k+m-1}^{(1)}\right) \right\} +$$
$$\frac{1}{2}\sum_{k=1}^{N_f} H_k \left\{ \sum_{m=1}^{k} \varphi_{k-m+1} S_m^{(1)} + \sum_{m=1}^{N_f y-k-1} \left(\varphi_{k+m-1} S_m^{(1)} - \varphi_m S_{k+m-1}^{(1)}\right) \right\}$$

where $F1$, $F2$ and $F3$ are defined as in Appendix 2.1.

Appendix 3.1 Details of the Energy Balance Equation at the Interface in Curvilinear Coordinates

The interface position in the Cartician coordinate is expressed as

$$\mathbf{r} = \mathbf{E}_1 x^1 + \mathbf{E}_2 S$$

The normal vector $\mathbf{n}$ of the interface can be expressed as

$$\mathbf{n} = \frac{\mathbf{e}^2}{|\mathbf{e}^2|} \qquad \text{at} \qquad x^2 = S$$

The interface moving velocity in the direction $\mathbf{n}$ is

$$V_n = \frac{\partial S}{\partial t}\mathbf{E}_2 \cdot \mathbf{n} = \frac{\partial \xi^k}{\partial x^2}\mathbf{e}_k \cdot \mathbf{e}^2/|\mathbf{e}^2|\frac{\partial S}{\partial t}$$

$$= \frac{\partial \xi^2}{\partial x^2}/|\mathbf{e}^2|\frac{\partial S}{\partial t}$$

The flux terms under the curvilinear coordinate can be written as

$$\nabla T^l \cdot \mathbf{n} = \mathbf{e}^i \nabla_i T^l \cdot \mathbf{e}^2/|\mathbf{e}^2|$$

$$= \mathbf{e}_j g^{ij} \nabla_i T^l \cdot \mathbf{e}^2/|\mathbf{e}^2|$$

$$= g^{22} \nabla_2 T^l/|\mathbf{e}^2|$$

and

$$\nabla T^s \cdot \mathbf{n} = \tilde{\mathbf{e}}^i \nabla_i T^s \cdot \mathbf{e}^2 / |\mathbf{e}^2|$$

$$= \tilde{\mathbf{e}}_2 \tilde{g}^{i2} \nabla_i T^s \cdot \mathbf{e}^2 / |\mathbf{e}^2|$$

$$= \tilde{g}^{22} \frac{\partial T^s}{\partial \eta^2} \frac{\partial \xi^k}{\partial \eta^2} \mathbf{e}_k \cdot \mathbf{e}^2 / |\mathbf{e}^2|$$

$$= \tilde{g}^{22} \frac{\partial T^s}{\partial \eta^2} \frac{\partial \xi^2}{\partial \eta^2} / |\mathbf{e}^2|$$

where $\tilde{\mathbf{e}}_1 = \mathbf{e}_1$ at the interface and $\mathbf{e}_1 \cdot \mathbf{e}^2 = 0$ are used, and because

$$\frac{\partial \xi^2}{\partial \eta^2} \frac{\partial x^2}{\partial \xi^2} = \frac{\partial x^2}{\partial \eta^2}$$

the energy balance equation at the interface under the present curvilinear coordinate is expressed as

$$\frac{\partial S}{\partial \tau} = -Ste^l \; g^{22} \nabla_2 T^l \frac{\partial x^2}{\partial \xi^2} + Ste^s \; \tilde{g}^{22} \nabla_2 T^s \frac{\partial x^2}{\partial \eta^2}$$

$$= -Ste^l \frac{(x^1_{\xi^1})^2 + (x^2_{\xi^1})^2}{x^1_{\xi^1} J^l} \frac{\partial T^l}{\partial \xi^2}\Big|_{\xi^2=1} + Ste^s \frac{(x^1_{\eta^1})^2 + (x^2_{\eta^1})^2}{x^1_{\eta^1} J^s} \frac{\partial T^s}{\partial \eta^2}\Big|_{\eta^2=0}$$

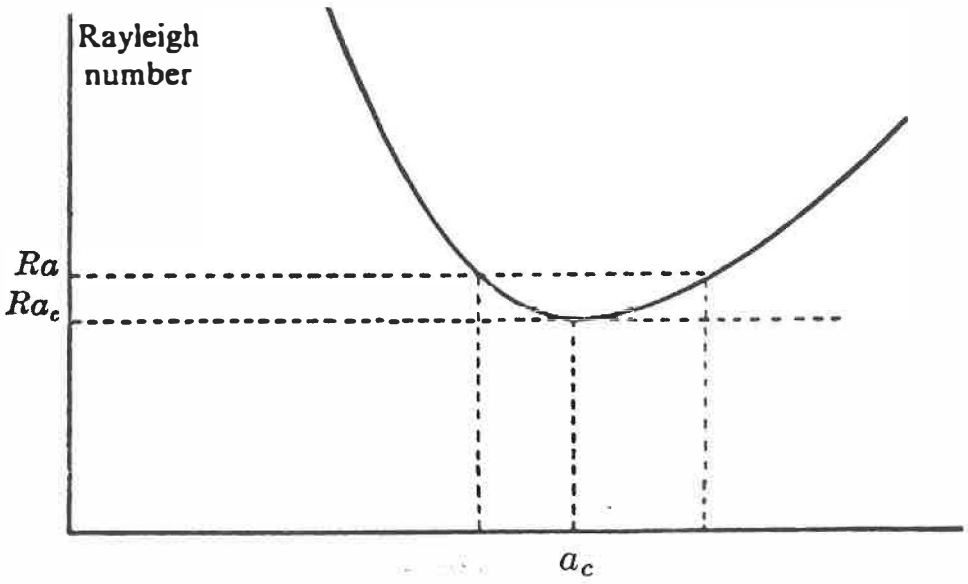

Fig.1.1 Neutral Stability Curve

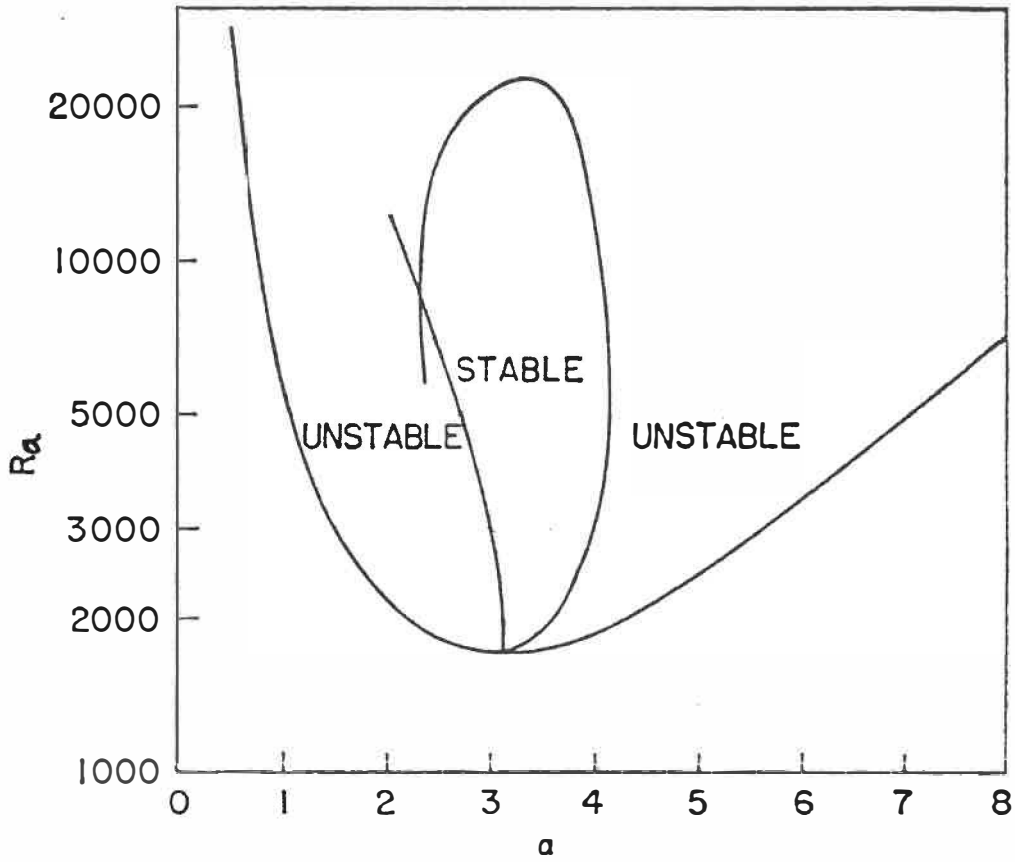

Fig.1.2 Busse's Stability Region

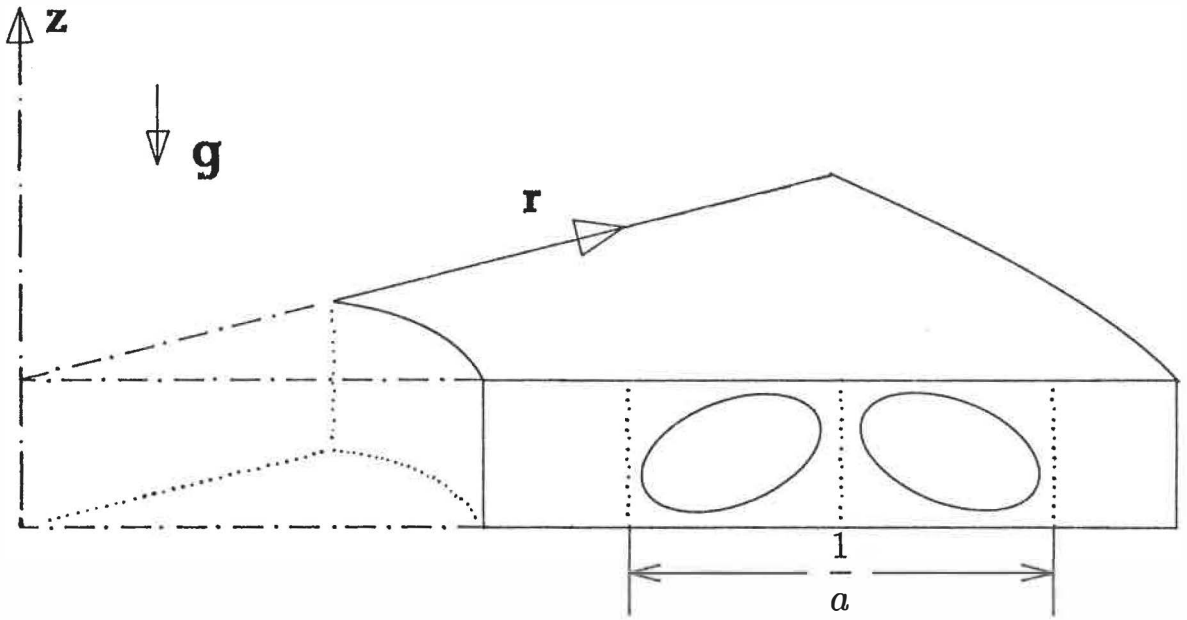

Fig.1.3 Axisymmetric Geometry

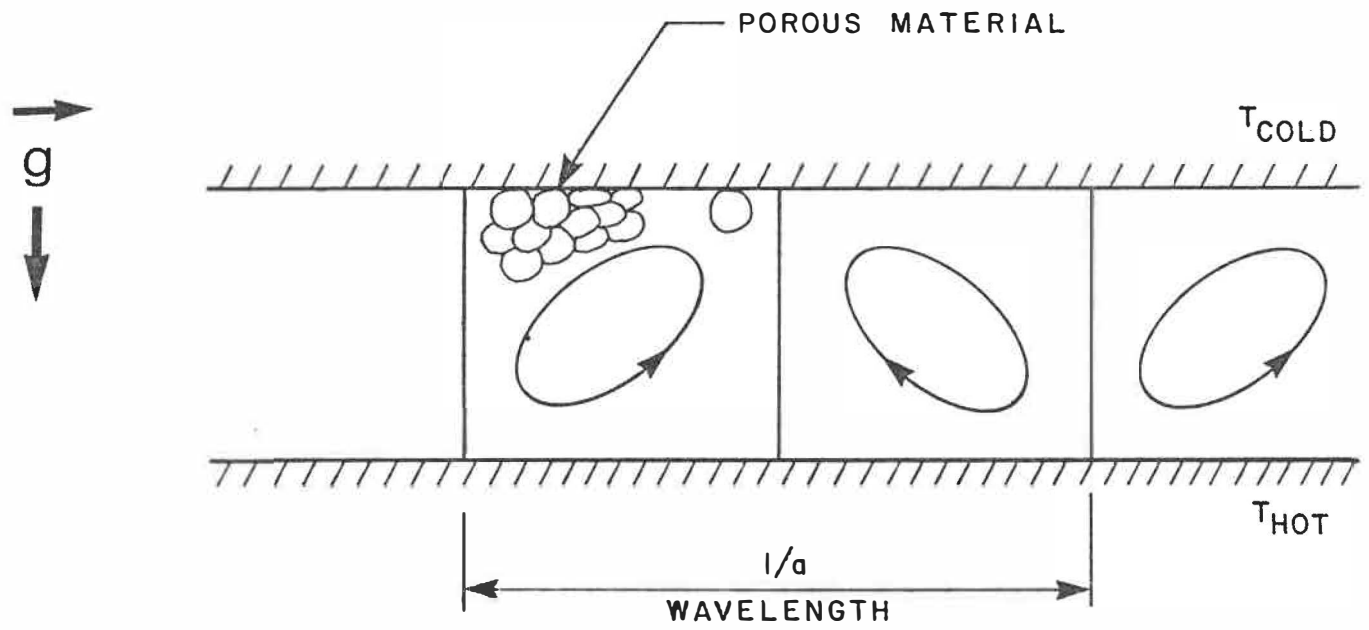

Fig.1.4 Bénard convection in a porous layer

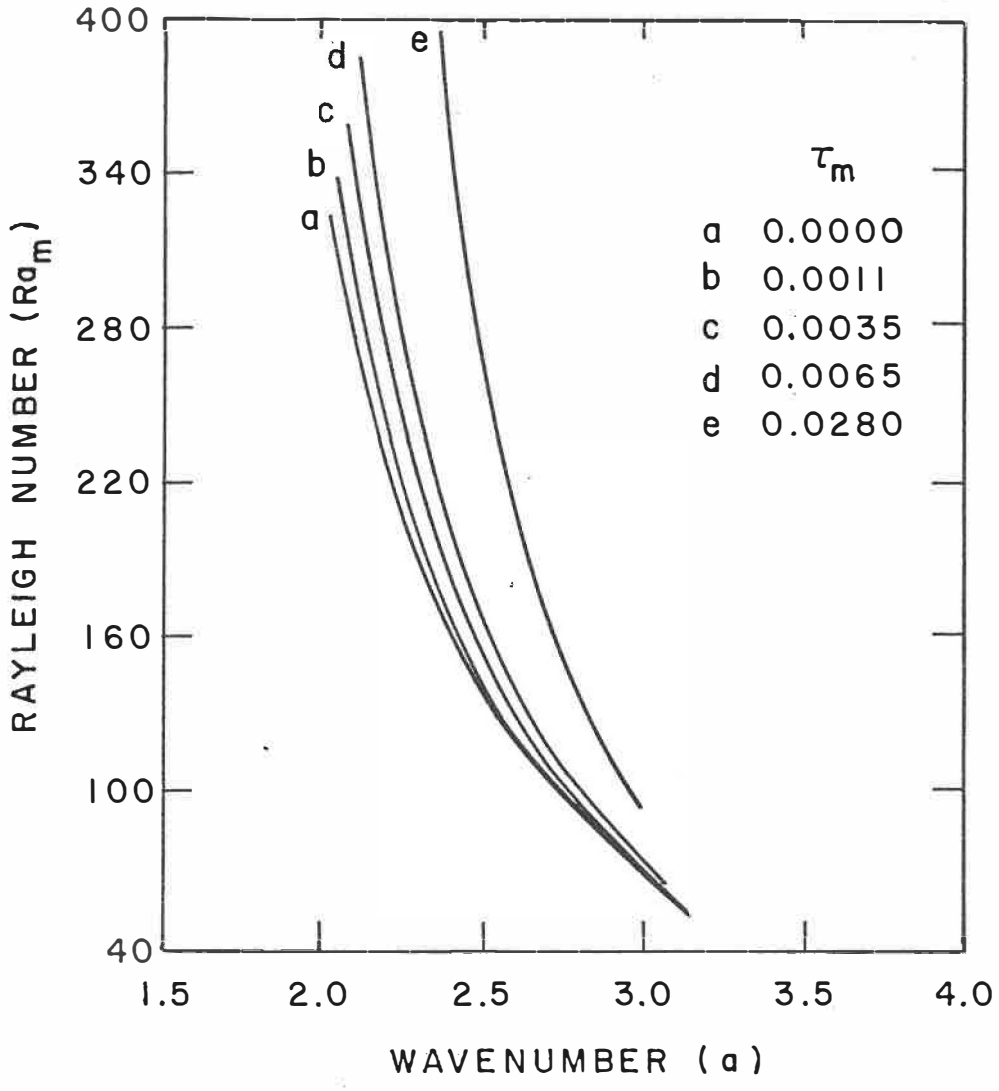

Fig.1.5 Preferred wavenumbers versus Ra_m with different τ_m

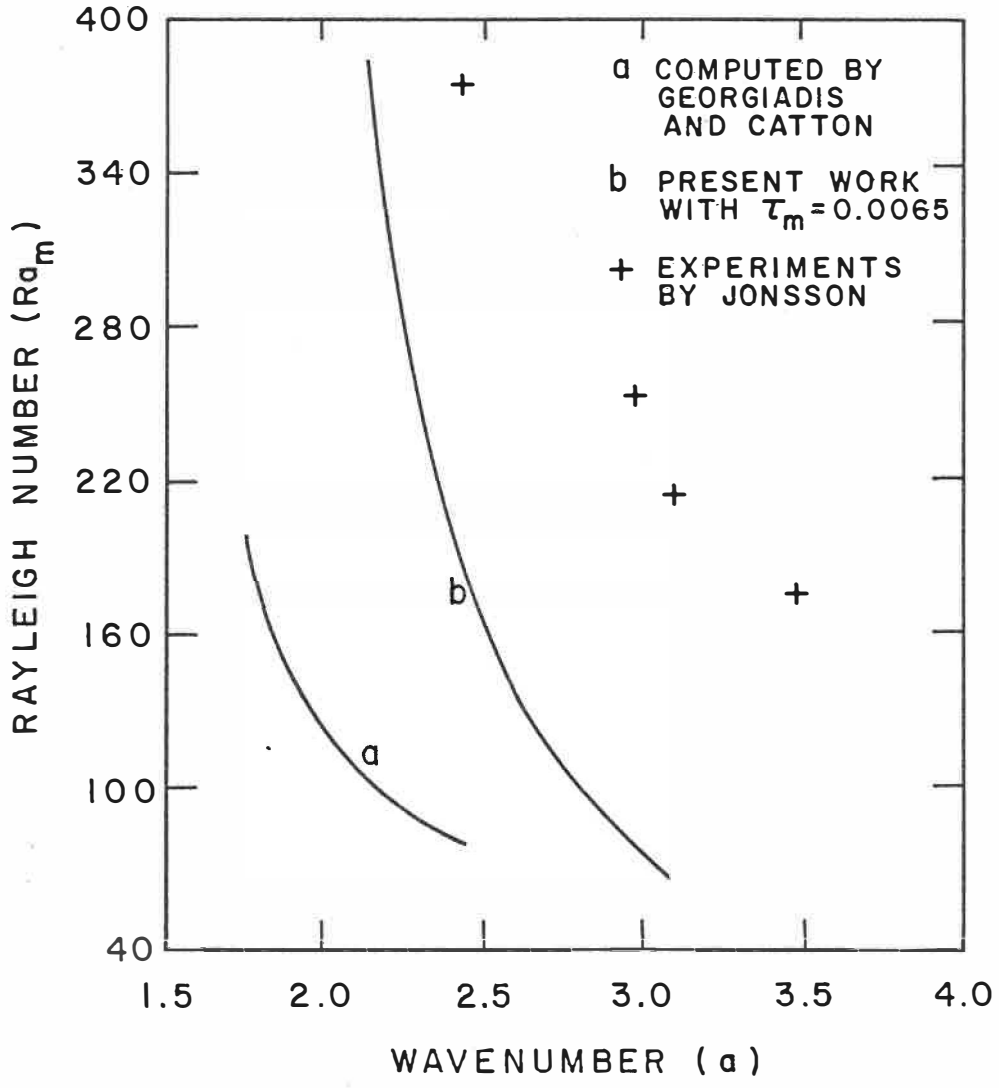

Fig.1.6 Comparison of present results with previous work

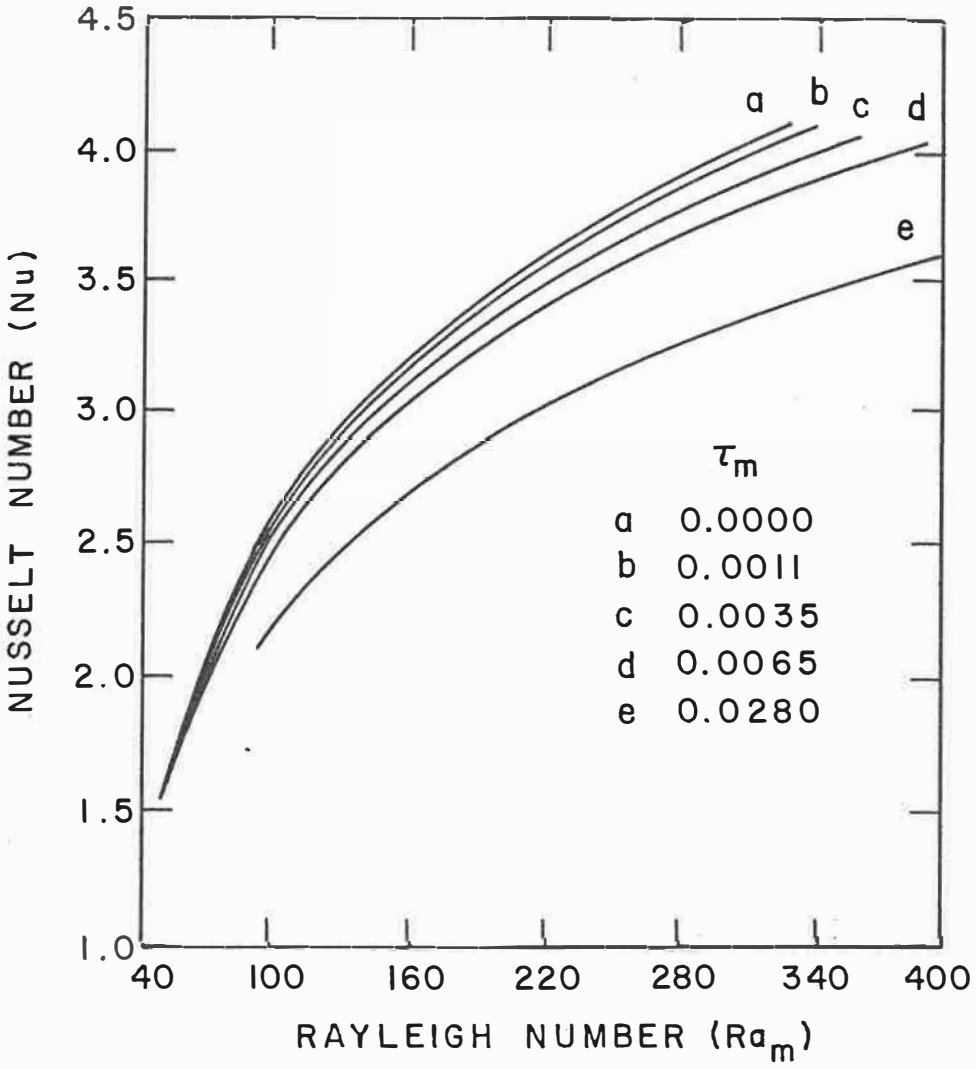

Fig.1.7 Nusselt number versus Ra_m with different τ_m

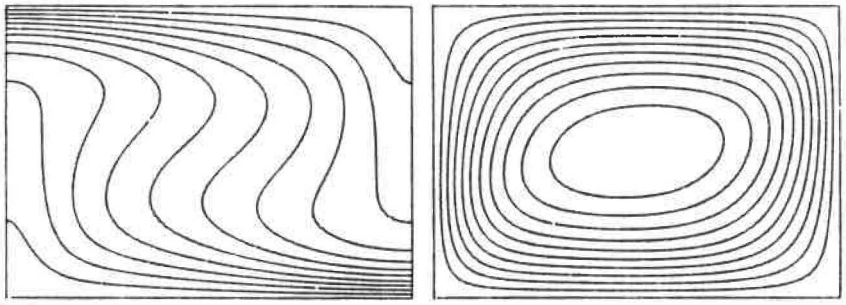

a

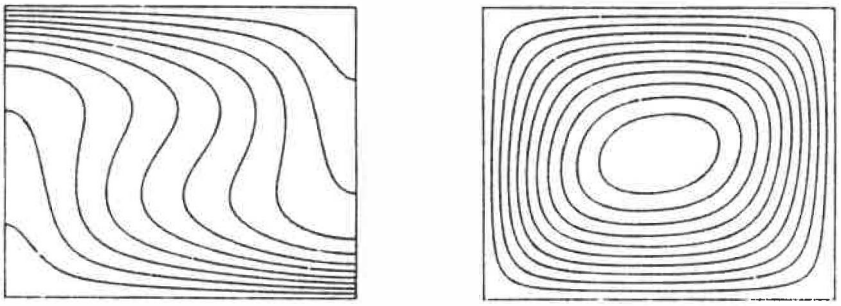

b

Fig.1.8 Streamline pattern and isotherm (non-Darcy fluid)

a: $Ra_m = 200, \tau_m = 0.000$
b: $Ra_m = 200, \tau_m = 0.028$

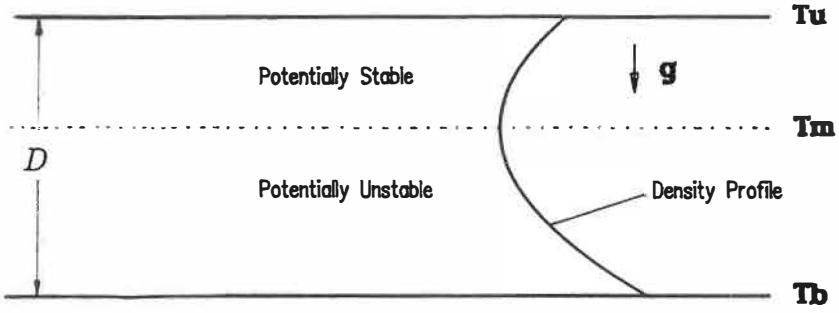

Fig.2.1 Definition Sketch of Penetrative Convection

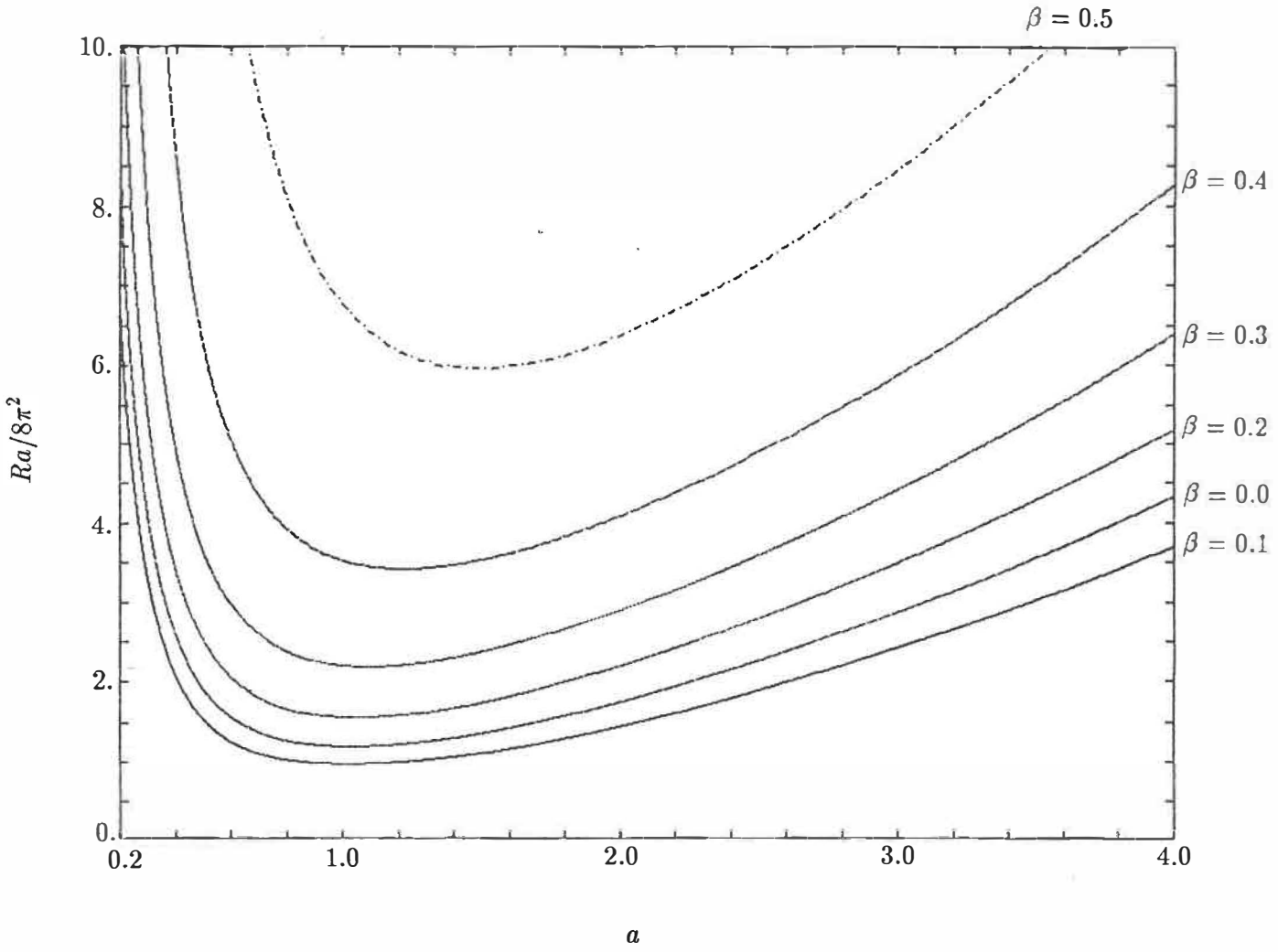

Fig.2.2 Results from the linear analysis (with penetration)

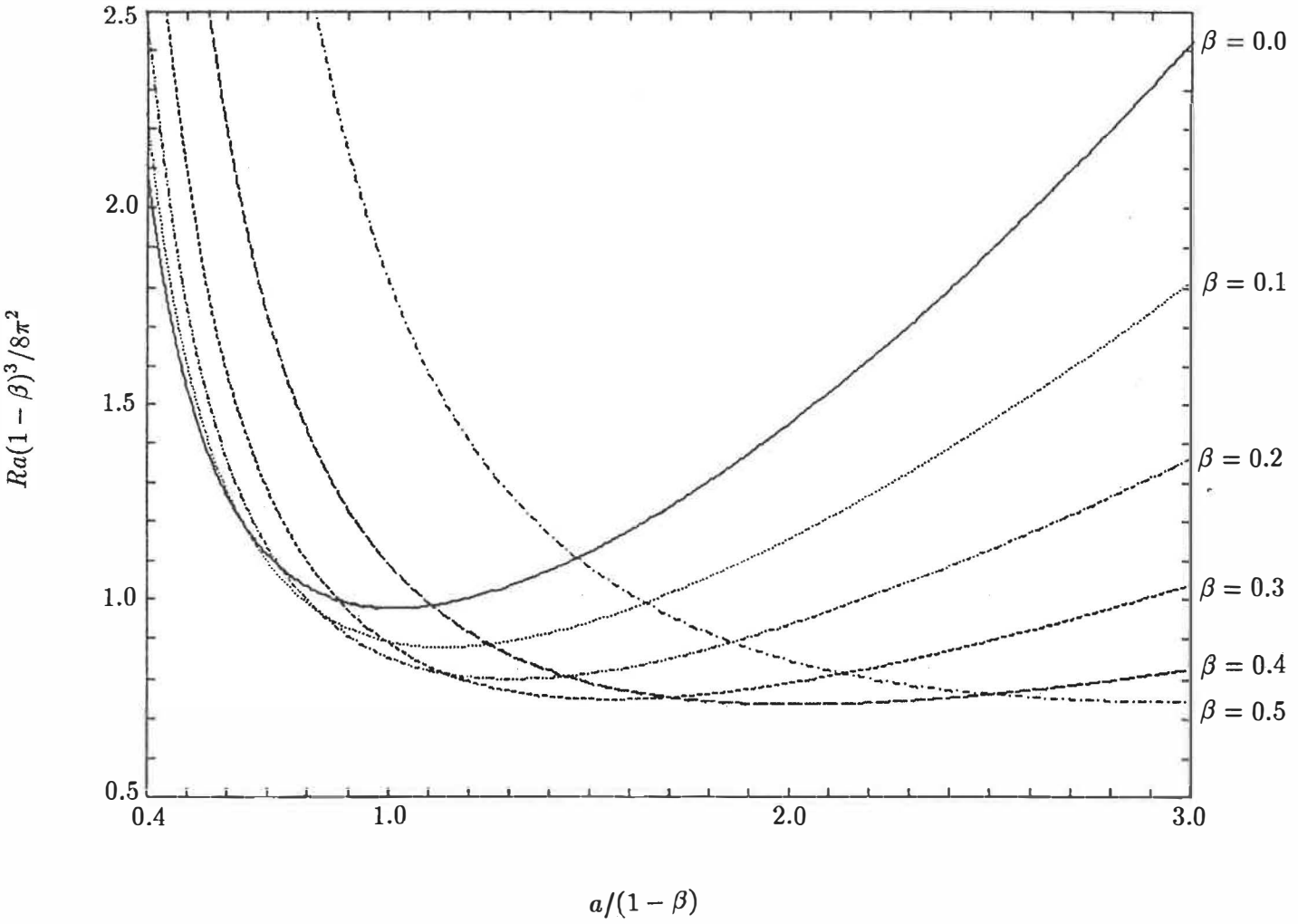

Fig.2.3 Results from the linear analysis using the modified Ra (with penetration)

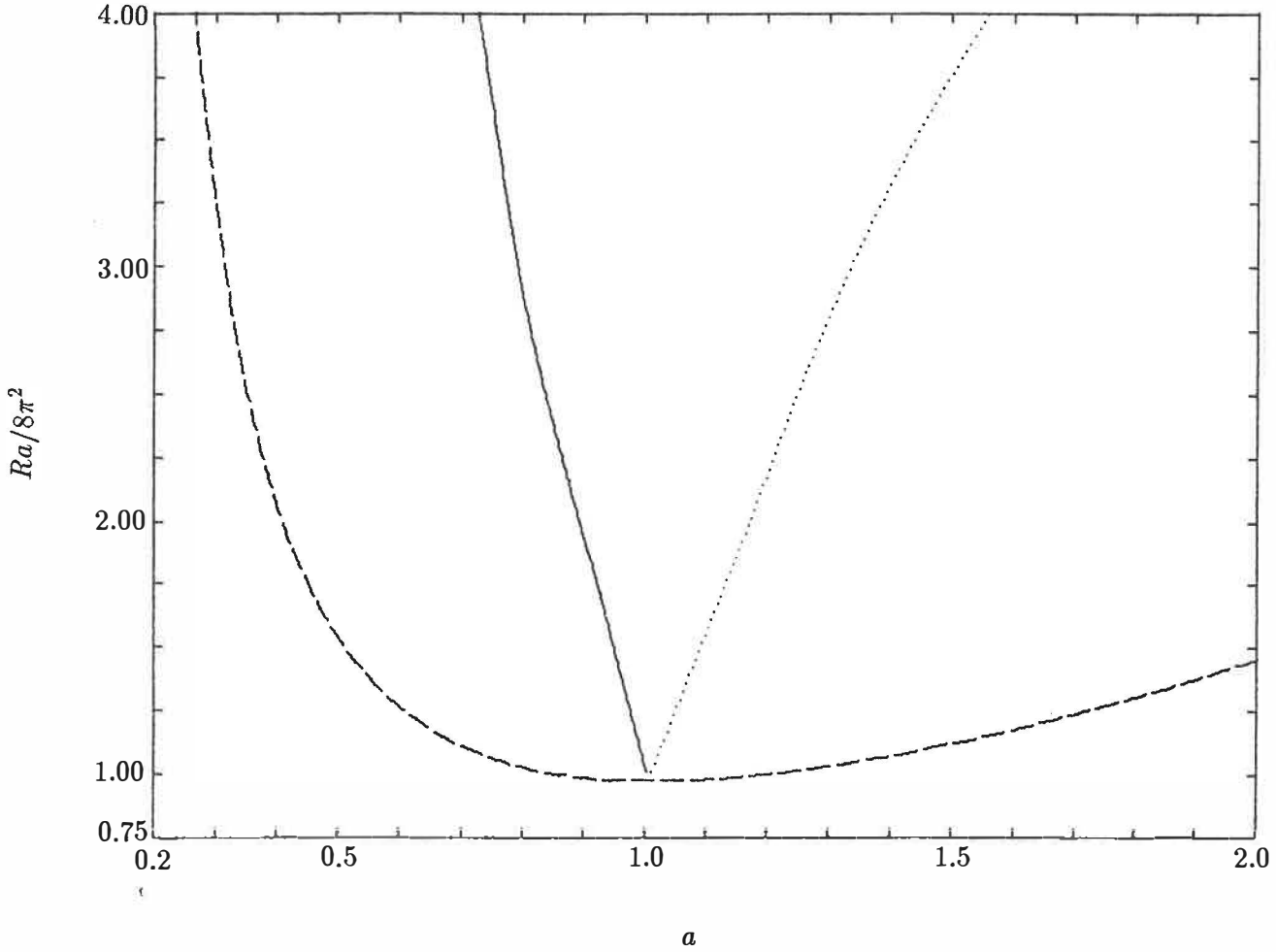

Fig.2.4 Preferred Wavenumbers ($\beta = 0.0$)

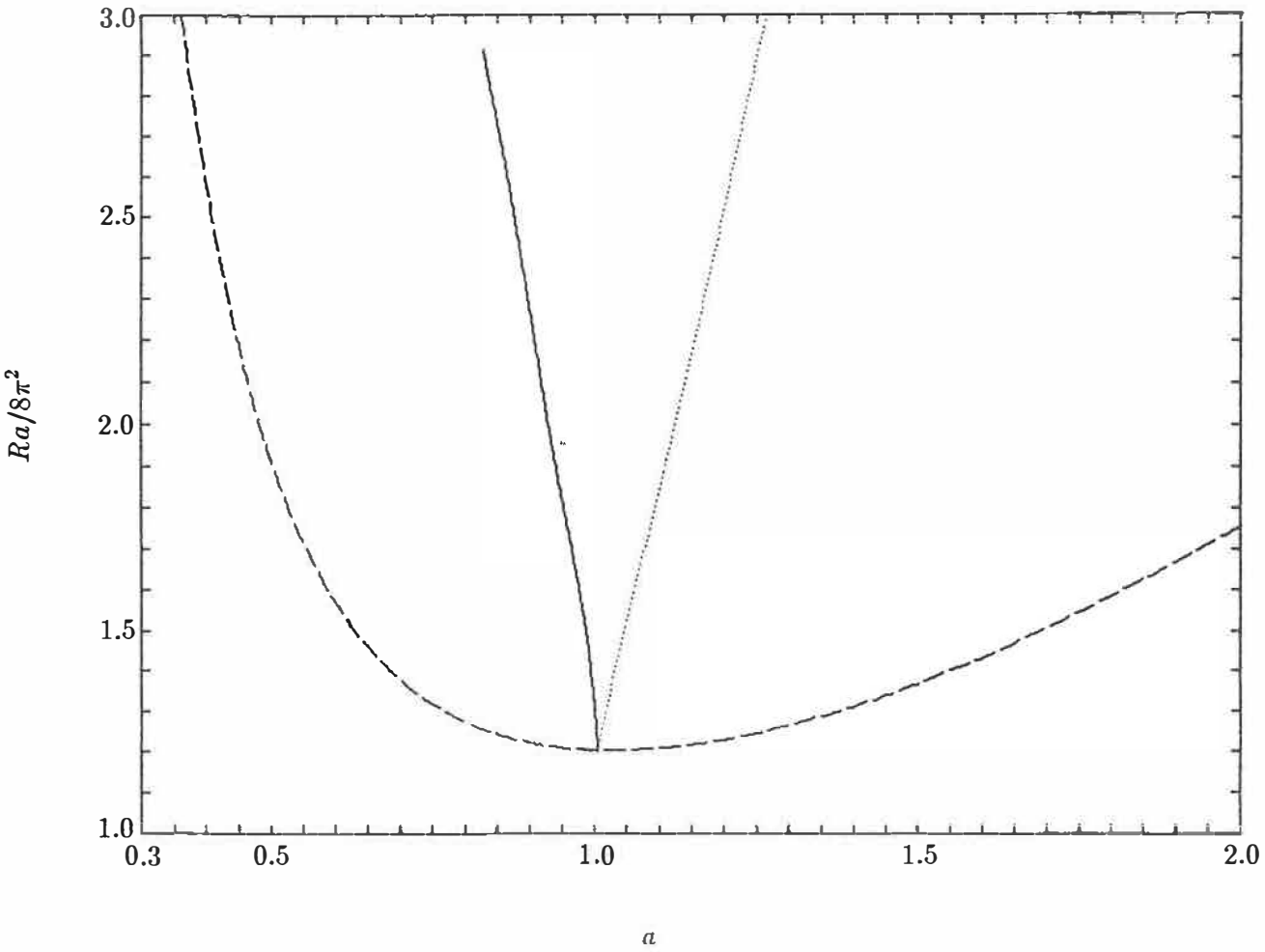

Fig.2.5 Preferred Wavenumbers ($\beta = 0.1$)

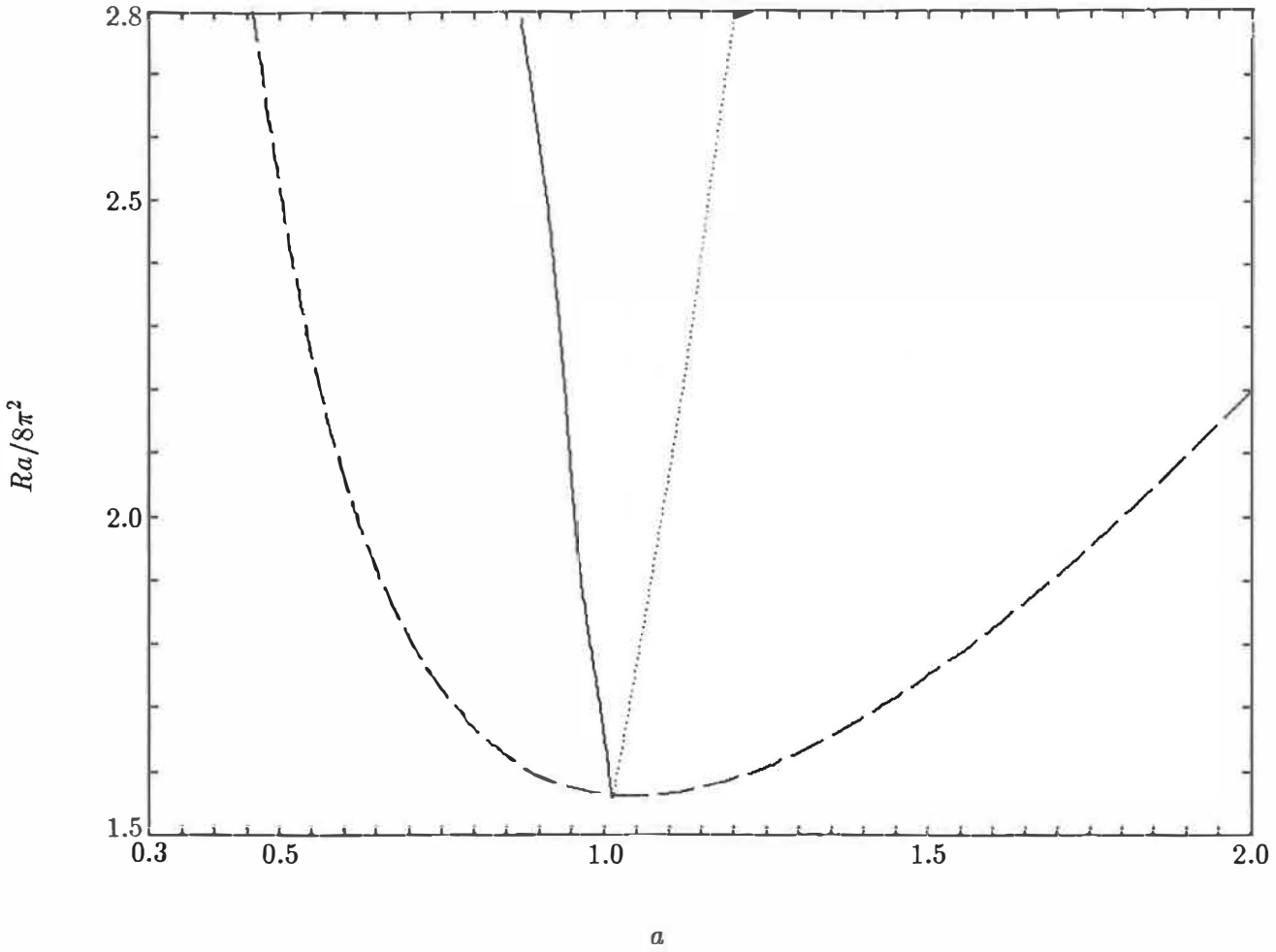

Fig.2.6 Preferred Wavenumbers ($\beta = 0.2$)

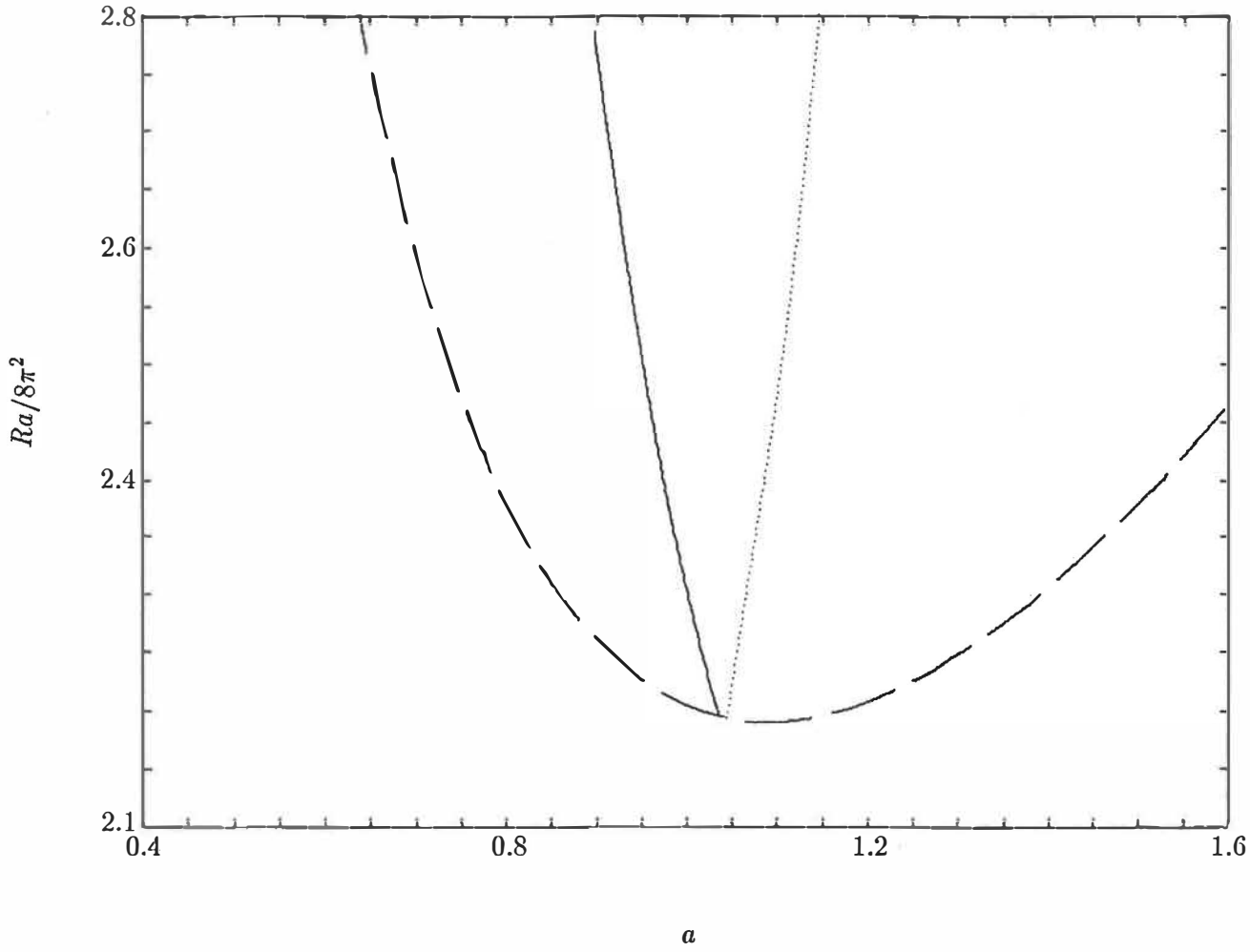

Fig.2.7 Preferred Wavenumbers ($\beta = 0.3$)

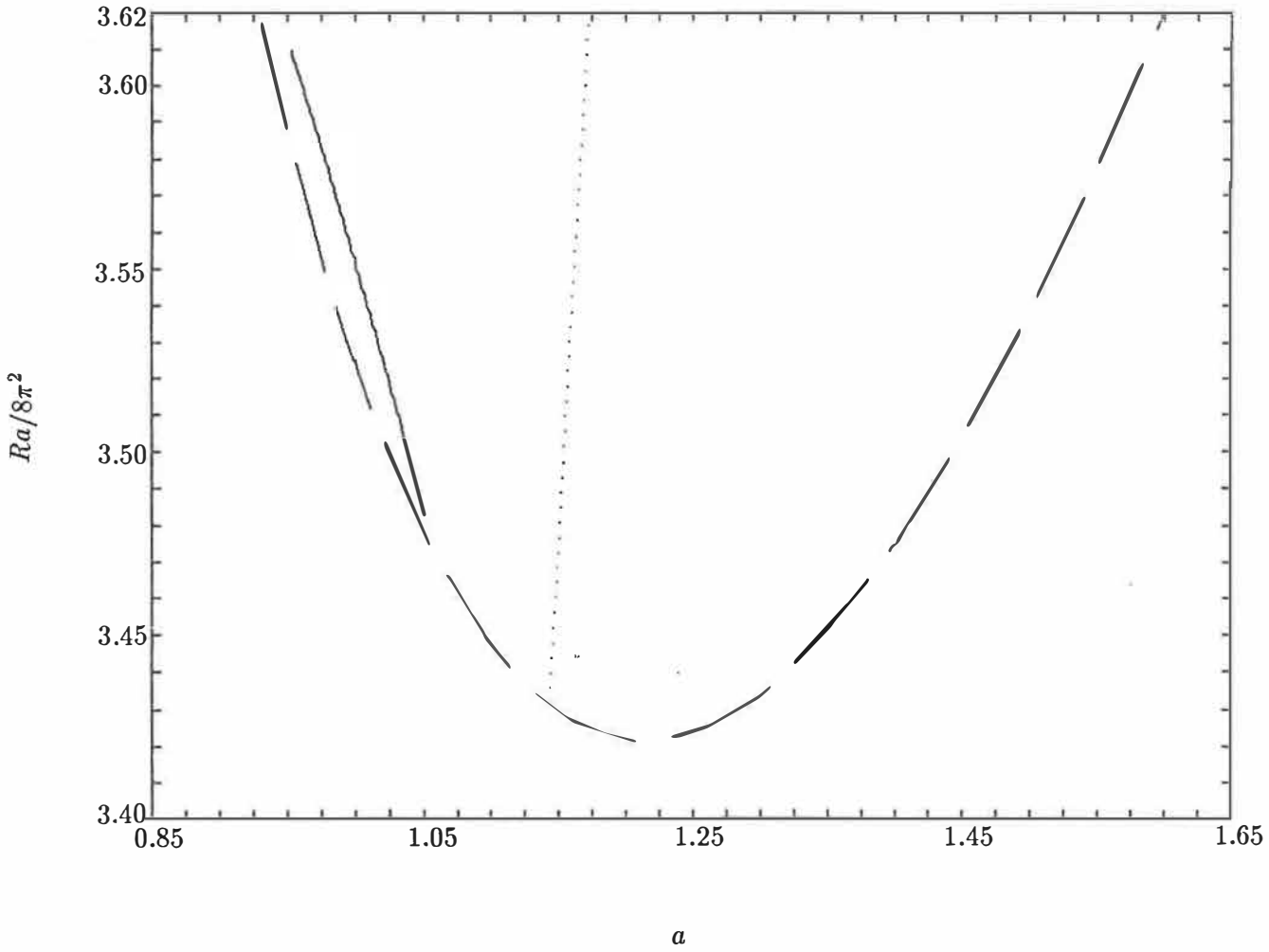

Fig.2.8 Preferred Wavenumbers ($\beta = 0.4$)

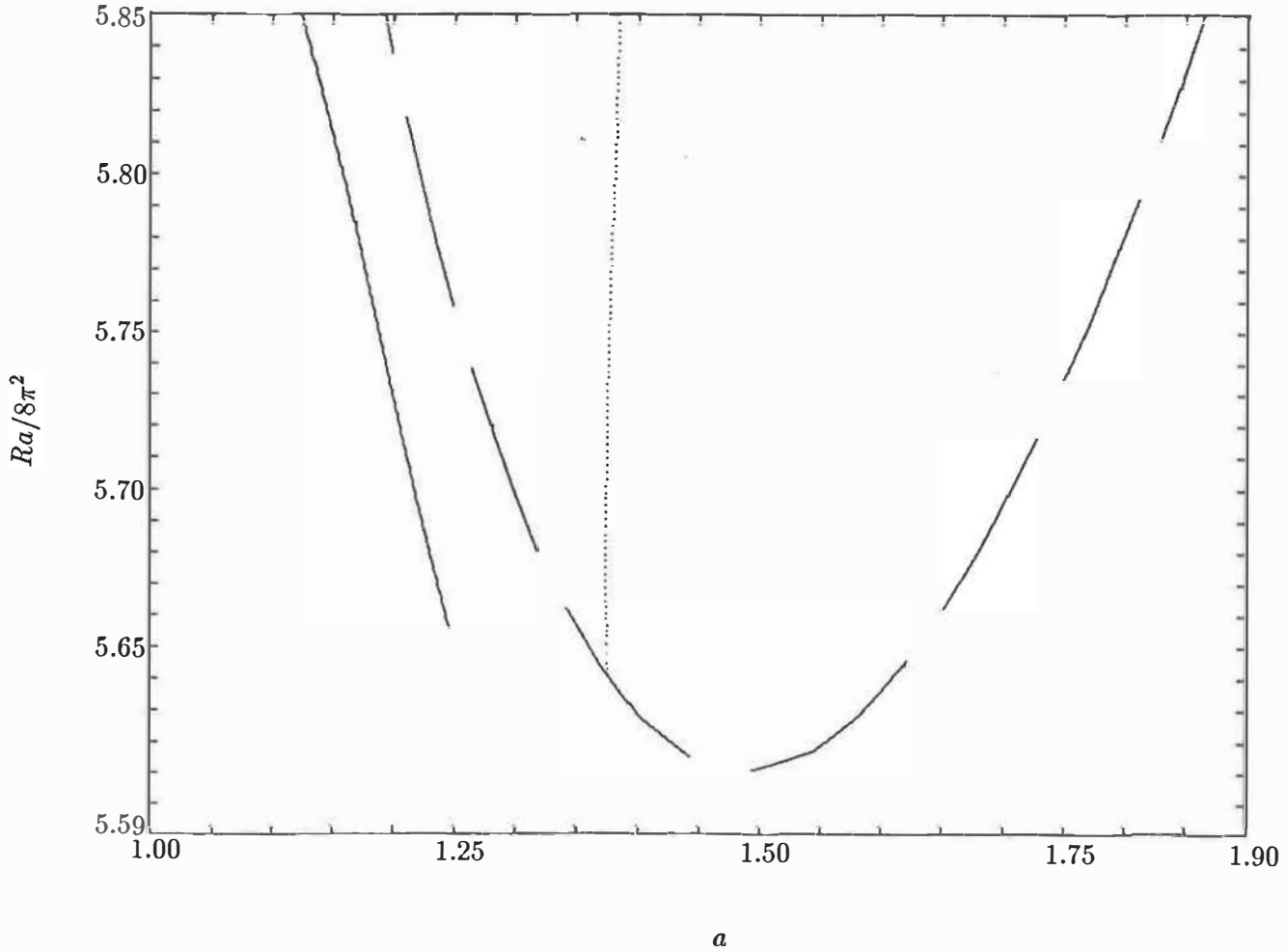

Fig.2.9 Preferred Wavenumbers ($\beta = 0.5$)

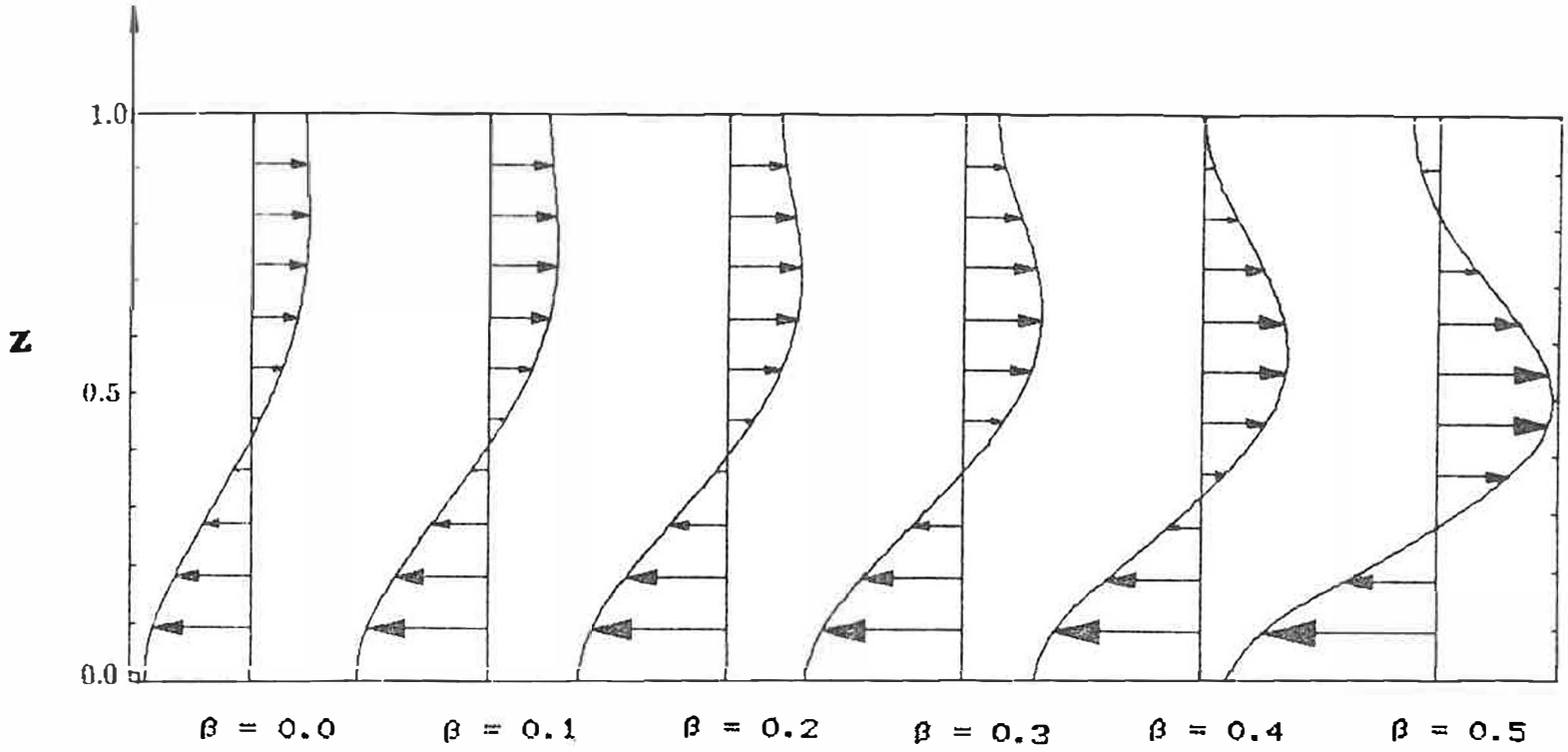

Fig.2.10 Average Velocity Profiles

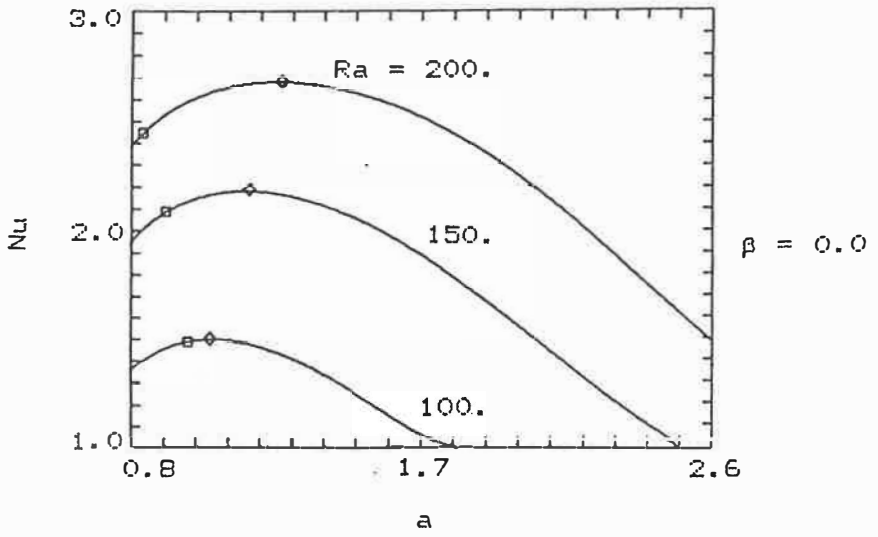

Fig.2.11 Nusselt numbers versus wavenumbers ($\beta = 0.0$)

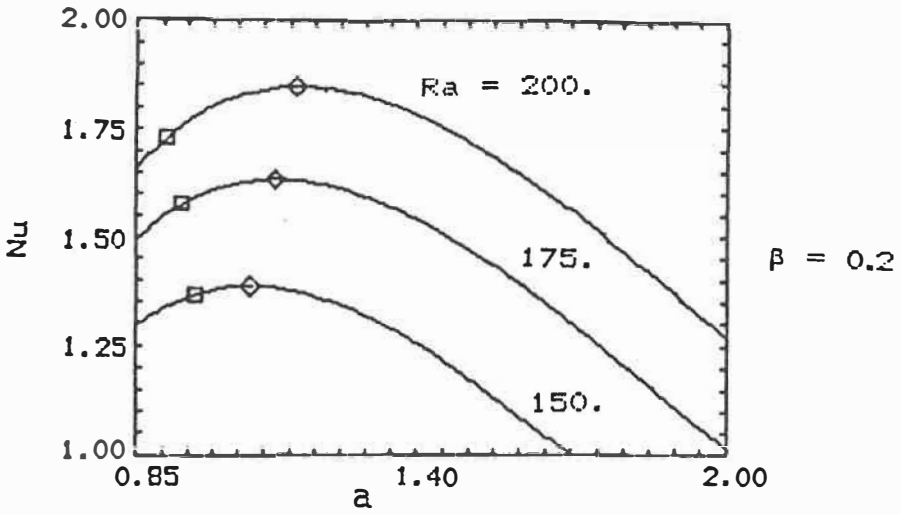

Fig.2.12 Nusselt numbers versus wavenumbers ($\beta = 0.5$)

□ Nusselt Number with the Preferred Wavenumber
◇ Maximum Nusselt Number

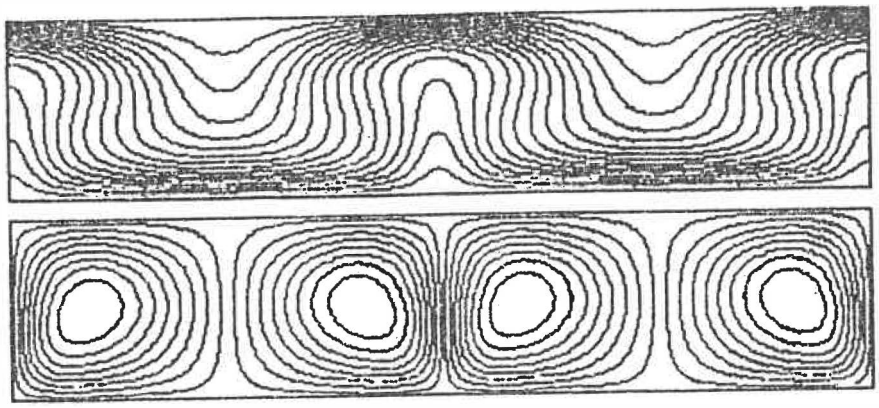

Fig.2.13 Isotherms and Streamlines ($\beta = 0.0$)

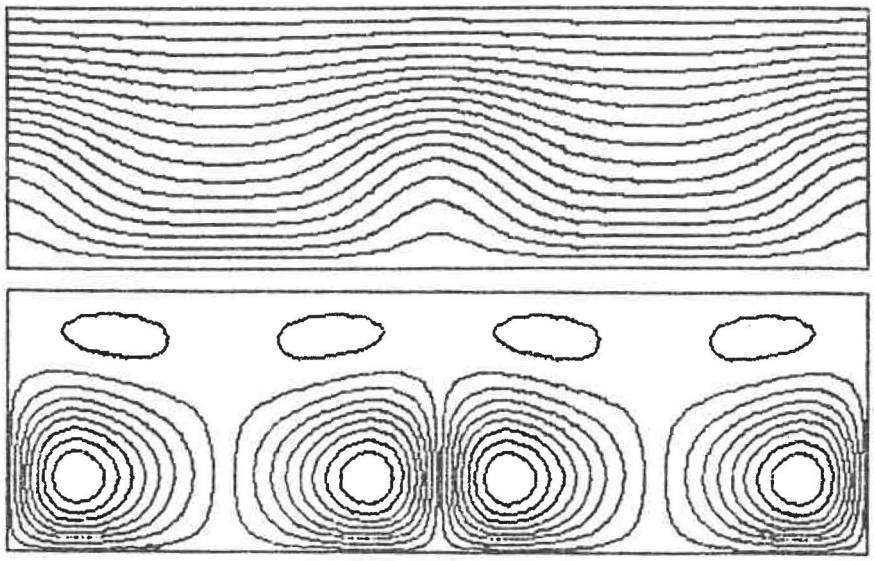

Fig.2.14 Isotherms and Streamlines ($\beta = 0.5$)

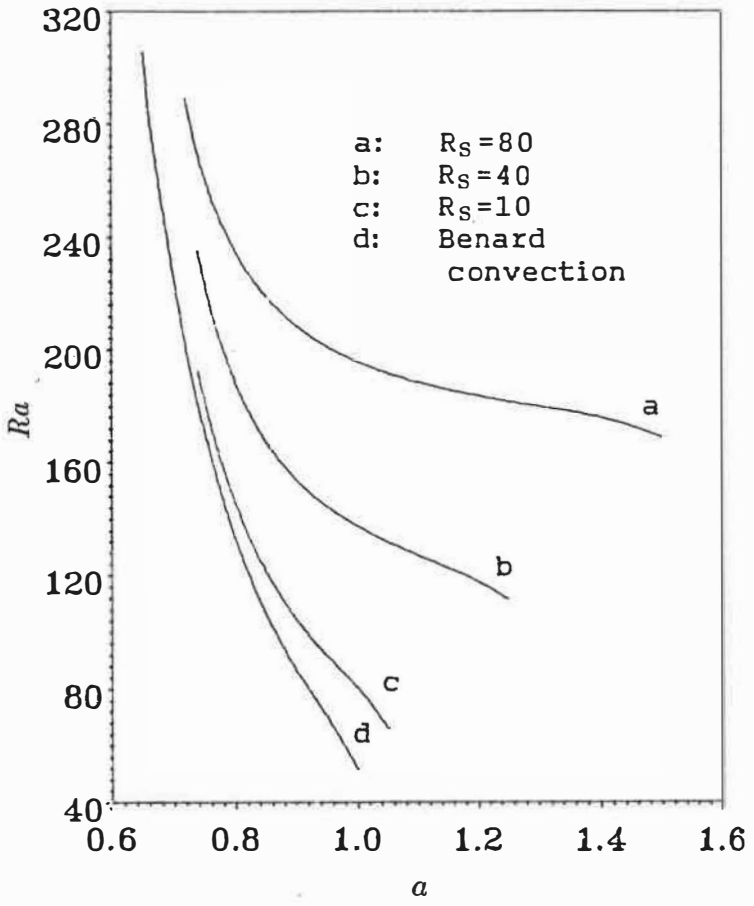

Fig.2.15 Preferred wavenumber versus Ra with S_c of $10^{-1/2}$

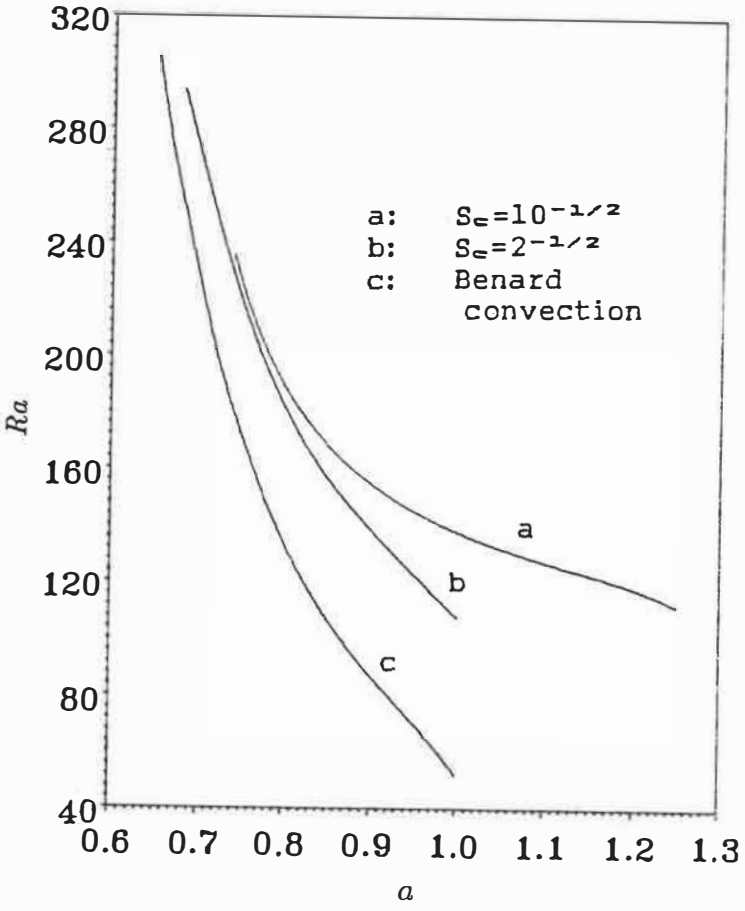

Fig.2.16 Preferred wavenumber versus Ra with R_S of 40

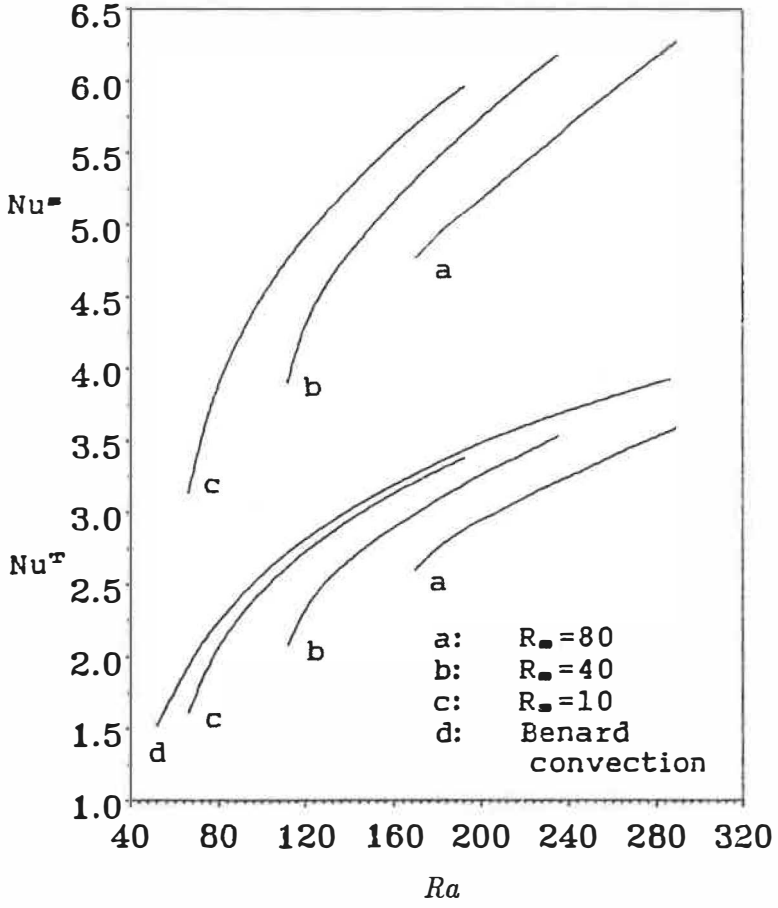

Fig.2.17 Nusselt number versus Ra with S_c of $10^{-1/2}$

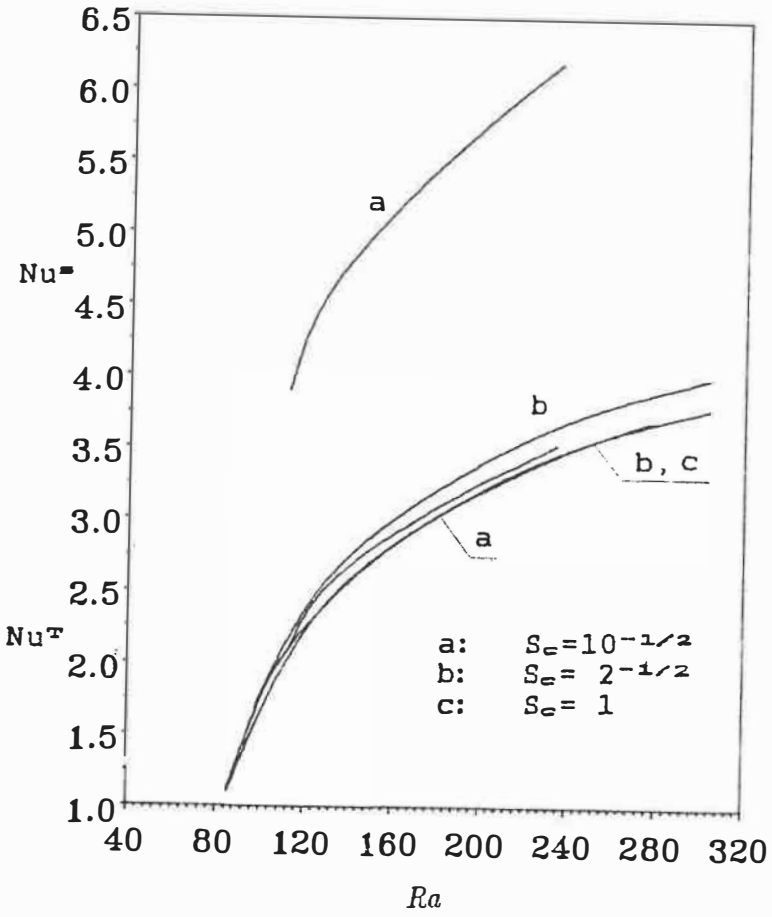

Fig.2.18 Nusselt number versus Ra with R_s of 40

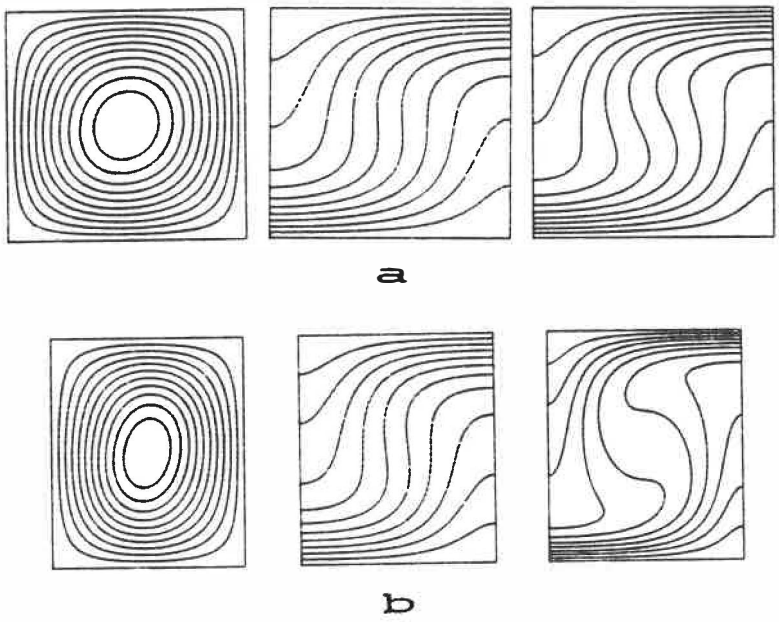

Fig.2.19 Streamlines, isotherms and iso-concentration lines constant concentration lines for $R_s=40$, $R_T=120$ and (a) $S_c=2^{-1/2}$, (b)$=10^{-1/2}$

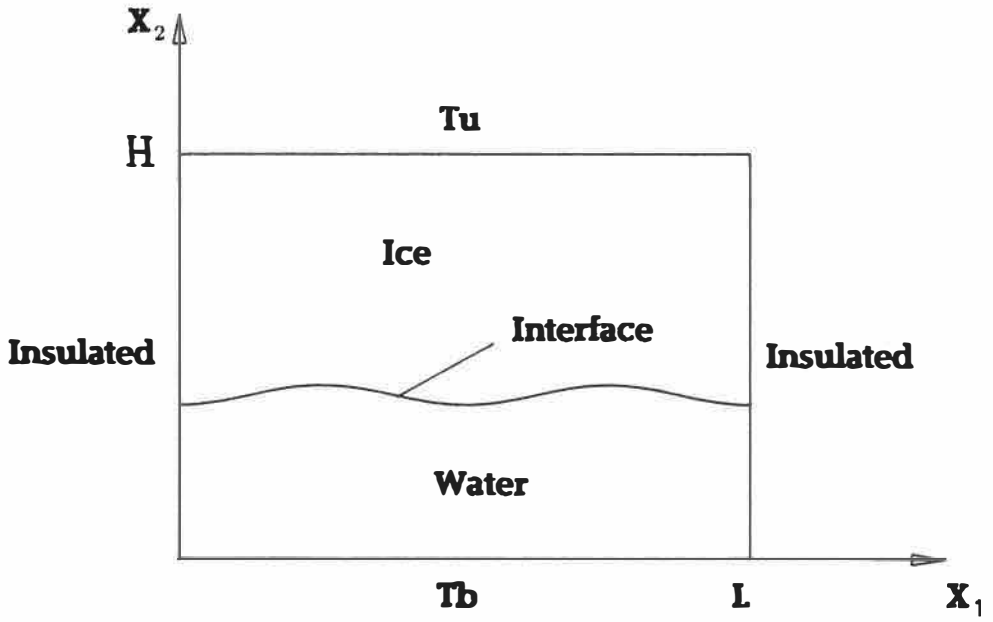

Fig.3.1 Definition Sketch for the Melting of Ice in a bounded Porous Layer

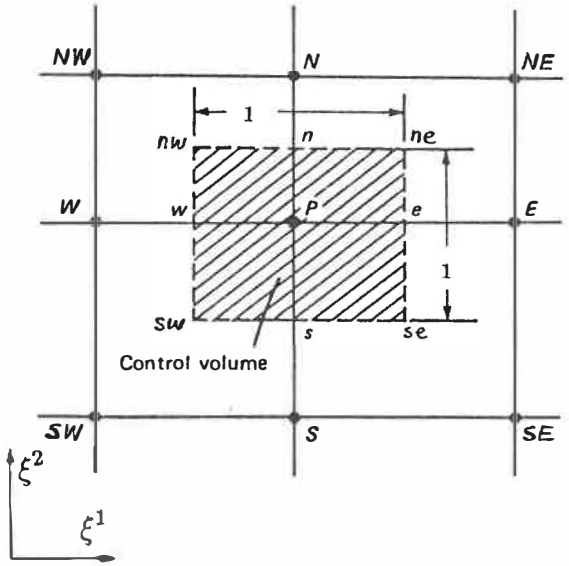

Fig.3.2 Sketch of Control Volume

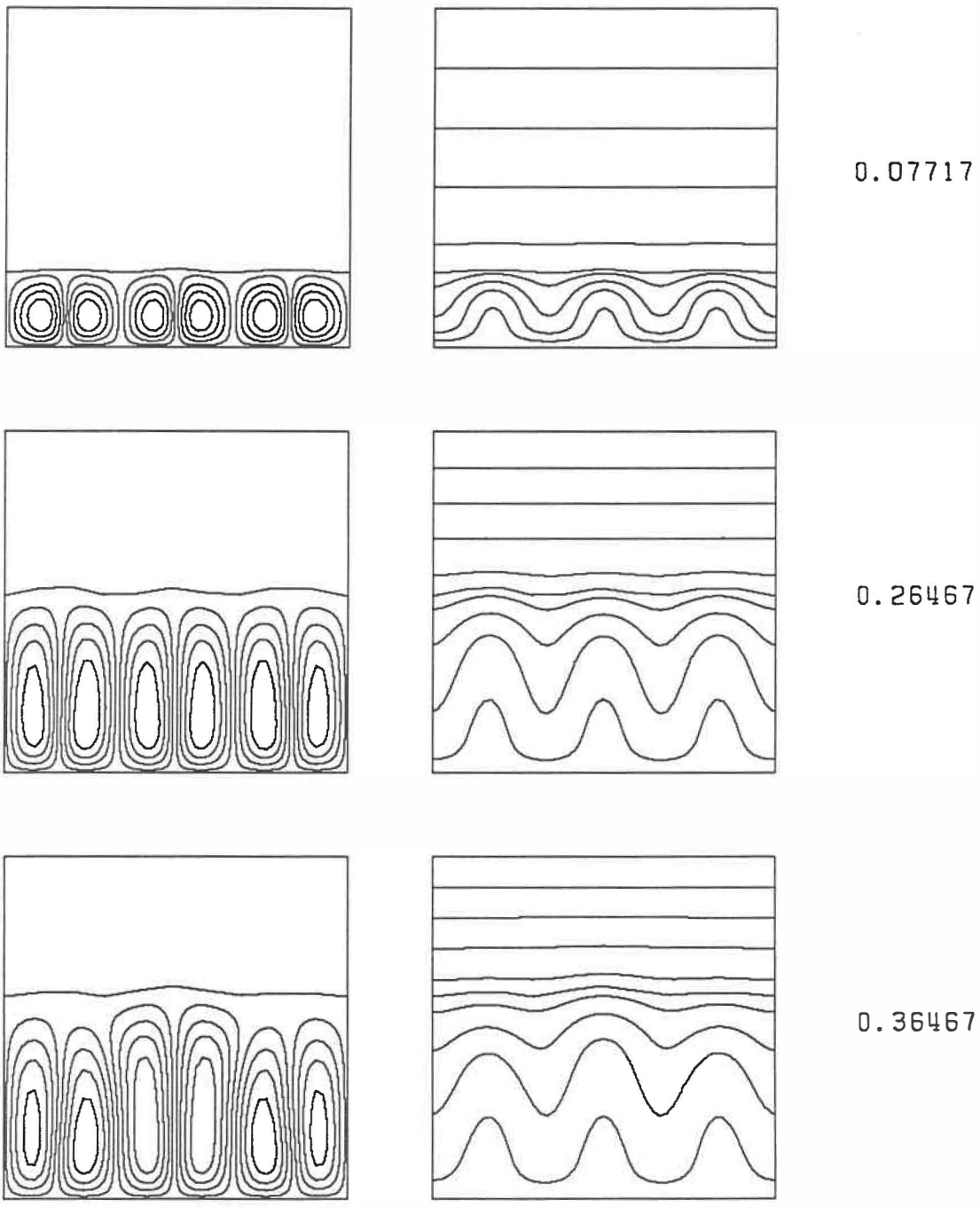

Fig.3.3 Time Evolution of Streamlines and Isotherms (Exp.1)

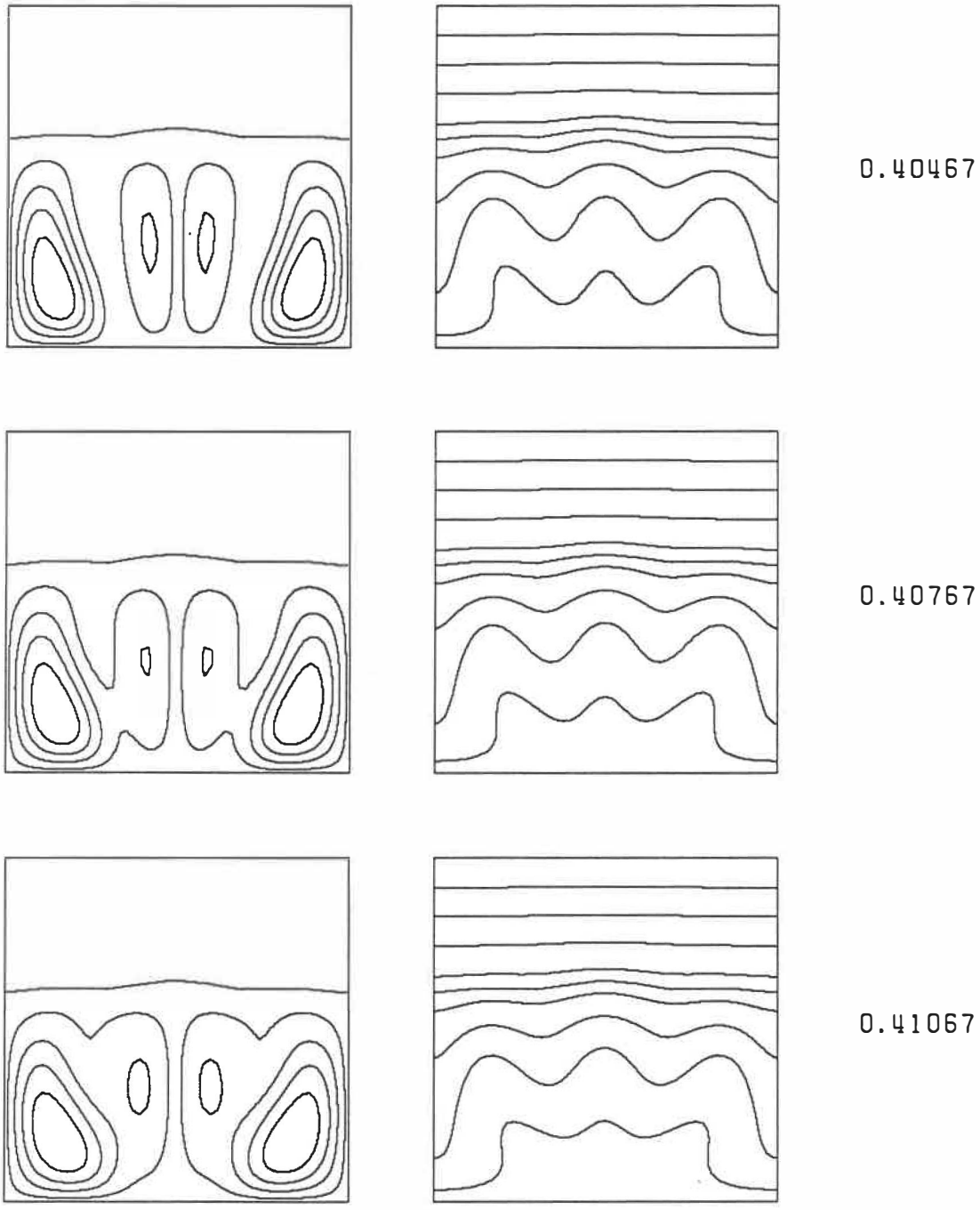

Fig.3.3 (continued)

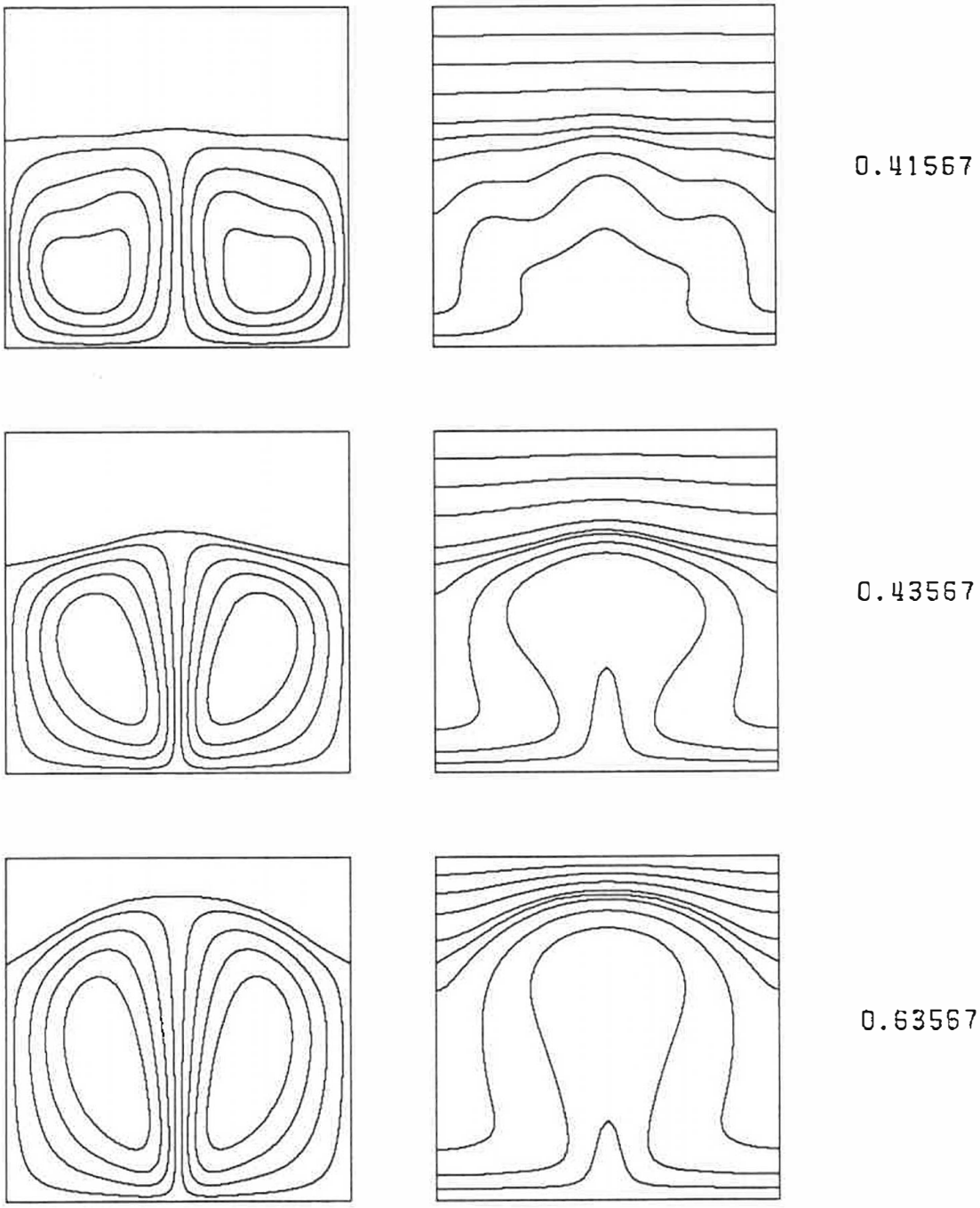

Fig.3.3 (concluded)

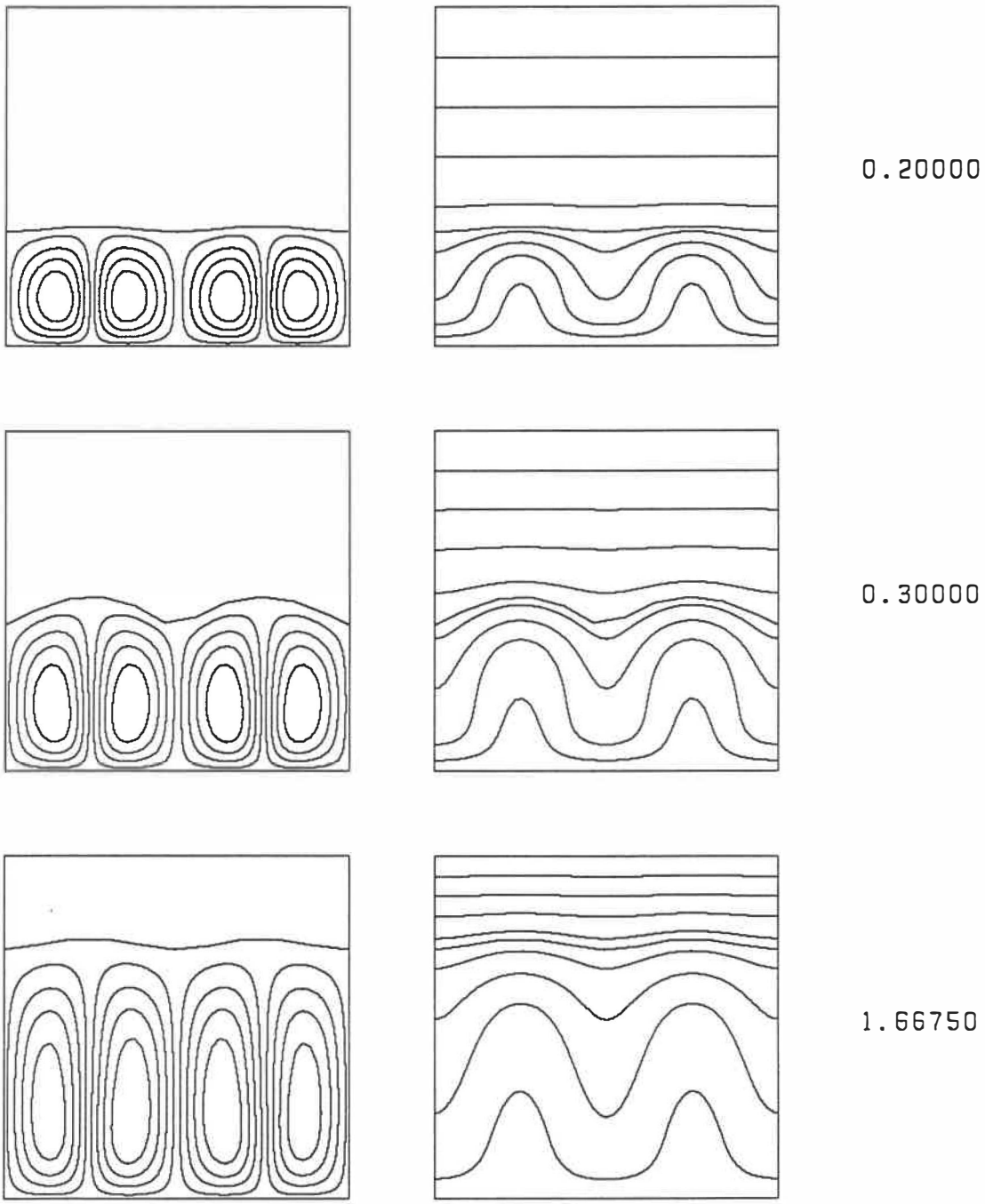

Fig.3.4 Time Evolution of Streamlines and Isotherms (Exp.2)

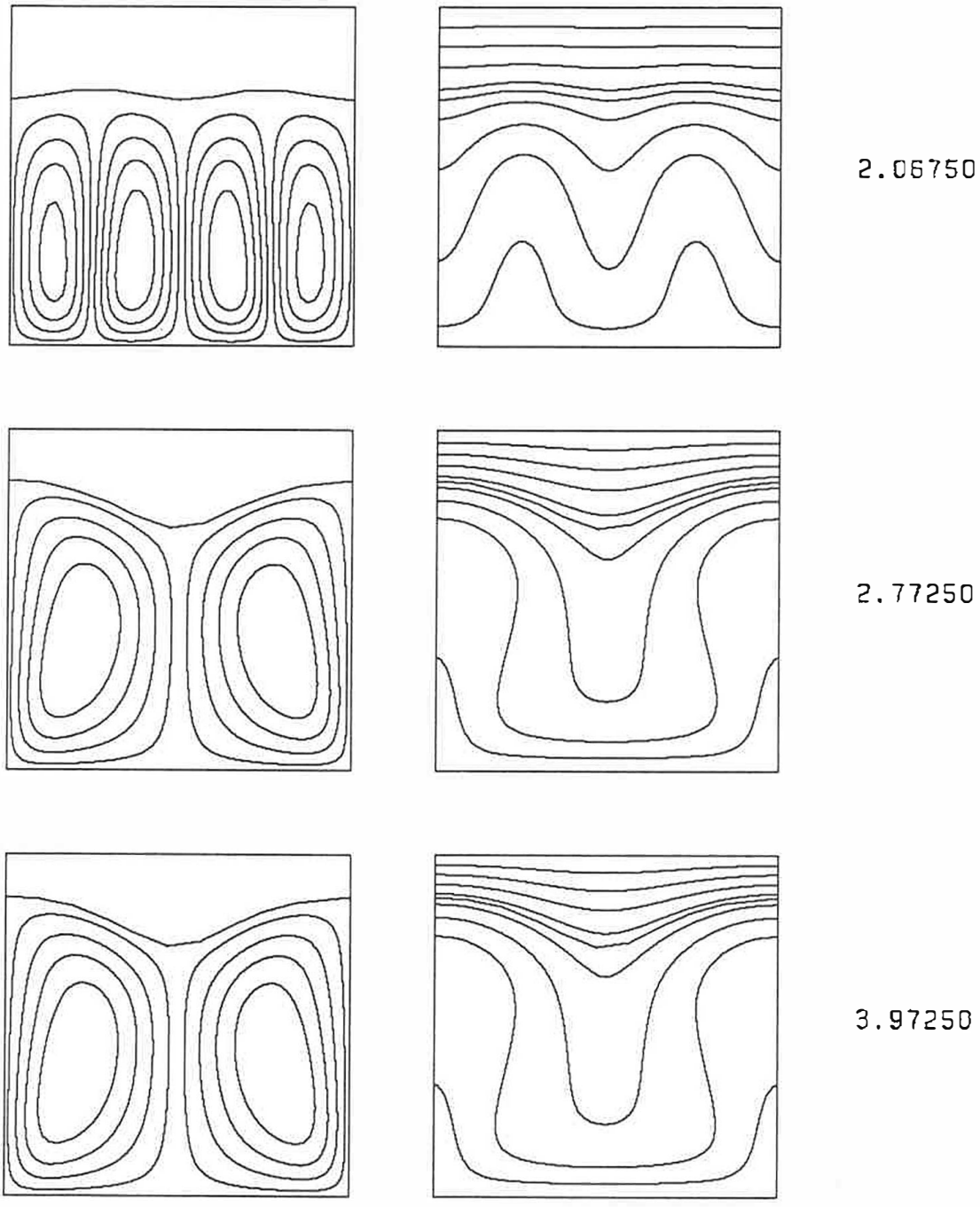

Fig.3.4 (concluded)

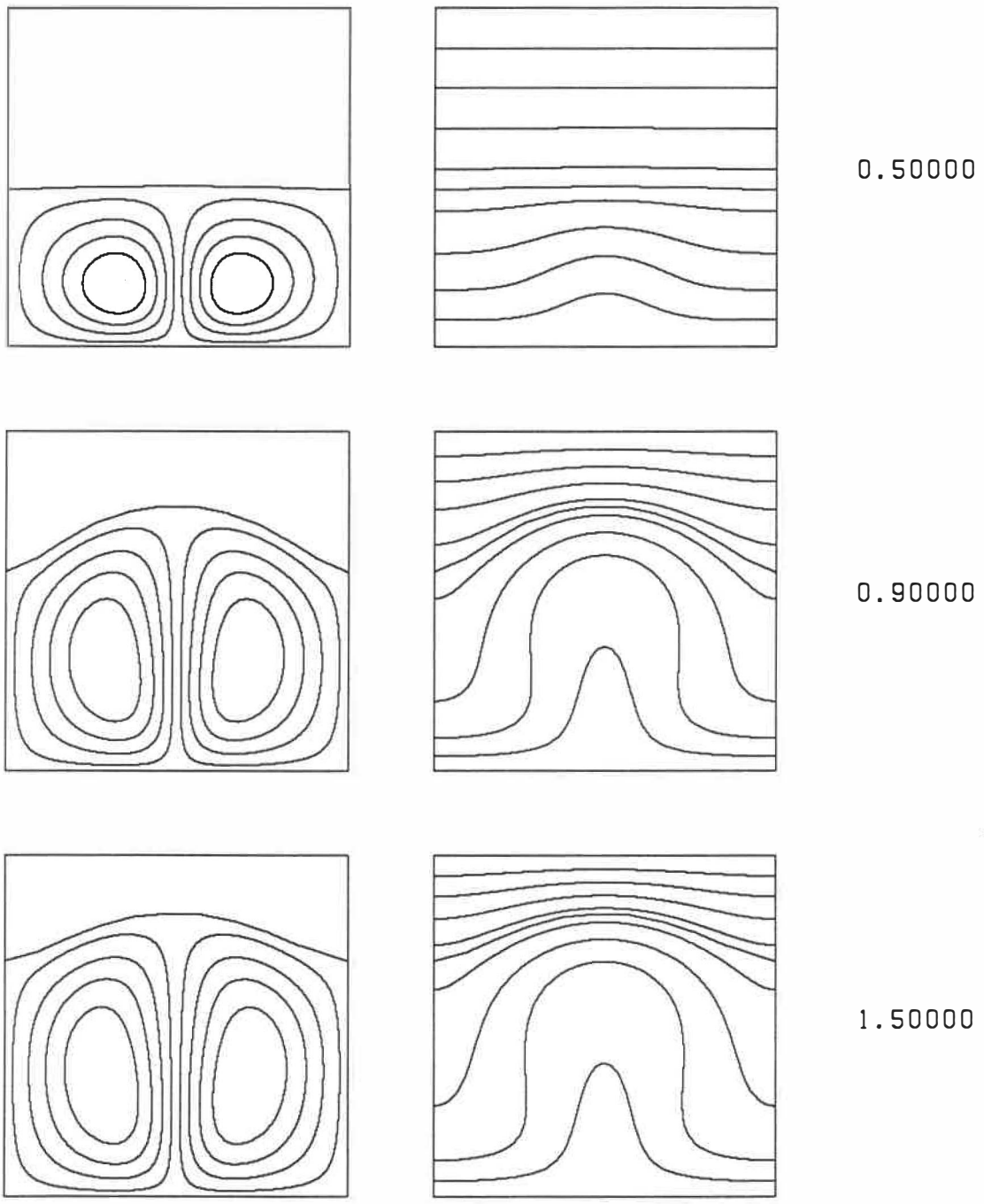

Fig.3.5 Time Evolution of Streamlines and Isotherms (Exp.3)

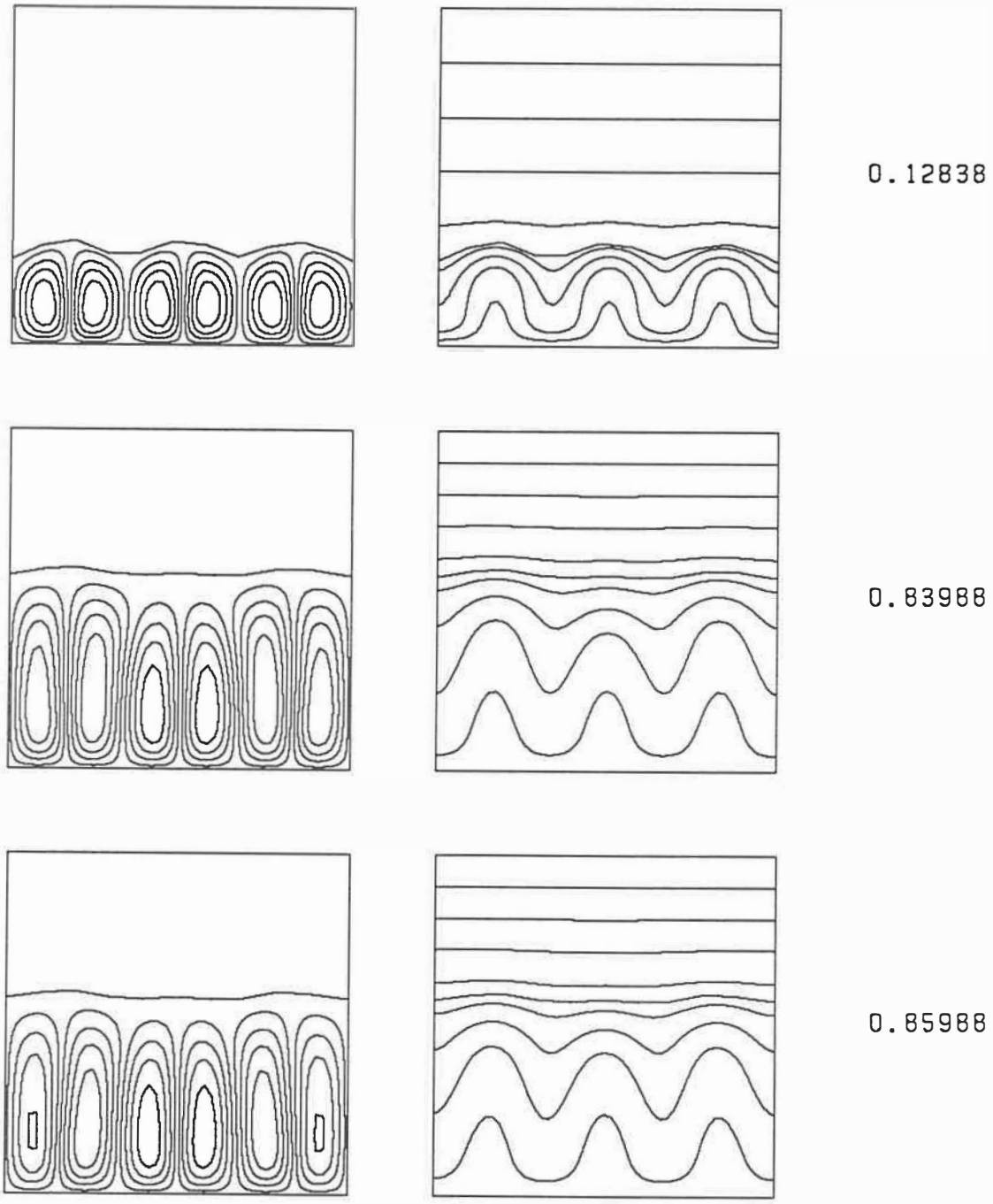

Fig.3.6 Time Evolution of Streamlines and Isotherms (Exp.5)

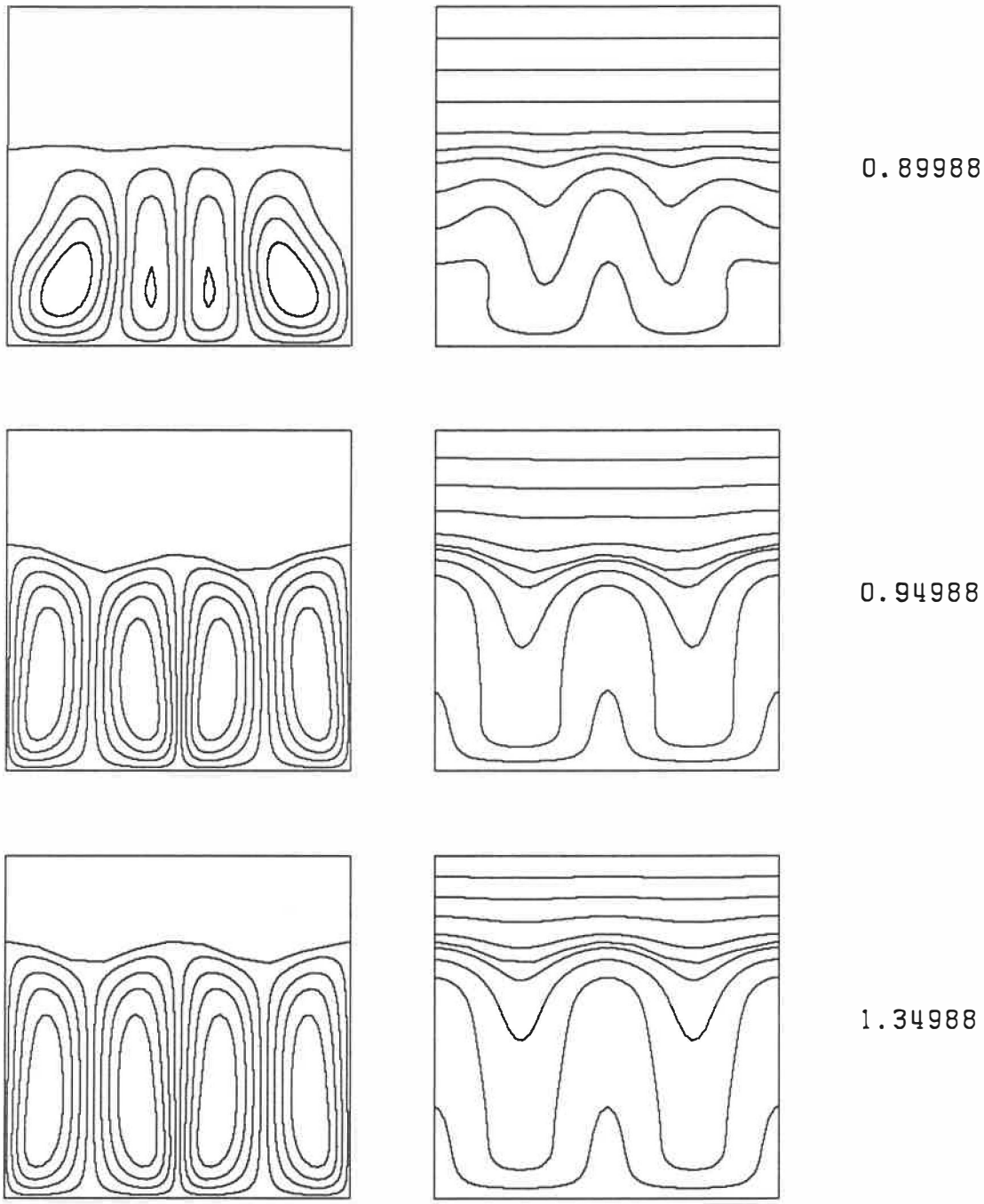

Fig.3.6 (concluded)

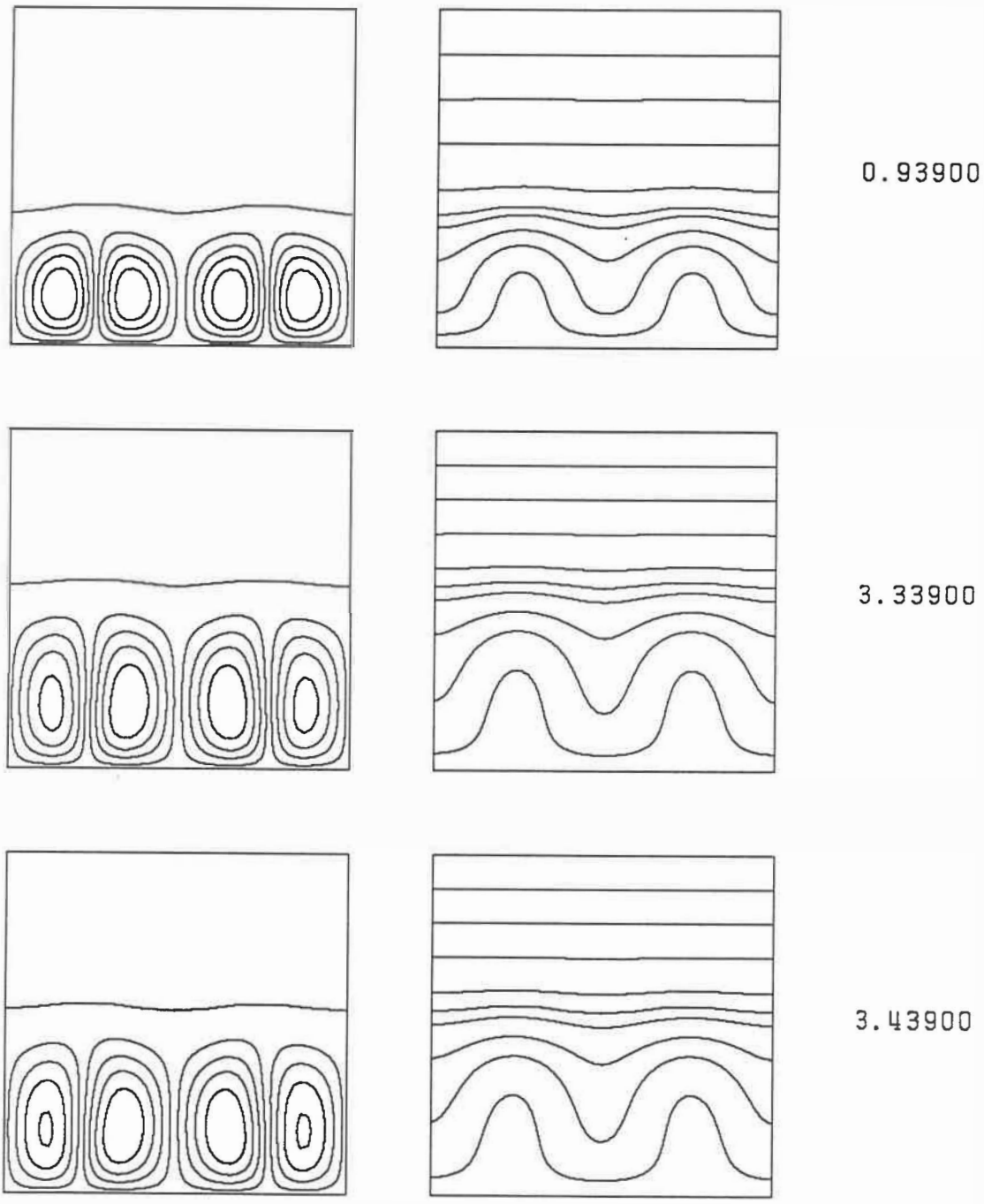

Fig.3.7 Time Evolution of Streamlines and Isotherms (Exp.6)

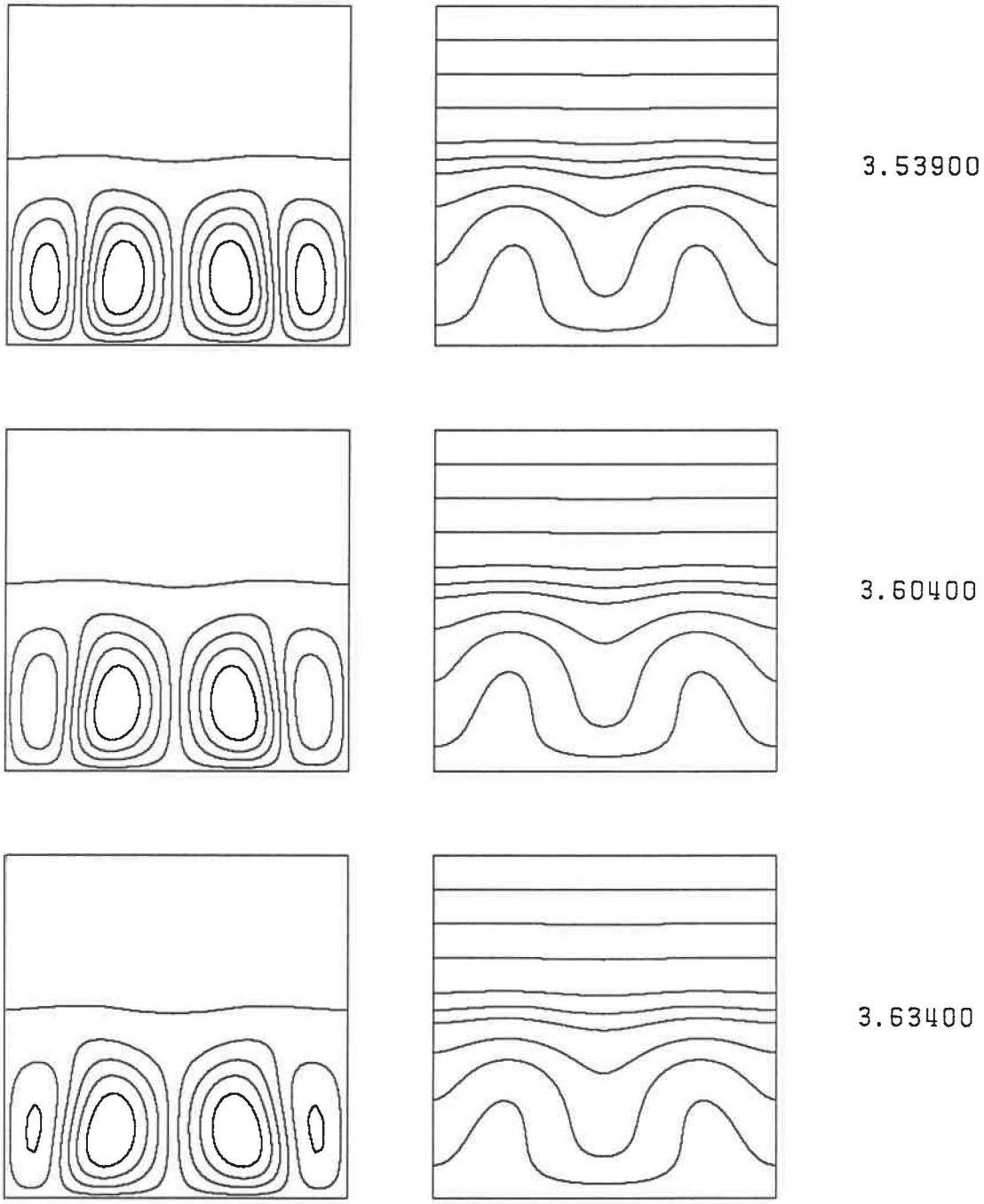

Fig.3.7 (continued)

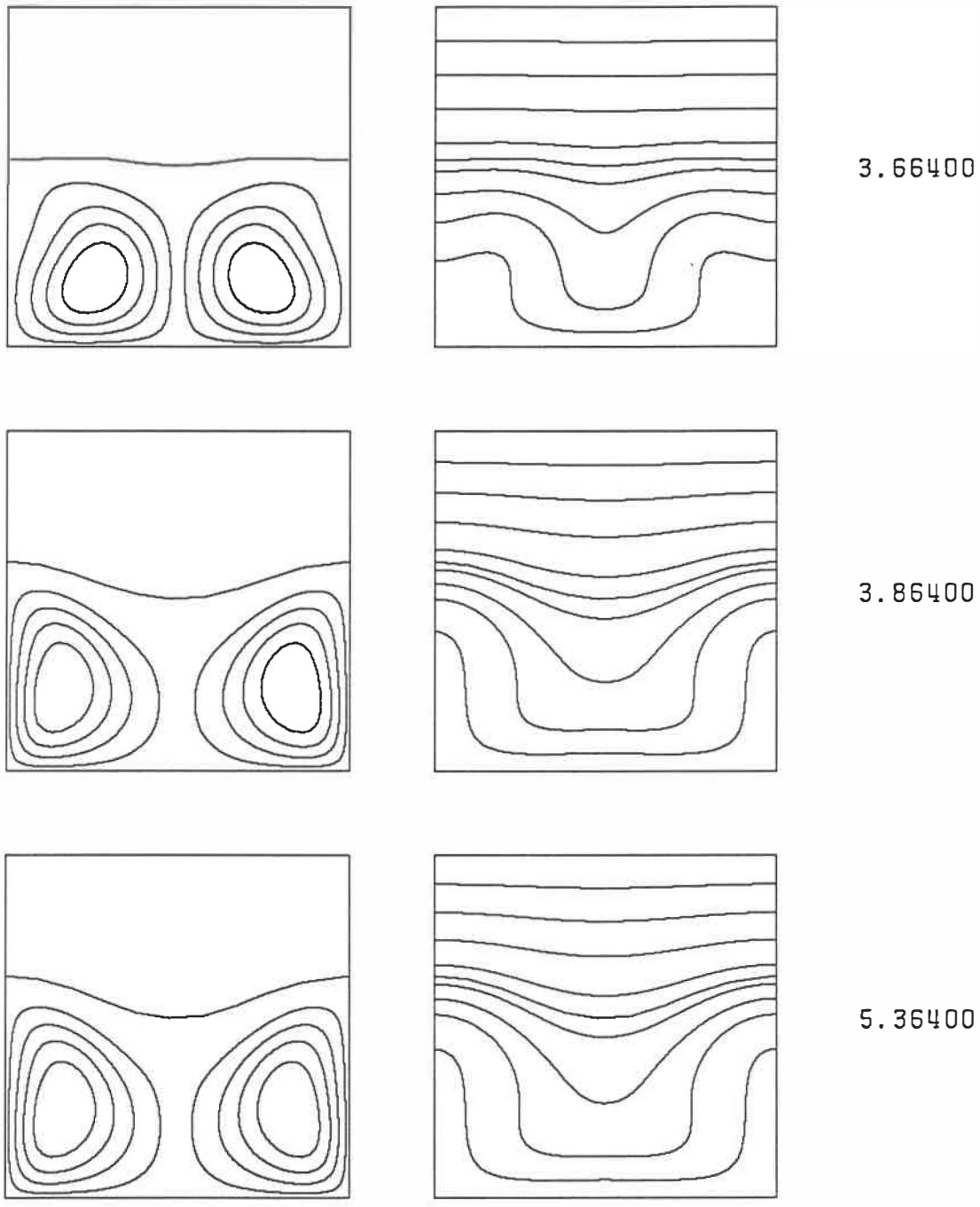

Fig.3.7 (concluded)

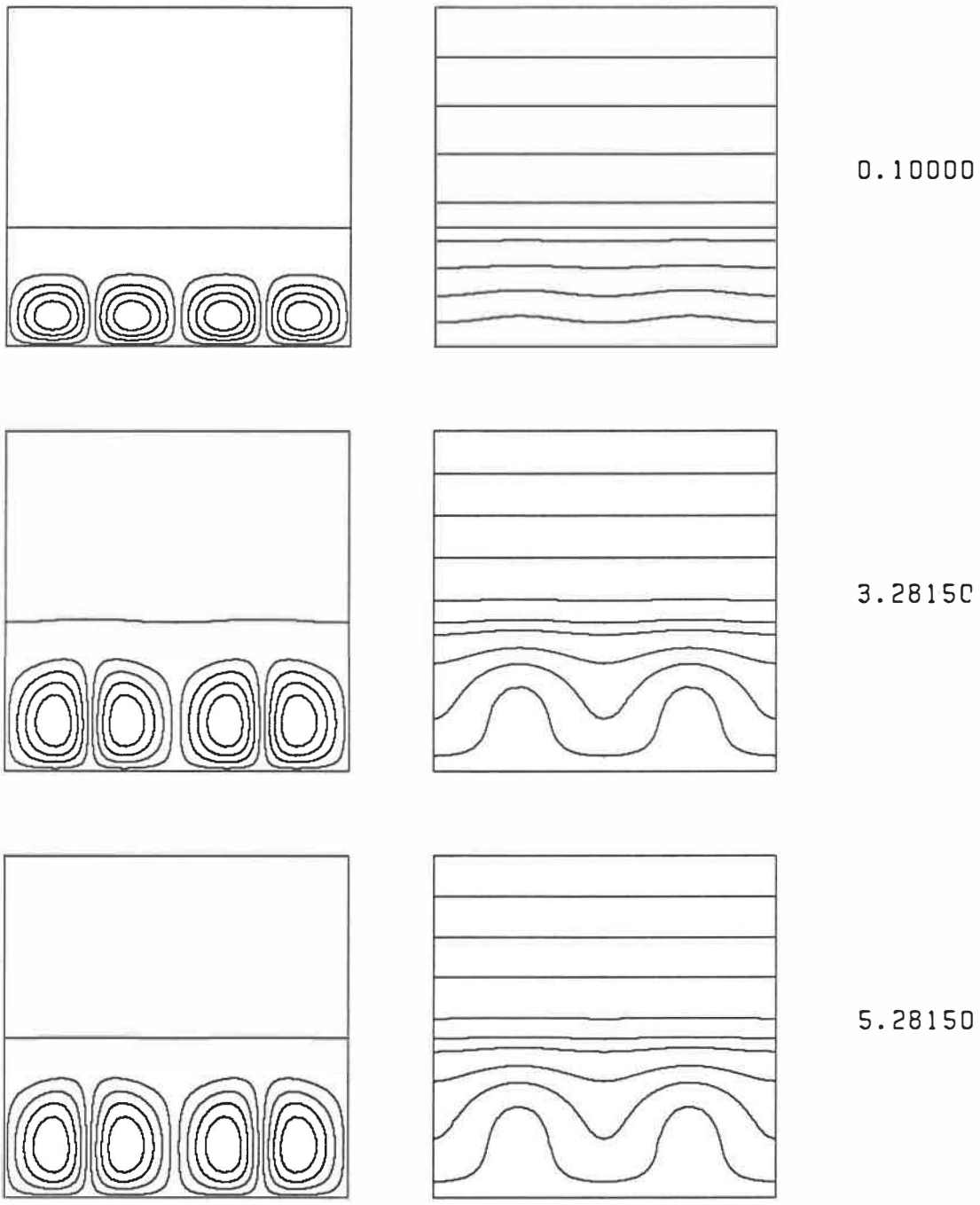

Fig.3.8 Time Evolution of Streamlines and Isotherms (Exp.8)

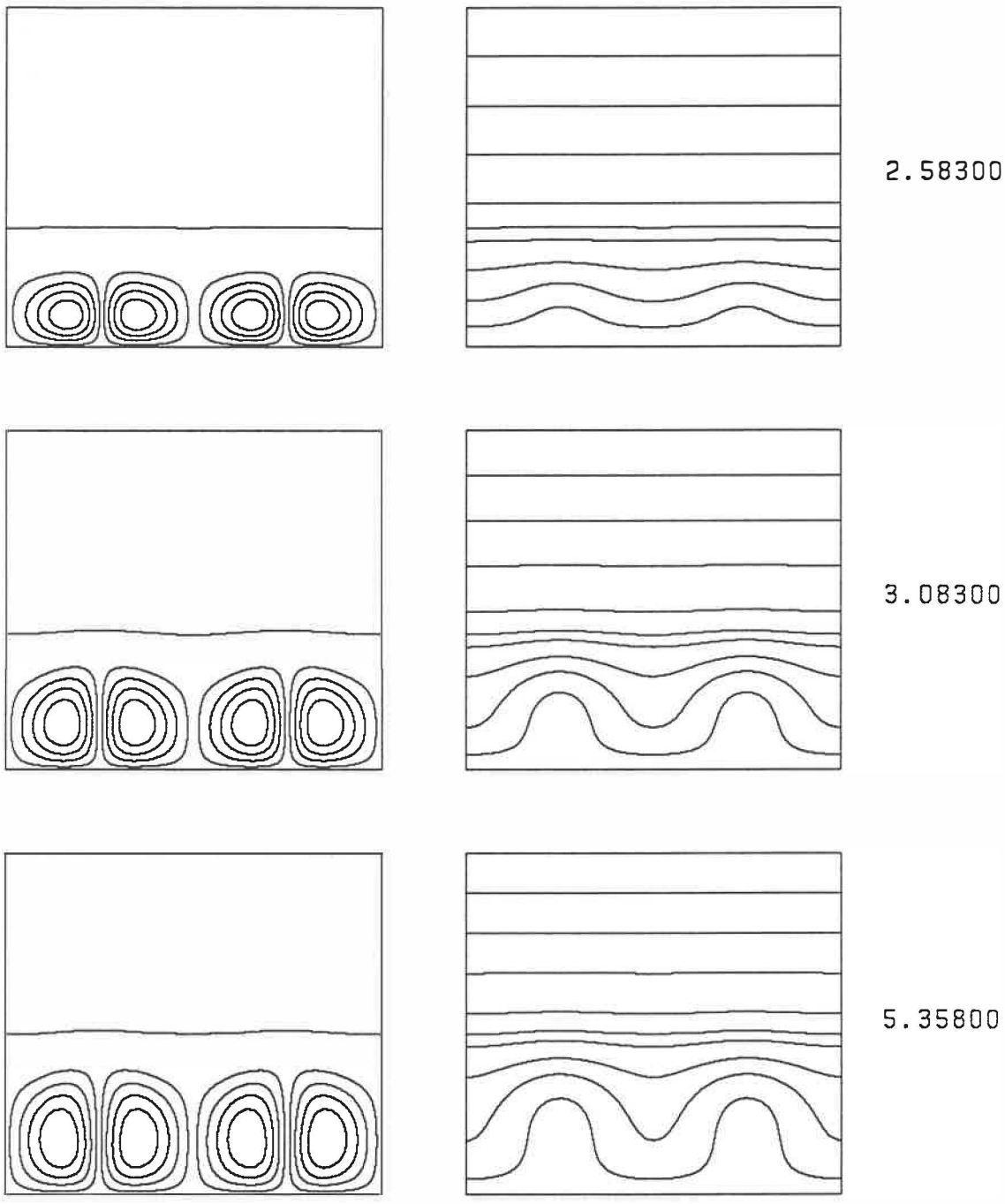

Fig.3.9 Time Evolution of Streamlines and Isotherms (Exp.9)

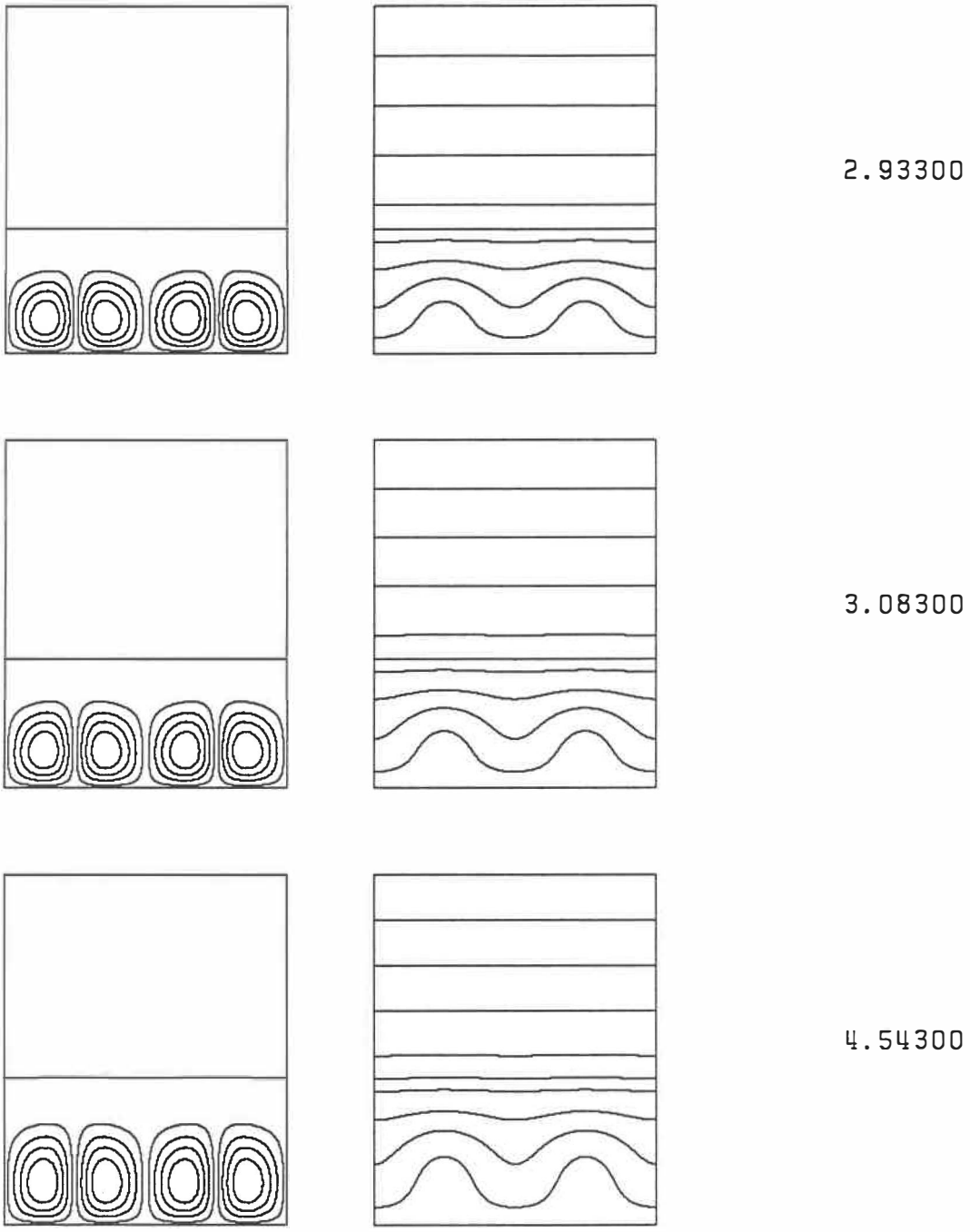

Fig.3.10 Time Evolution of Streamlines and Isotherms (Exp.10)

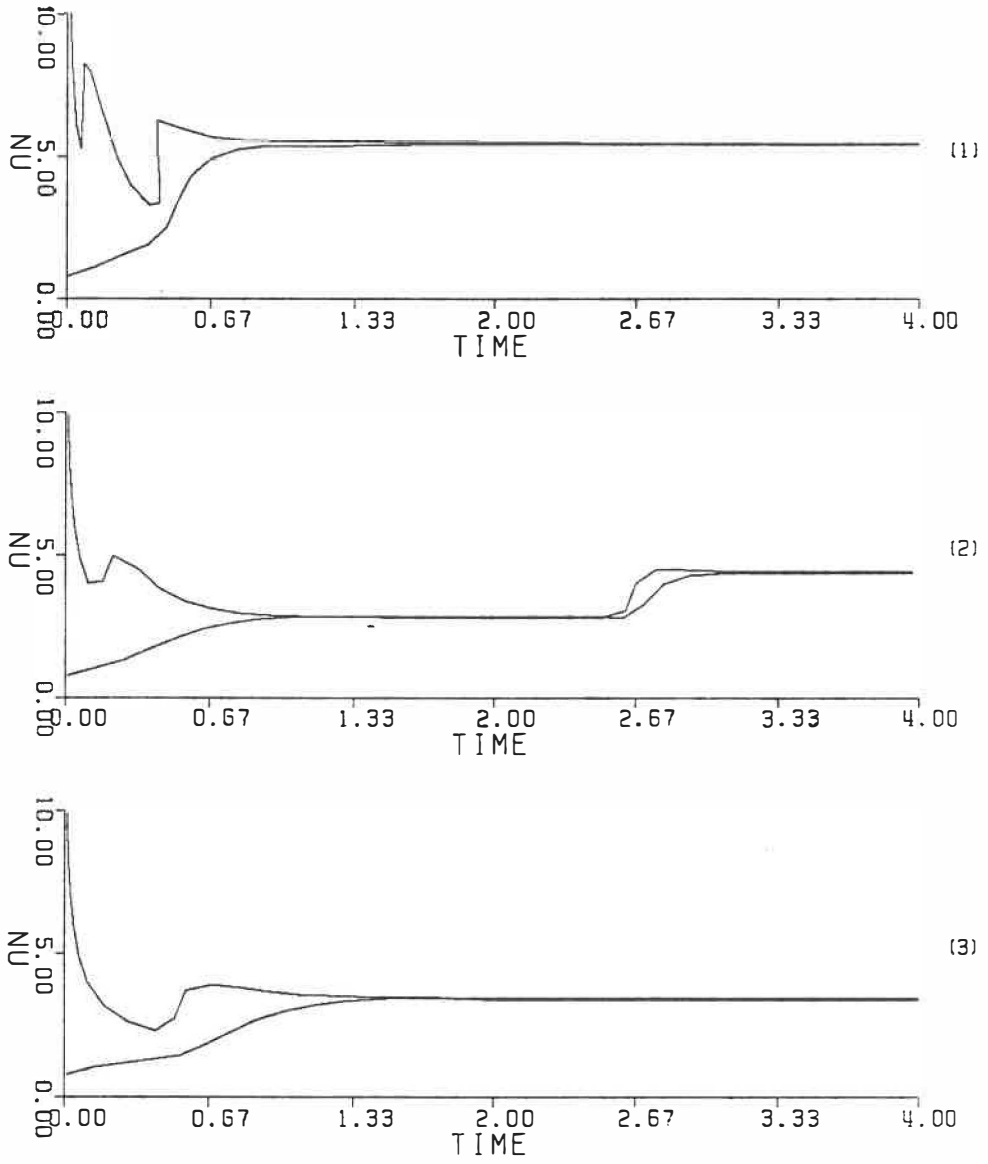

Fig.3.11 Influence of Rayleigh number on heat transfer rate

(1): $Ra = 478.$, **Experiment 1**

(2): $Ra = 300.$, **Experiment 2**

(3): $Ra = 200.$, **Experiment 3**

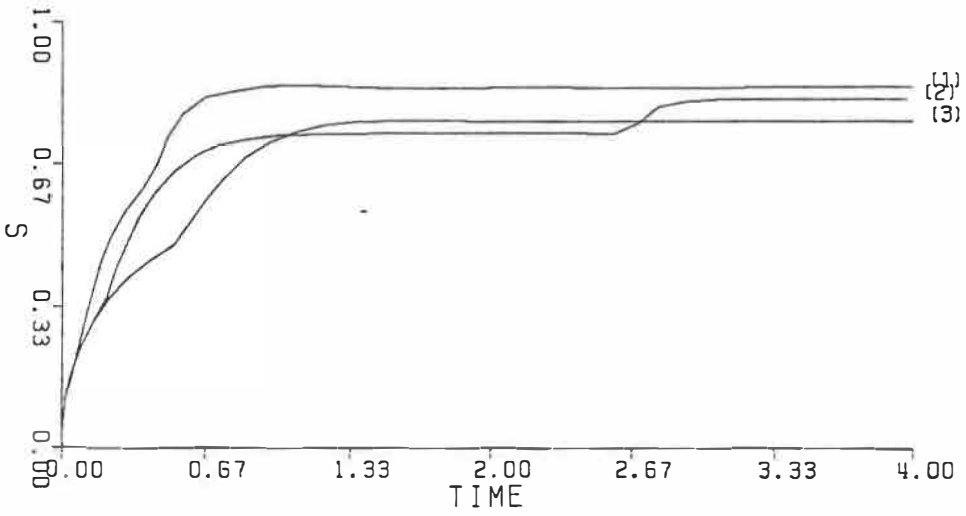

Fig.3.12 Influence of Rayleigh number on interface position

(1): $Ra = 478.$, **Experiment 1**

(2): $Ra = 300.$, **Experiment 2**

(3): $Ra = 200.$, **Experiment 3**

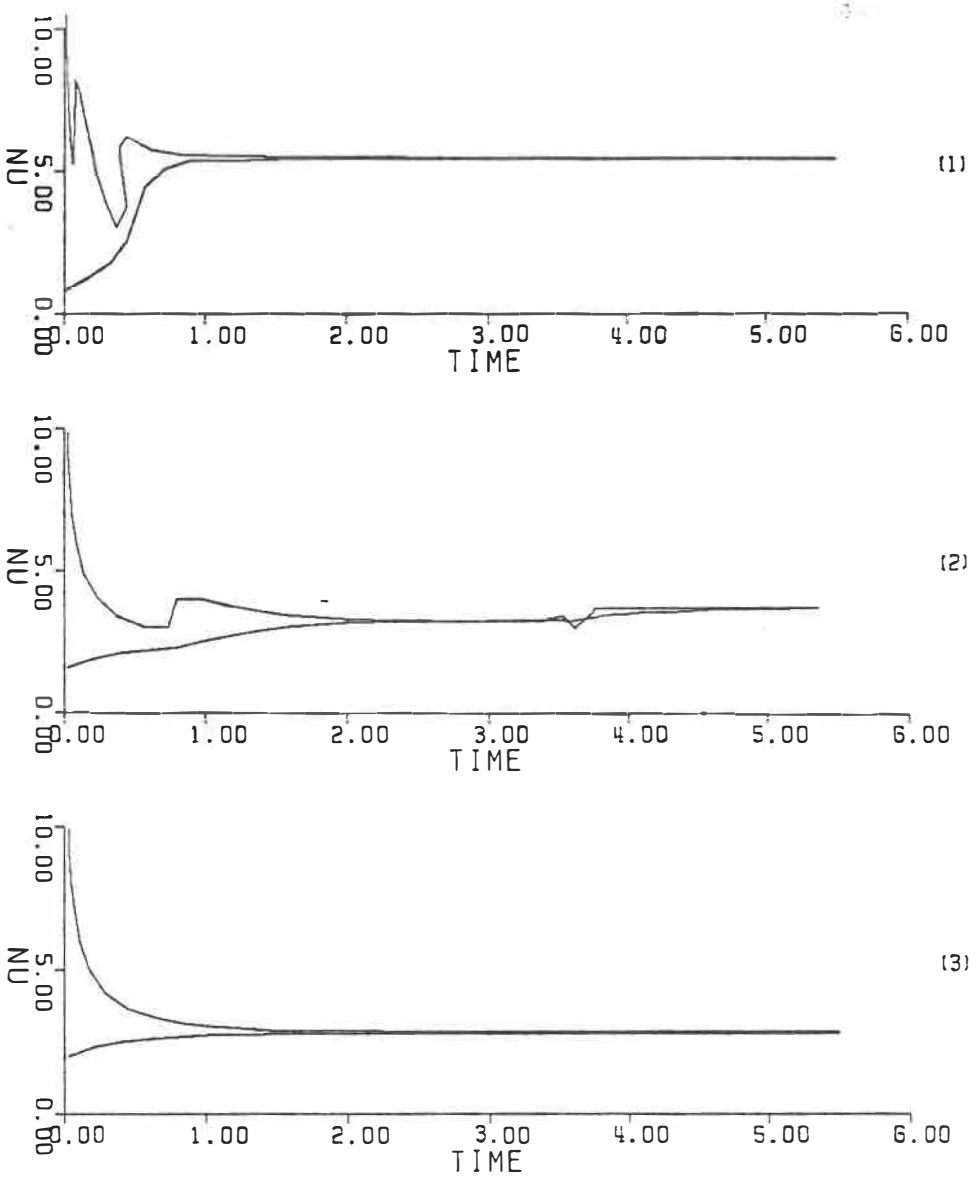

Fig.3.13 Influence of β on heat transfer rate

(1): $\beta = 0.2$, Experiment 1

(2): $\beta = 0.4$, Experiment 6

(3): $\beta = 0.5$, Experiment 11

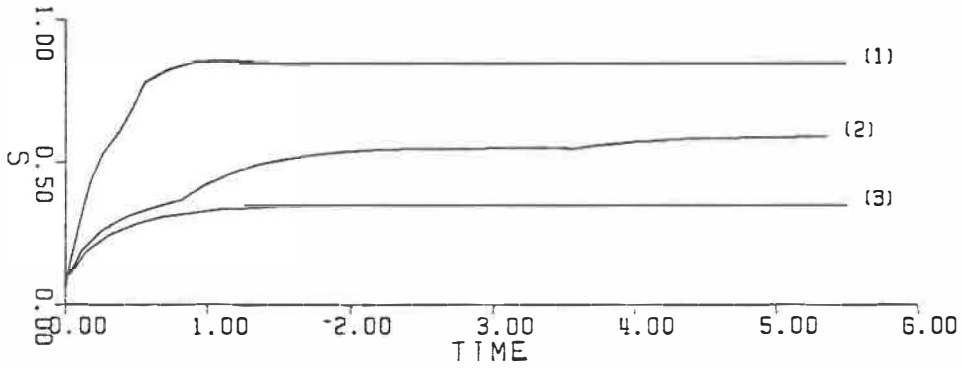

Fig.3.14 Influence of β on interface position

(1): $\beta = 0.2$, Experiment 1

(2): $\beta = 0.4$, Experiment 6

(3): $\beta = 0.5$, Experiment 11

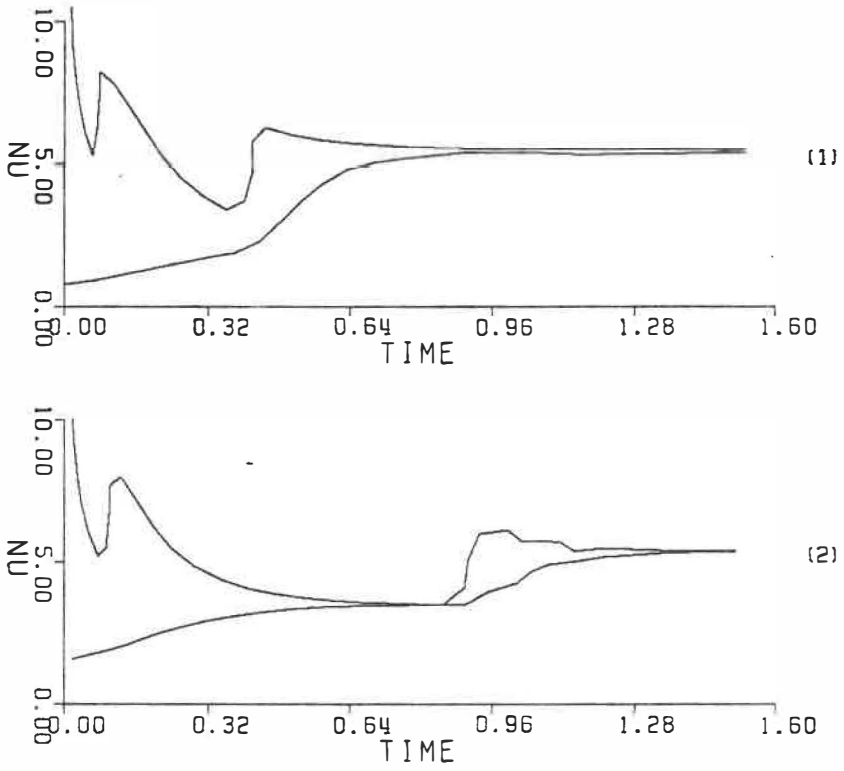

Fig.3.15 Influence of Ste^s on heat transfer rate

(1): $Ste^s = 0.3068$, **Experiment 1**

(2): $Ste^s = 0.6136$, **Experiment 5**

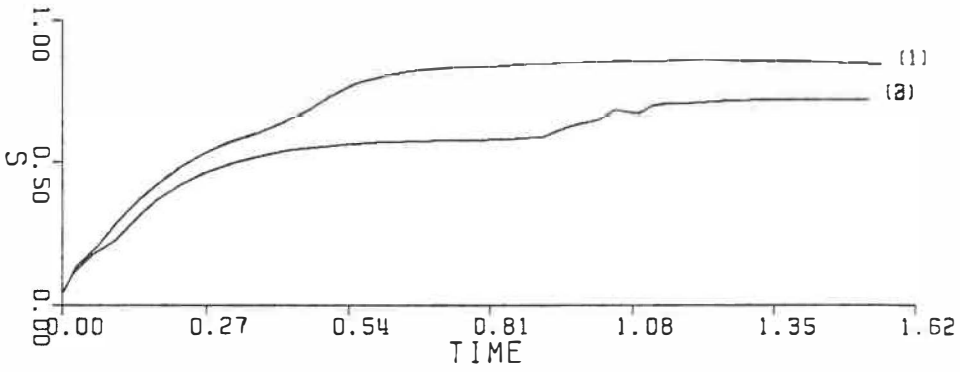

Fig.3.16 Influence of Ste^s on interface position

(1): $Ste^s = 0.306S$, **Experiment 1**

(2): $Ste^s = 0.6136$, **Experiment 5**

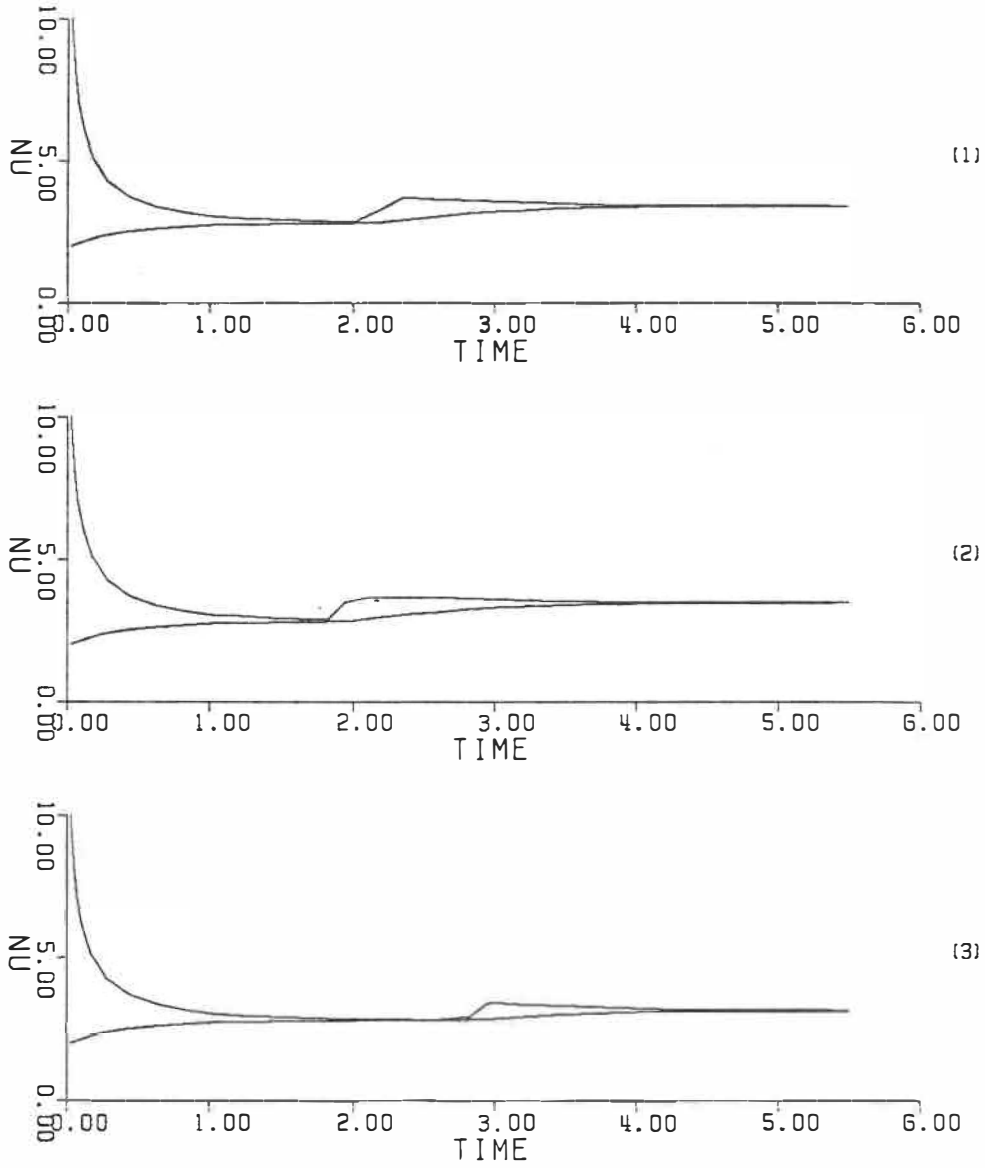

Fig.3.17 Influence of XL on heat transfer rate

(1): $XL = 1.0$, **Experiment 8**

(2): $XL = 1.1$, **Experiment 9**

(3): $XL = 0.8$, **Experiment 10**

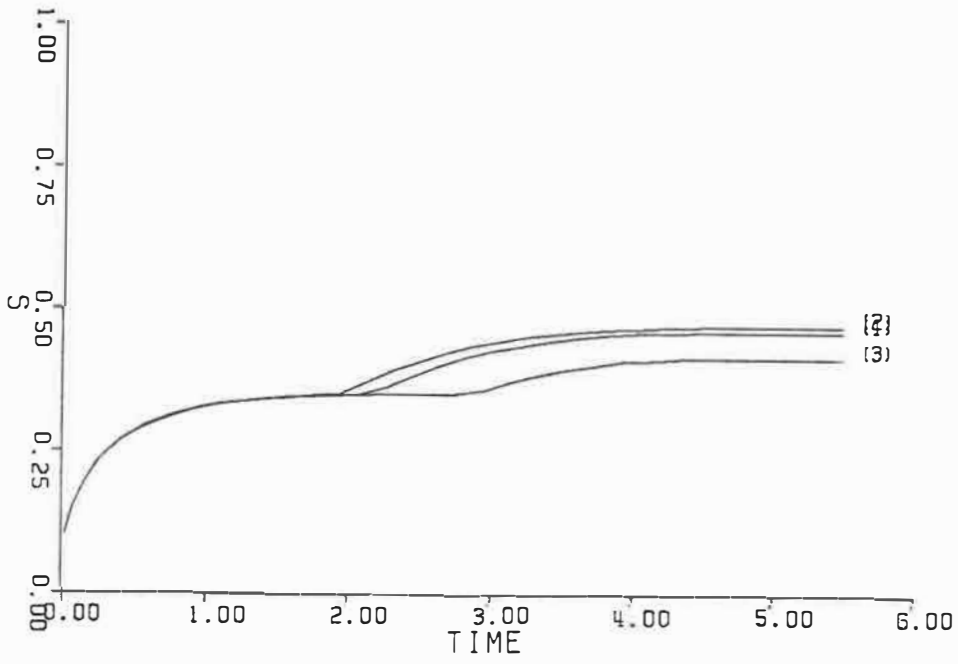

Fig.3.18 Influence of XL on interface position

(1): $XL = 1.0$, Experiment 8

(2): $XL = 1.1$, Experiment 9

(3): $XL = 0.8$, Experiment 10